

## Perception and sensing for autonomous vehicles under adverse weather conditions: A survey

**Yuxiao Zhang<sup>a,\*</sup>, Alexander Carballo<sup>b,c,d</sup>, Hanting Yang<sup>a</sup>, Kazuya Takeda<sup>a,c,d</sup>**

<sup>a</sup> Graduate School of Informatics, Nagoya University, Furo-cho, Chikusa-ward, Nagoya, 464-8601, Japan

<sup>b</sup> Faculty of Engineering and Graduate School of Engineering, Gifu University, 1-1 Yanagido, Gifu City, 501-1193, Japan

<sup>c</sup> Institute of Innovation for Future Society, Nagoya University, Furo-cho, Chikusa-ku, Nagoya, 464-8601, Japan

<sup>d</sup> TierIV Inc., Nagoya University Open Innovation Center, 1-3, Mei-eki 1-chome, Nakamura-Ward, Nagoya, 450-6610, Japan



### ARTICLE INFO

#### Keywords:

Perception and sensing  
Adverse weather conditions  
Autonomous driving  
LiDAR  
Sensor fusion  
Deep learning

### ABSTRACT

Automated Driving Systems (ADS) open up a new domain for the automotive industry and offer new possibilities for future transportation with higher efficiency and comfortable experiences. However, perception and sensing for autonomous driving under adverse weather conditions have been the problem that keeps autonomous vehicles (AVs) from going to higher autonomy for a long time. This paper assesses the influences and challenges that weather brings to ADS sensors in a systematic way, and surveys the solutions against inclement weather conditions. State-of-the-art algorithms and deep learning methods on perception enhancement with regard to each kind of weather, weather status classification, and remote sensing are thoroughly reported. Sensor fusion solutions, weather conditions coverage in currently available datasets, simulators, and experimental facilities are categorized. Additionally, potential ADS sensor candidates and developing research directions such as V2X (Vehicle to Everything) technologies are discussed. By looking into all kinds of major weather problems, and reviewing both sensor and computer science solutions in recent years, this survey points out the main moving trends of adverse weather problems in perception and sensing, i.e., advanced sensor fusion and more sophisticated machine learning techniques; and also the limitations brought by emerging 1550 nm LiDARs. In general, this work contributes a holistic overview of the obstacles and directions of perception and sensing research development in terms of adverse weather conditions.

### 1. Introduction

Perception and sensing are at the core of Autonomous Vehicles (AVs) and robots. An autonomous vehicle, also known as a self-driving car, is a vehicle that has the ability to sense its surrounding environment and navigate safely with little or no human input. Driverless vehicles are meant to change the way people and goods are transported fundamentally and could benefit the future society in significant ways ([Yurtseven et al., 2020](#); [University of Michigan, 2021](#)). However, incidents and casualties involving vehicles equipped with Automated Driving Systems (ADS) are still rising. For the merits of autonomous vehicles to be recognized more extensively, the immediate problem of ADS must be appropriately dealt with, namely, the perception and sensing ability in adverse weather conditions ([Carballo et al., 2020](#)).

Weather phenomena have various negative influences. Averagely, global precipitation occurs 11.0% of the time ([Trenberth and Zhang, 2018](#)). It has been proven that the risk of accidents in rain conditions is 70% higher than normal ([Andrey and Yagar, 1993](#)). 77% of the countries in the world receive snow. The United States national statistics



\* Corresponding author.

E-mail address: [yuxiao.zhang@g.sp.m.is.nagoya-u.ac.jp](mailto:yuxiao.zhang@g.sp.m.is.nagoya-u.ac.jp) (Y. Zhang).

show that each year over 30,000 vehicle crashes occur on snowy or icy roads or during snowfall or sleet ([National Oceanic and Atmospheric Administration, 2021](#)). Phenomena like fog, haze, sandstorms, and

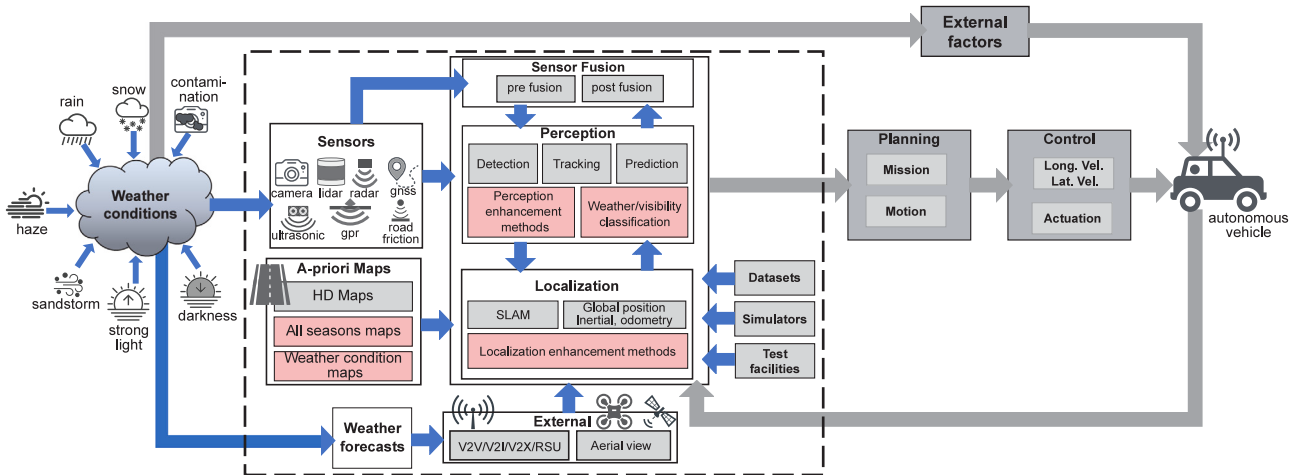


**Fig. 2.** An architecture for self-driving vehicles agnostic to adverse weather conditions. Red blocks denote weather-related modules. Blue arrows denote the relationships among weather and perception and sensing modules. Gray arrows denote the relationships among ADS modules including external weather factors such as wind and wet road surfaces. This survey mainly focuses on the area enclosed in the dashed rectangle. (For interpretation of the references to color in this figure legend, the reader is referred to the web version of this article.)

strong light severely decrease visibility and raise driving risks (Mehra et al., 2021). Secondary problems directly or circumstantially caused by weather, such as heat and coldness, and contamination also have unpredictable or undesirable effects on both manned and autonomous cars.

With some rapid development during recent years, there are already many autonomous cars in operation all over the world, and with the help of LiDAR (Light Detection And Ranging, sometimes Light Imaging Detection And Ranging for the image-like resolution of modern 3D sensors) technology, some manufacturers claim to have achieved or about to deliver vehicles with autonomy equivalent to level 4 of SAE standard (SAE On-Road Automated Driving, 2014) such as Waymo's commercial self-driving taxi service in Phoenix, Arizona (Laris, 2018), the Sensible4<sup>1</sup> autonomous bus (Fig. 1(a)), and the Mcity driver-less shuttle project of the University of Michigan (Fig. 1(b)) (Briefs, 2015). However, weather conditions directly affect the environmental states and impair ADS sensors' ability to perceive, and further increase difficulties for ADS to complete perception tasks such as object recognition. The environmental state changes also create discrepancies between the sensing results and map information, affecting localization accuracy. As a result, an explicit acknowledgment of adverse weather condition influences on sensors is necessary, and a clear picture of how the current adverse weather models are working on perception enhancement, weather classification, and localization to help the perception and sensing module of autonomous driving is useful to the research community, as well as the prospects of the rapidly developing technologies including V2X and aerial imagery.

There have been various adverse weather models all over the world to address the perception and sensing problems in weather. Lots of researchers work on a particular sensor's better ability in dealing with rain and fog, and some on snow. Besides overviews on the driveability assessment in autonomous driving (Guo et al., 2020), there are literature reviews on common sensors' performance evaluations used in ADS in weather conditions (Zang et al., 2019; Mohammed et al., 2020; Yoneda et al., 2019). There is no paper right now that has inclusively covered all the adverse weather phenomena and all the common ADS sensors. Neither has any paper covered both sensor hardware solutions, i.e. sensor fusion, and computer vision and enhancement algorithms based on machine learning in a comprehensive way. So, in addition to filling the void of literature, this paper's main contributions include:

- Holistic presentation of the influences on ADS sensors induced or circumstantially brought by weather.
- Sensor fusion solutions, perception enhancement algorithms, classification, and localization algorithms are thoroughly reported. In the meantime, quick index access to the corresponding literature is provided.
- Experimental validations of several solutions for perception enhancement under adverse weather are conducted.
- Perspectives of trends and future research directions regarding adverse weather conditions are proposed. Also, the limitations that research currently faces are discussed.

Fig. 2 shows the relationships among weather conditions, adverse weather models, and perception and sensing modules, which are the main content covered in this paper. The remainder of this paper is written in 3 parts with 8 sections. The first part is about the sensors: Section 2 introduces the major ADS sensors and presents the challenges and influences that weather brings to them. Section 3 introduces sensor fusion solutions targeting certain weather. The second part is about algorithms and deep learning based methods that help ease the weather effects and improve object recognition: Section 4 presents perception enhancement methods and experimental validation results with regard to each kind of weather; Section 5 states weather classification methods and algorithms that help improve localization accuracy in weather.

The third part is to provide tools for weather research and point out the directions of this area: Section 6 summarizes the datasets, simulators, and experimental facilities that support weather conditions. Section 7 provides analyses of trends, limits, and developing research directions. Section 8 summarizes and concludes this work.

## 2. Adverse weather influences on sensors of autonomous vehicles

Weather challenges have been an impediment to ADS deployment and it is necessary to first acknowledge their influences on sensors. Over a decade ago, Rasshofer et al. (2011) had already attempted to analyze the influences of weather on LiDAR. They proposed a method previous to real tests and artificial environment—synthetic target simulation, which is to reproduce the optical return signals measured by reference laser radar under real weather conditions. Signal parameters like pulse shape, wavelength, and power levels were replicated and the influences of weather were presented in an analytical way. However, such an approach is no longer sufficiently reliable considering the real world is not invariant, and synthetic targets are hard to reach exhaustivity.

<sup>1</sup> <https://sensible4.fi/>.

**Table 1**

The influence level of various weather conditions on sensors.

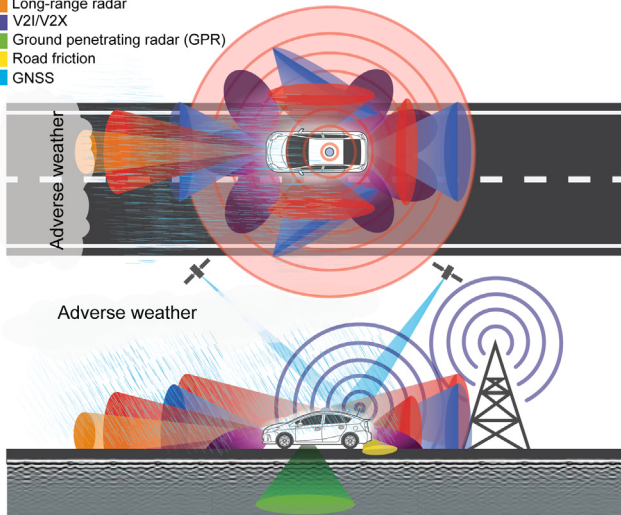
Modality	Light rain <4 mm/h	Heavy rain >25 mm/h	Dense smoke /Mist vis<0.1 km	Fog vis<0.5 km	Haze/Smog vis>2 km	Snow	Strong light	Contamination (over emitter)	Operating Temperature (°C)	Installation complexity	Cost
LiDAR ( $\lambda$ 850–950 nm and 1550 nm)	2	3	5	4	1	5	2	3	−20 to +60 (Velodyne, 2021d)	Easy	High
Radar (24, 77 and 122 GHz)	0	1	2	0	0	2	0	2	−40 to +125 (Texas Instruments, 2021)	Easy	Medium
Ground- Penetrating Radar (100–400 MHz)	0	0	0	0	0	1	0	2	−5 to +50 (Cornick et al., 2016)	Hardest	Medium to high
Camera	3	4	5	4	3	2 (dynamic) 3 (static)	5	5	−20 to +40 (Garmin Ltd., 2021)	Easiest	Lowest
Stereo camera	Almost same as regular camera							0 to +45 (Ricoh, 2021)	Easy	Low	
Gated NIR camera (Bright Way Vision, 2021) ( $\lambda$ 800–950 nm)	2	3	2	1	0	2	4	3	Normally 0 to +65 (SenS HiPe, 2021) for InGaAs cameras	Easy	Low
Thermal FIR Camera <sup>a</sup> ( $\lambda$ 2–10 $\mu$ m)	2	3	3	1	0	2	4	3	−40 to +60 (Axis Com- munications, 2021)	Easy	Low
Road-friction sensor <sup>b</sup> (Lufft, 2021) (infrared)	2	3	3	2	1	2	1	5	−40 to +60	Medium	Low

The effect level each phenomenon causes to sensors:

- 0 - negligible: influences that can almost be ignored.
- 1 - minor: influences that barely cause detection error.
- 2 - slight: influences that cause small errors on special occasions.
- 3 - moderate: influences that cause perception error up to 30% of the time.
- 4 - serious: influences that cause perception error more than 30% but lower than 50% of the time.
- 5 - severe: noise or blockage that causes false detection or detection failure.

<sup>a</sup>Thermal camera is considered to be installed outside of cabin and without glass housings.<sup>b</sup>Road-friction sensor operating relative humidity is <95% but is able to measure 0~100% humidity.

- Ultrasound/short-range radar
- Camera (RGB/Thermal FIR/Stereo/Gated NIR)
- LiDAR
- Long-range radar
- V2I/V2X
- Ground penetrating radar (GPR)
- Road friction
- GNSS

**Fig. 3.** An illustration of sensors configuration in an autonomous vehicle, towards driving under adverse weather conditions. Sensor coverage denotes the general operating directions instead of real operating conditions, for reference only.

**Fig. 3** contains the perception and sensing sensors that are covered in this paper when adverse weather is present. In order to better demonstrate the influences of some major weather conditions on ADS sensors, a detailed comparison is given in **Table 1**. It is worth noticing that level 3 influences (moderate), that cause perception error up to 30% of the time in this table, could also mean up to 30% of the LiDAR point cloud is affected by noise, or up to 30% of the pixels in the camera images are affected by distortion or obscure. The same applies to level 4 influences (serious), as well.

This section will introduce 5 types of major perceptive sensors used in current AVs and the influences that adverse weather has on them.

## 2.1. LiDAR

LiDAR is one of the core perception sensors in the autonomous driving field. The use of 3D-LiDAR on cars has not exceeded much more than a decade and has already demonstrated its indispensability in ADAS (advanced driver-assistance system) with high measurement accuracy and illumination independent sensing capabilities (Thrun et al., 2006). This 3D laser scanning technology has some key attributes: measurement range, measurement accuracy, point density, scan speed and configuration ability, wavelength, robustness to environmental changes, form factor, and cost (Carballo et al., 2020).

Modern LiDARs possess internal property flexibility. Many LiDAR models are equipped with the modality switch among the strongest signal return (strongest echo), the first signal return (first echo) and the last signal return (last echo), and all give relatively similar point cloud

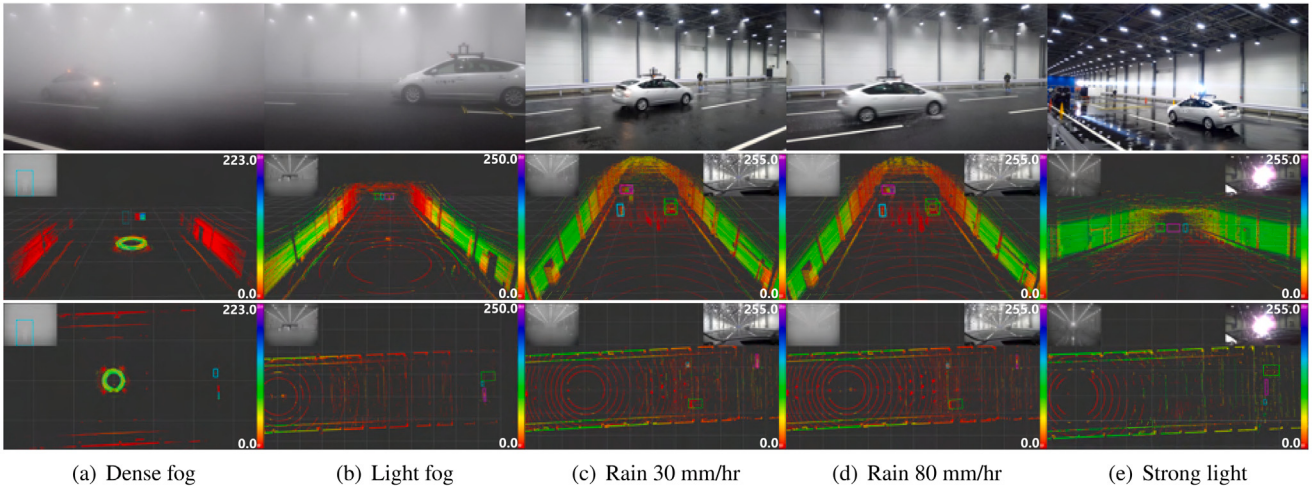


**Fig. 4.** Adverse weather results, top row depicts sample conditions, middle and bottom rows show the 3D LiDAR point cloud, thermal camera image and RGB camera image (not available for fog experiments), targets of interest (human/mannequin, car, and reflective targets) are highlighted. (a) dense fog with visibility of 17 m, color bar denotes intensity range from 0.0 to 223.0. (b) light fog with visibility 162 m, color bar denotes intensity range from 0.0 to 250.0. (c) rainfall setting of 30 mm/h and average humidity of 89.5%, color bar denotes intensity range from 0.0 to 255.0. (d) rainfall setting of 80 mm/h and average humidity of 93%, color bar denotes intensity range from 0.0 to 255.0. Rainfall and visibility measurements using a VAISALA PWD12 laser disdrometer (Vaisala, 2022) at 875 nm, humidity was measured at 4 different stations, strong light used a 6000 W source with a color temperature of 6000 K and maximum current of 155 A. (For interpretation of the references to color in this figure legend, the reader is referred to the web version of this article.)

configurations for driving conditions under clear weather, especially in the observed area in front of the car (Heinzler et al., 2019). However, suppose in a condition where fog is getting denser, the last return shows a larger overlap with the reference point cloud than the strongest return. LiDARs such as the Velodyne HDL64-S3D (Velodyne, 2021b) also provide the function of output laser power and noise ground level manual adjustment. While higher power output guarantees a longer detecting range, the right noise level choice can help improve accuracy, with the help of compatible de-noising methods (Bijelic et al., 2018a).

LiDAR's measurement range, measurement accuracy, and point density are among the key factors that could be interfered with by weather conditions. People have done tests and validations on LiDAR under adverse weather conditions (Zang et al., 2019) in artificial environments like fog chambers (Carballo et al., 2020), real-world snowfields (Jokela et al., 2019), or simulation environments (Fersch et al., 2016).

### 2.1.1. Rain and fog

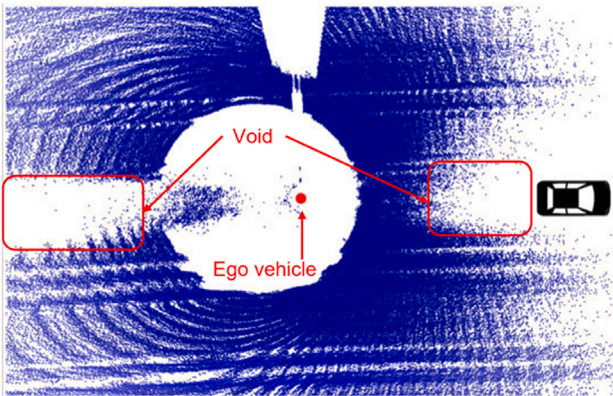
Normal rain does not affect LiDAR functions very much according to the research of Fersch et al. (2016) on small aperture LiDAR sensors. The power attenuation due to scattering by direct interaction between laser beam and raindrops of comparable is almost negligible: the percentage diminution caused by rain at the criteria of how much signal stays above 90% of the original power is at the scale of two decimal spaces, and even for a more stringent criterion (99.5%) a loss of more than 10% of signal power has shown to be very unlikely. The effect from the wetting of the emitter window varies based on drop size, from max attenuation around 50% when the water drops are relatively small, to a minimal of 25% when the drop is about half the aperture size. It seems like wetness does not really impact LiDARs but it is still worth noticing that when the atmosphere temperature is just below the dew point, the condensed water drops on the emitter might just be smaller than the lowest drop size in Fersch et al. (2016) and a signal with a power loss over 50% can hardly be considered a reliable one. Additionally, the influence of rain on LiDAR may not merely lie in signal power level but the accuracy and integrity of the point cloud could also be impacted which is hard to tell from a mathematical model or simulation.

Filgueira et al. (2017) thought of quantifying the rain's influences on LiDAR. They put a stationary LiDAR by the roadside and compared

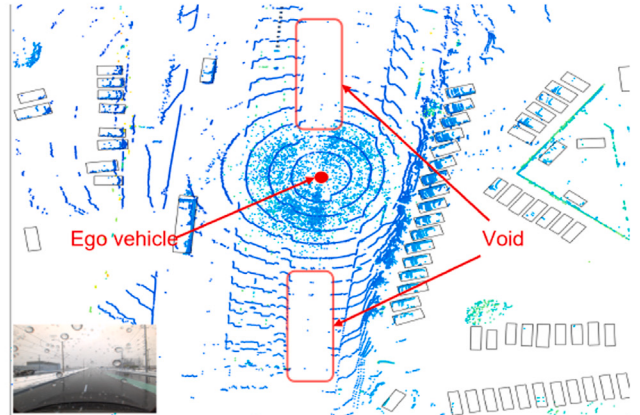
the range detection change, signal intensity change, and the number of detected points changes with regard to several detection areas including road signs, building facades, and asphalt pavement. Their results show range variations up to 20 cm when the rain rate is below 8 mm/h. The problem is that asphalt pavement is almost perpendicular to the falling rain and the building facade is almost parallel to the rain falling direction, and this affects the impartiality of quantifying standards.

Though drizzling and light rain barely affect LiDAR, we do fear it when the rain rate rises. Rains with a high and non-uniform precipitation rate would most likely form lumps of agglomerate fog and create fake obstacles to the LiDARs. As a result, we treat heavy rain the same as dense fog or dense smoke when measuring their effects. Hasirlioglu et al. (2016) proved that the signal reflection intensity drops significantly at a rain rate of 40 mm/h and 95 mm/h by using the method of dividing the signal transmission path into layers in simulation and validating the model with a laser range finder in a hand-made rain simulator. Considering a precipitation rate of more than 50 mm/h counts as violent rain and happens pretty rare even for tropical areas (Jebson, 2007), the referential value here is relatively low in real life. Tests with real commercial LiDARs give a more direct illustration.

We can see from the LIBRE Dataset collected by Carballo et al. (2020) and Lambert et al. (2020) that the point clouds of LiDARs in Fig. 4 show discouraging results due to fog, rain, and wet conditions. In the fog test, the highlighted human presence is only detectable by the LiDAR 13 m ahead in the dense setting but very few points to attempt recognition, and from 47 m ahead in the less dense setting. In the rain test, the highlighted objects were detected 24 m from the LiDAR, and the difference is the level of noise due to the different rain settings. The artificial rain generated in a fog chamber, the Japan Automobile Research Institute (JARI) weather experimental facilities as shown in the first row of Fig. 4 in this case, raised a new problem that most LiDARs detect the water comes out of the sprinklers as falling vertical cylinders which muddle the point cloud even more as illustrated in the third row of Figs. 4(c) and 4(d). Fog chambers have come a long way from over a decade ago when researchers were still trying to stabilize the visibility control for a better test environment (Colomb et al., 2008). However, real weather tests might not completely be ready to be replaced by fog chambers until a better replication system is available. We include an extensive review of weather facilities in Section 6.2.



(a) Ouster OS1-64 point cloud in snow swirl. A few points of powder snow around the ego vehicle; missing view on both forward and back due to the turbulent snow caused by the leading vehicle and ego vehicle itself.



(b) Snow swirl effect without a leading vehicle. Black rectangles correspond to surrounding vehicles. Similar voids can be observed both in front of and behind the ego vehicle. The falling snow is sensed as similar to dense fog clouds around the ego vehicle. Point cloud scene from CADC Dataset. Points color depth indicates intensities: dark blue corresponds to points with higher intensity (cars); light blue corresponds to points with medium intensities (snowfall); cyan corresponds to points with lower intensities (buildings).

**Fig. 5.** LiDAR point clouds with swirl effect in snow weather. Image (a) courtesy of Dr. Maria Jokela [Jokela et al. \(2019\)](#), VTT Technical Research Centre of Finland Ltd.<sup>2</sup>

### 2.1.2. Snow

Different from rain, snow consists of solid objects, snowflakes, and could easily shape themselves into much larger solid objects and become obstacles that either cause false detection of LiDAR or block the line of sight for useful detection. Very few tests on snow effects have been done given the fact that a snow test ground, like the fog chamber, is less easy to access, and the apparent danger of driving in snow.

Jokela et al. (2019) tested LiDAR performance in Finland and Sweden's snow conditions, mainly focused on the snow swirl caused by a leading car. Fig. 5(a) shows the point cloud of accumulating multiple 3D scans as the ego vehicle moved behind the preceding vehicle. For an Ouster OS1-64 LiDAR, apart from some noise points near the sensor, the turbulent snow caused by the leading car and the ego car itself creates voids in the front and back view in the point cloud. It is worth noticing that this kind of point cloud is acquired in a condition where there is considerable accumulated snow on the ground with an interacting vehicle around, which is not very common in normal urban traffic and that is what makes it unique. We explored the Canadian adverse driving conditions dataset (Pitropov et al., 2021) and tried to identify a similar swirl effect on paved roads with no interacting vehicles ahead. It turned out that although the exact same result as Fig. 5(a) is hard to capture, similar voids both in front of and behind the ego vehicle can also be observed, as shown in Fig. 5(b). The voids can be caused by the swirl effect in heavy snowfalls, as in Jokela et al. (2019) findings, or due to accumulation of snowflakes on the optical window, or melted snow as water drops like shown in the bottom left inset of Fig. 5(b). In a word, it is safe to say that snow swirl in the atmosphere or whirled from the ground could cause anomalies in LiDAR's point cloud and shorten the view distance.

One other factor in snow conditions, low temperature, is also of concern. A Velodyne VLP-16 LiDAR like the one used in Jokela et al. (2019), whose designed lowest operating temperature is  $-10^{\circ}\text{C}$ , might not even stand a chance in a colder environment which is not that rare in the northern hemisphere. When the temperature change is at a large scale, such as from an extremely cold ( $-20^{\circ}\text{C}$ ) to an extremely hot ( $+60^{\circ}\text{C}$ ) environment, the time delay of LiDAR measurement would increase about 6.8 ns, which widens the LiDAR ranging by over a 1 meter and lowers the precision at near field (Gao et al., 2018), not to mention the sensibility of photodetectors and range measurement.

### 2.1.3. Sandstorm and smog

There are more weather phenomena that cause problems to transportation, such as sandstorms and smog. As rare as they might appear, they could be more serious problems than rain and snow for some regions like the Middle East or desert areas. Particles from road dirt attached to the outer surface of the emitter window could worsen the LiDAR signal attenuation (Trierweiler et al., 2020). Tests with near-homogeneous dust particles being distributed on the surface of a scanner show a 75% reduction in LiDAR maximum range (Trierweiler et al., 2019). Besides Waymo's experience in a dust storm in Arizona, evaluations in such weather are scarce. The part where LiDAR is involved in sandstorms or haze-smog weather is beyond the road—airborne or space. The CALIPSO high spectral resolution LiDAR (Rogers et al., 2014) is used in satellites to monitor the Earth's atmosphere and can look through haze and sandstorms. Single-photon LiDARs are also frequently used in airborne LiDARs for 3D terrain mapping. Although such technology normally serves meteorology and oceanology (Swatantran et al., 2016), there is already single-photon avalanche diode (SPAD) LiDAR that has been used in automotive applications (SONY Semiconductor Solutions Corporation, 2021) due to its advantages in long-range capabilities (kilometers), excellent depth resolution (centimeters), and use of low-power (eye-safe) laser sources (Rapp et al., 2020). Future aerial LiDARs and UAVs (Unmanned Aerial Vehicles) are facing additional weather challenges as the situation in the sky is not quite the same as on the ground. Atmosphere turbulence can produce wind-affected and time-varying refractive gradients which lead to scintillation, beam spreading, and wander (Osche and Young, 1996). The particular effect of such adversarial conditions on aerial LiDARs and UAVs has not been studied in a methodically way as they are still at the stage of developing in the autonomous driving area, but it is safe to assume that they are going to need to overcome this problem to be able to serve the intelligent transportation system under hazy and turbulent conditions in the future.

<sup>2</sup> <https://www.vtresearch.com/en>.

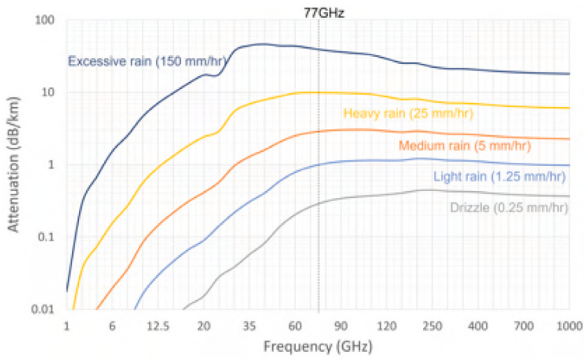


**Fig. 6.** Electromagnetic power attenuation vs. frequency in different rain rates (International Telecommunication Union, 2021; Olsen et al., 1978).

## 2.2. Radar

The automotive radar system consists of a transmitter and a receiver. The transmitter sends out radio waves that hit an object (static or moving) and bounce back to the receiver, determining the object's distance, speed and direction. Automotive radar typically operates at bands between 24 GHz and 77 GHz which are known as mm-wave frequencies, while some on-chip radar also operates at 122 GHz. Radar can be used in the detection of objects and obstacles like in the parking assistance system, and also in detecting positions, and speed relative to the leading vehicle as in the adaptive cruise control system (Patole et al., 2017).

There is also an FMCW (Frequency Modulated Continuous Wave) form for radar where the frequency of the transmitted signal is continuously varied at a known rate which makes the difference between the transmitted and the reflected signal proportional to the time of flight. Besides the speed measurement advantage, FMCW radar shows superior range resolution and accuracy (Navtech Radar, 2021b; Gao et al., 2021).

Radar seems to be more resilient in weather conditions. In order to intuitively see the difference, we plotted a chart of electromagnetic power attenuation in different rain rates (International Telecommunication Union, 2021; Olsen et al., 1978). From Fig. 6, we can observe that the attenuation for radar at 77 GHz is at the level of 10 dB/km in a 25 mm/h heavy rain, while 905 nm LiDAR's attenuation is about 35 dB/km under the same visibility below 0.5 km condition (Ijaz et al., 2012; Gultepe, 2008). According to Sharma and Sergeyev's simulation on non-coherent photonics radar which possesses lower atmosphere fluctuation, the detection range of the configuration of a linear frequency-modulated 77 GHz and 1550 nm continuous-wave laser could reach 260 m in heavy fog, 460 m in mild fog and over 600 m in heavy rain with SNR (signal-to-noise ratio) threshold at 20 dB (Sharma and Sergeyev, 2020). Norouzian et al. (2019) also tested radar's signal attenuation in snowfall. A higher snow rate yields larger attenuation as expected, and wet snow shows higher attenuation because of the higher water absorption and larger snowflakes. Considering a snowfall with 10 mm/h already has quite low visibility (< 0.1 km) (Rasmussen et al., 1999), we estimate that the specific attenuation for a 77 GHz radar in a 10 mm/h snow is about 6 dB/km, which is seemingly acceptable given the rain data.

In the research of Zang et al. (2019), the rain attenuation and back-scatter effects on mm-wave radar and the receiver noise were mathematically analyzed. They conducted simulations on different scenarios with radar detecting cars or pedestrians under different levels of rain rate. Results show that the back-scatter effect leads to the degradation of the signal-to-interference-plus-noise ratio when the radar cross-section area is small. However, the degradation is at the single-digit level at a 100 mm/h rain rate and their simulation expands the

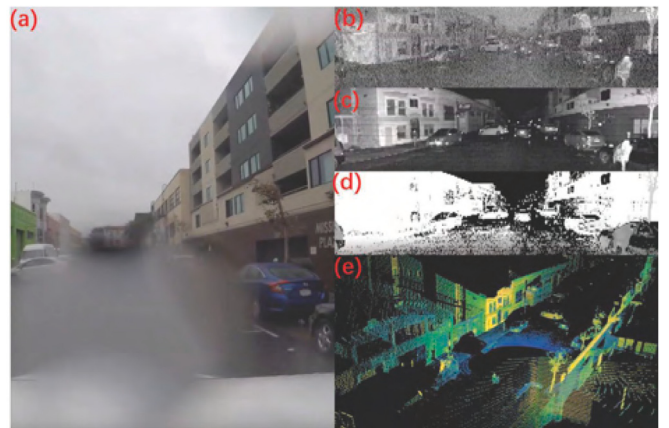


**Fig. 7.** Camera vs. LiDAR in rain condition (Mardirosian, 2021). (a) camera perspective; (b) intensity; (c) reflectivity; (d) noise; (e) 3D point cloud colored by intensity. Image courtesy of Ms. Kim Xie, Ouster Inc.<sup>3</sup> (For interpretation of the references to color in this figure legend, the reader is referred to the web version of this article.)

test variables up to a 400 mm/h rain rate which is basically unrealistic in real-world because even if such an enormously high rain rate occurs, the condition of driving would be highly difficult. Therefore, rain attenuation and back-scatter effects on the mm-wave radar are not serious.

No doubt that radar is objectively better adaptive to wet weather, but when compared with LiDAR, radar often receives criticism for its insufficient ability in pedestrian detection, object shape, and size information classification due to low spatial resolution. Akita and Mita (2019) have improved this by implementing long-short-term memory (LSTM) which can treat time-series data. What is more, one of the sensors used by the radar extension of Oxford RobotCar dataset (Barnes et al., 2020) is a Navtech Radar CTS350-X 360° FMCW scanning radar (Navtech Radar, 2021a) which possesses a measurement range up to 100–200 m and can handle Simultaneous Localization and Mapping (SLAM) solely in the dark night, dense fog and heavy snow conditions (Hong et al., 2020; Gadd et al., 2020). Recently, by adding an additional time dimension, 4D radars with Multiple Input Multiple Output (MIMO) antenna arrays are now able to measure the object's height above road level so as to achieve higher classification accuracy (Palfy et al., 2022). Furthermore, high-resolution mapping of urban environments agnostic to many kinds of weather conditions can be achieved by the application of synthetic aperture radar (SAR) (Tebaldini et al., 2022). So the usefulness of radar has much more potential.

## 2.3. Camera

Camera is one of the widest-used sensors in perception tasks, while also one of the most vulnerable in adverse weather conditions. Adhered to the interior windshield, sometimes rear or other windows, dashcams (dashboard cameras) continuously record the surroundings of a vehicle with an angle as wide as 170° (Rexing, 2021). Numerous autonomous driving datasets started with dashcam recordings at an early stage while nowadays professional camera sets and fisheye lens cameras are being deployed for an even larger field of view (Yogamani et al., 2019). Cameras with specialties under particular situations such as night vision will be further discussed in sensor fusion in Section 3.2 and potential sensor candidates in Section 7.1.2.

<sup>3</sup> <https://ouster.com/>.

### 2.3.1. Rain and fog

A camera in rain, regardless of how high resolution, can be easily incapacitated by a single water drop on the emitter or lens (Mardirosian, 2021), as shown in Fig. 7. The blockage and distortion in the image would instantly make the system lose the sense of input data and fail to process correctly. As for fog, based on its density, it creates near-homogeneous blockages at a certain level which is a direct deprivation of information to cameras. Reway et al. (2018) proposed a Camera-in-the-Loop method to evaluate the performance of the object detecting algorithm under different weather conditions. The environment model data are acquired by a set of cameras and processed by an object classification algorithm, the result is then fed to the decision maker which re-engages in the simulation environment and completes a closed loop. The result of up to 40% rise in miss rate in the night or fog proves that camera-only perception under the influences of weather is not safe enough.

### 2.3.2. Snow

Winter weather like snow could affect the camera in one similar way as rain does when the snowflakes touch the lens or the camera's optical window and melt into ice-slurry immediately. What is worse, those ice water mixtures might freeze up again quickly in low temperatures and form an opaque blockage.

Heavy snow or hail could fluctuate the image intensity and obscure the edges of the pattern of a certain object in the image or video which leads to detection failure (Zang et al., 2019). Besides the dynamic influence, snow can extend itself to a static weather phenomenon by accumulating on the surface of the earth and blocking road marks or lane lines (Naughton, 2021). Under such situations, the acquisition of data sources is compromised for cameras, and the process of perception would be interrupted at the very beginning.

### 2.3.3. Light conditions

A particular weather phenomenon, strong light, which could be directly from the sun, from skyscrapers' light pollution, or from bright beam light of other cars approaching the ego vehicle may also cause severe trouble to cameras. Even LiDAR suffers from strong light in extreme conditions (Carballo et al., 2020), showing a large area of black around the light source. As shown in Fig. 4(e) upper right insets, too high an illumination can degrade the visibility of a camera down to almost zero, and glares reflected by all kinds of glossy surfaces could make the camera exposure selection a difficult task (Radecki et al., 2016). HDR camera specializes in tough light conditions which will be introduced in Section 7.1.2.

Another correlative issue caused by light is the reflection off reflective surfaces. If the reflection happens to be ideal, it might confuse the camera into believing it and transmitting a false signal due to the lack of stereoscopic consciousness. Sometimes the reflections are an inferior mirage due to high road surface temperatures, and sometimes are mirror images of the car's interiors. It would be preferable to have a sense of depth in three-dimension to help a normal camera handle changes in light and illumination conditions.

## 2.4. Ultrasonic sensors

Ultrasonic sensors are commonly installed on the bumpers and all over the car body serving as parking assisting sensors and blindspot monitors (Carullo and Parvis, 2001). The principle of ultrasonic sensors is pretty similar to radar, both measuring the distance by calculating the travel time of the emitted electromagnetic wave, only ultrasonic operates at ultrasound band, around 40 to 70 kHz. In consequence, the detecting range of ultrasonic sensors normally does not exceed 11 m (Frenzel, 2021), and that restricts the application of ultrasonic sensors to close-range purposes such as backup parking. Efforts have been done to extend the effective range of ultrasonic and make it fit for long-range detecting (Kamemura et al., 2008). For example, Tesla's

"summon" feature uses ultrasonic to navigate through park space and garage doors (Tesla, 2021a).

Ultrasonic is among the sensors that are hardly considered in the evaluation of weather influences, but it does show some special features. The speed of sound traveling in air is affected by air pressure, humidity, and temperature (Varghese et al., 2015). The fluctuation of accuracy caused by this is a concern to autonomous driving unless enlisting the help of algorithms that can adjust the readings according to the ambient environment which generates extra costs. Nonetheless, ultrasonic does have its strengths, given the fact that its basic function is less affected by harsh weather compared to LiDAR and camera. The return signal of an ultrasonic wave does not get decreased due to the target's dark color or low reflectivity, so it is more reliable in low visibility environments than cameras, such as high-glare or shaded areas beneath an overpass.

Additionally, the close proximity specialty of ultrasonic can be used to classify the condition of the road surface. Asphalt, grass, gravel, or dirt road can be distinguished from their back-scattered ultrasonic signals (Bystrov et al., 2016), so it is not hard to imagine that the snow, ice, or slurry on the road can be identified and help AV weather classification as well.

## 2.5. GNSS/INS

Navigation or positioning systems are among the most basic technology found in robots, AVs, UAVs, air crafts, marine vessels, and even smartphones. Groves (2014) provides a list of diverse measurement types and corresponding positioning methods.

The global navigation satellite system (GNSS) is an international system of multiple constellations of satellites, including systems such as GPS (United States), GLONASS (Russia), BeiDou (China), Galileo (European Union), and other constellations and positioning systems. GNSS operates in the L-Band (1 to 2 GHz) which can pass through clouds and rain, with a minimum impact on the transmitted signal in terms of path attenuation. GNSS sensors include one or more antennas, reconfigurable GNSS receivers, processors, and memory. GNSS is often in combination with real-time kinematic positioning (RTK) systems using ground base-stations to transmit correction data.

Non-GNSS broadband radio signals are used for indoor, GNSS signal-deprived areas (i.e. tunnels), and urban positioning. Such systems include Wi-Fi-based positioning systems (WPS), Bluetooth and Ultra-Wideband (UWB) beacons, landmarks, vehicle-to-infrastructure (V2I) stations, radio frequency ID (RFID) tags, etc.

Odometry and inertial navigation systems (INS) use dead reckoning to compute position, velocity, and orientation without using external references. INS combines motion sensors (accelerometers), rotation sensors (gyroscopes), and also magnetic field sensors (magnetometers). For the advanced INS, fiber optic gyroscopes (FOG) are used: with no moving parts, and two laser beams propagating in opposite directions through very long fiber optic spools, the phase difference between the two beams is compared and it is proportional to the rate of rotation.

The combination of the above, such as GNSS with INS (GNSS+INS) and other sensors, with algorithms such as Kalman Filter and motion models, is a common approach to improve positioning accuracy and reduce drift. For example, the Spatial FOG Dual GNSS/INS of Advanced Navigation (Advanced Navigation, 2021) has 8 mm horizontal position accuracy and about 0.005° roll/pitch accuracy.

Signals from satellite-based navigation systems, such as GPS, Galileo and others, experience some attenuation and reflection with passing through water in the atmosphere and other water bodies. As analyzed by Gernot (2007), water is a dielectric medium and a conductor. Electromagnetic waves will experience attenuation due to the rotation of water molecules according to the electric field which causes energy dissipation. Also, moving charges in the water body will reflect and refract the wave, and this happens at the air–water and water–air interfaces.

**Table 2**

Sensor fusion configurations and their target adverse conditions.

Sensor fusion	Configuration	Target weather
RadarNet (Yang et al., 2020)	Radar + LiDAR	Potentially rain in the nuScenes dataset
MVDNet (Qian et al., 2021)	Radar + LiDAR	Fog
Liu et al. (2021a)	Radar + Camera	Rain, fog, nighttime
Fritzsche et al. (2018)	Mechanical pivoting radar (MPR) + LiDAR	Low visibility fog
FLIR automated emergency braking (AEB) sensor suite (FLIR, 2021)	[Thermal long-wave infrared (LWIR) camera + Radar + Visible camera]	Nighttime, tunnel exit into sun glare
Heatnet (Vertens et al., 2020)	Thermal camera + 2 RGB cameras	Nighttime
Spooren et al. (2016)	Near-infrared camera + RGB camera	Potentially rain, snow, smog
John et al. (2021)	Thermal camera + Visible cameras	Low illumination conditions, headlight glare
SLS-Fusion (Mai et al., 2021)	LiDAR + Camera	Fog
RobustSENSE (Kutila et al., 2016)	[LiDAR + 77 GHz radar + 24 GHz radar + Stereo camera + Thermal cameras]	Fog
Radecki et al. (2016)	LiDAR + Radar + Camera	Wet conditions, nighttime, glare, dust
Bijelic et al. (2020)	[A pair of stereo RGB cameras + NIR gated camera + 77 GHz radar + 2 LiDARs + Far-infrared (FIR) camera + weather station + road-friction sensor]	Rain, fog, snow
Rawashdeh et al. (2021)	Cameras + LiDAR + Radar	Snow pathfinding
Vachmanus et al. (2021)	Thermal camera + RGB cameras	Snow
Brunner et al. (2013)	Thermal camera + Visible cameras	Strong light, smoke, fire, extreme heat

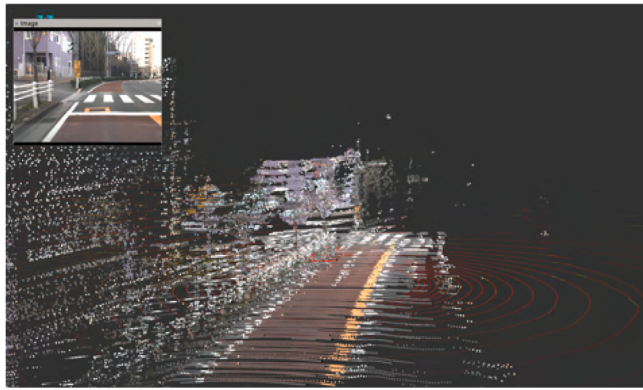


**Fig. 8.** Fusion of 3D point cloud data and camera imagery: point cloud colored by the corresponding RGB color information. (For interpretation of the references to color in this figure legend, the reader is referred to the web version of this article.)

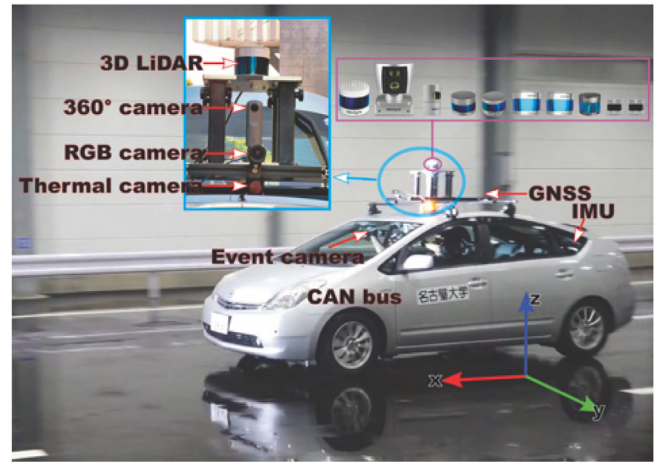


**Fig. 9.** The Toyota Prius used for ADS tests from Nagoya University. The LiDAR sensor, alongside other sensors, is bolted on a plate mounted firmly on top of the car.

Balasubramaniam and Ruf (2020) studied the effects of rain and winds on GNSS reflectometry (GNSS-R), their model considers path attenuation, modified surface roughness and downdraft winds. Their study finds very little attenuation in the L-Band due to raindrops, with about 96% transmissivity for mild rain below 30 mm/h. While the L-Band is able to penetrate even heavy rain, the effect of wind tends to increase attenuation.

In Gernot's work (Gernot, 2007), GPS signal experienced a significant loss over 9.4 dB when passing through a 1 mm layer of liquid water, but only 0.9 dB when passing through a 4 cm layer of snow, and 1.7 dB for a 14 cm layer of snow. This experiment suggests that bodies of water in the form of wet roads and puddles will further affect the signal-to-noise ratio of GNSS.

### 3. Sensor fusion solutions

The serious influences that weather causes on autonomous driving encourage people to work on solutions. For example, industry solutions typically use directed air flows to remove drops of water from the camera. With the wild spread use of machine learning and the rapid development of powerful sensors, multiple-sensor modalities and additional sensor components are brought to help mitigate the effects of weather. Table 2 shows the sensor fusion configurations and the adverse conditions they are targeting.

It can be inferred from the previous section that an individual sensor is not going to navigate through adverse weather conditions with

enough safety assurance. But multiple forces combining together could improve the perception ability as shown in the enhanced point cloud from a LiDAR + camera fusion in Fig. 8. Yeong et al. (2021) pointed out that a sensor fusion outdoes every sensor on its own including LiDAR, camera, and radar, not only in weather conditions but also the overall perception performance. As a result, groups from all over the world come up with their own combinations with the addition of radar, infrared cameras, gated cameras, stereo cameras, weather stations, and other weather-related sensors. An example of a sensor fusion setup on a test AV is shown in Fig. 9. Sensor diversity improves the perception ability's general lower bound, and the intelligent choice of sensor weighting and accurately quantified parameters based on the particular weather determine the ceiling of robustness and reliability.

#### 3.1. Radar appendage

The addition of radar can be observed in many cases due to its intrinsic robustness against adverse conditions. Yang et al. (2020) brought up RadarNet, which exploits both radar and LiDAR sensors for perception. Their early fusion exploits the geometric information by concatenating both LiDAR and radar's voxel representation together along the channel dimension, and the attention-based late fusion is designated to specifically extract the radar's radial velocity evidence. They validated their method on the nuScenes dataset (Caesar et al.,

2020) without specifically mentioning the performances under adverse weather conditions even though rain conditions in Boston and Singapore are presented in nuScenes. Basically, the significance of such classic fusion is proven, especially in the improvement of long-distance object detection and velocity estimation.

Liu et al. (2021a) raised a robust target recognition and tracking method combining radar and camera information under severe weather conditions, with radar being the main hardware and camera the auxiliary. They tested their scheme in rain and fog including night conditions when visibility was the worst. Results show that radar has pretty high accuracy in detecting moving targets in wet weather, while the camera is better at categorizing targets and the combination beats LiDAR only detection by over a third. Their radar also shows good stability in tracking vertical targets but not horizontal targets due to the limited field of view (FOV). Radar and camera together reach close to the LiDAR tracking ability and they concluded that this mixture stands a good chance in adverse weather conditions.

Fritzsche et al. (2018) used a 2D high bandwidth scanner, the mechanical pivoting radar (MPR) (Fritzsche et al., 2016), to fuse with LiDAR data to achieve SLAM in a low visibility fog environment. The MPR only has a 15 m measurement range but the ability to penetrate fog is more than enough to prove itself useful in landmark searching and make up for what the LiDAR is missing. This fusion was tested on a robot instead of an AV.

Qian et al. (2021) introduced a Multimodal Vehicle Detection Network (MVDNet) featuring LiDAR and radar. It first extracts features and generates proposals from both sensors, and then the multimodal fusion processes region-wise features to improve detection. They created their own training dataset based on the Oxford Radar Robotcar (Barnes et al., 2020) and the evaluation shows much better performance than LiDAR alone in fog conditions.

Kutila et al. (2016) raised an architecture called the RobustSENSE project. They integrated LiDAR with long (77 GHz) and short (24 GHz) range radar, stereo, and thermal cameras while connecting the LiDAR detection layer and performance assessment layer. That way, the data gathered by the supplementary sensors can be used in the vehicle control layer for reference when the LiDAR performance is assessed as degrading down to a critical level. They tested the architecture with a roadside LiDAR in a foggy airport and collected performance data while keeping the hardware components' cost at a considerably low price (< 1000 Euros). Although the comparability with an AV test drive is not ideal, the concept of hardware and software complementation is proven.

### 3.2. Specialized camera appendage

Cameras with certain specialties such as thermal imaging also often dominate fusions, especially in pure vision solutions. FLIR System Inc. (FLIR, 2021) and the VSI Labs (VSILabs, 2021) tested the world's first fused automated emergency braking (AEB) sensor suite in 2020, equipped with a thermal long-wave infrared (LWIR) camera, a radar, and a visible camera. LWIR covers the wavelength ranging from 8 μm to 14 μm and such cameras known as the uncooled thermal camera operate under ambient temperature. This sensor suite was tested along with several cars with various AEB features employing radar and visible cameras against daytime, nighttime, and tunnel exit into sun glare. The comparison showed that although most AEB systems work fine in the daytime, normal AEB almost hit every mannequin under those adverse conditions, which did not happen once to the LWIR sensor suite. As a matter of fact, LWIR camera also exhibits superior performance in thick fog conditions when scattering loss is very high compared to MWIR (3 μm–5 μm) and SWIR (0.85 μm–2 μm) (Judd et al., 2019). It is worth noticing that LWIR thermal cameras normally would not be installed behind windows because the radiation of over 5 μm wavelength will not go through glasses.

Vertens et al. (2020) went around the troublesome nighttime images annotation and leveraged thermal images. They taught their network to adapt and align an existing RGB-dataset to the nighttime domain and completed multi-modal semantic segmentation. Spooren et al. (2016) came up with a multi-spectral active gated imaging system that integrated RGB and NIR cameras for low-light-level and adverse weather conditions. They designed customized filters to achieve a parallel acquisition of both the standard RGB channels and an extra NIR channel. Their fused image is produced with the colors from the RGB image and the details from the NIR. John et al. (2021) also proposed a visible and thermal camera deep sensor fusion framework that performs both semantic accurate forecasting as well as appropriate semantic segmentation. These might be some of the most cost-effective solutions for weather conditions but particular gated CMOS imaging systems are still being developed (Bright Way Vision, 2021).

It should be noted that even though thermal cameras can have better performance than regular cameras and can definitely be tested in winter, the operating temperatures provided by the manufacturers have certain lower bounds as shown in Table 1, which might seriously restrain the practical use of such sensors during cold winter even if it is a clear day. The durability of such temperature-sensitive devices needs further validation in real environments in the future to ensure their usefulness.

Mai et al. (2021) applied fog to the public KITTI dataset to create a Multifog KITTI dataset for both images and point clouds. They performed evaluation using their Spare LiDAR Stereo Fusion Network (SLS-Fusion) based on LiDAR and camera. By training their network with both clear and foggy data, the performance was improved over a quarter, on the basis of the original performance was reduced by almost a half, which is another good example of making the best of sensor fusion.

Vachmanus et al. (2021) also included imagery of thermal cameras to perform the autonomous driving semantic segmentation task. RGB camera input might not be enough to represent every pertinent object with various colors in the surroundings, or pedestrians involved in the snow driving scenario, which happens to be the thermal camera's strong point. Their architecture contains two branches of encoders, one for RGB camera and thermal camera each to extract features from their own input. The temperature feature in the thermal map perfectly supports the loss of image element due to the snow and the fusion model successfully improves snow segmentation compared to not only RGB camera alone, but several other state-of-art networks, based on the validation on several datasets including Synthia (Ros et al., 2016) and Cityscapes (Cordts et al., 2016). This network is very suitable for automated snowplows on roads with sidewalks, which serves beyond the traditional autonomous driving purpose.

Furthermore, Rawashdeh et al. (2021) include cameras, LiDAR, and radar in their CNN (Convolutional Neural Network) sensor fusion for drivable path detection. This multi-stream encoder-decoder almost complements the asymmetrical degradation of sensor inputs at the largest level. The depth and the number of blocks of each sensor in the architecture are decided by their input data density, of which camera has the most, LiDAR the second and radar the last, and the outputs of the fully connected network are reshaped into a 2-D array which will be fed to the decoder. Their model can successfully ignore the lines and edges that appeared on the road which could lead to false interpretation and delineate the general drivable area.

Bijelic et al. (2020) from Mercedes-Benz AG present a large deep multimodal sensor fusion in unseen adverse weather. Their test vehicle is equipped with the following: a pair of stereo RGB cameras facing front; a near-infrared (NIR) gated camera whose adjustable delay capture of the flash laser pulse reduces the backscatter from particles in adverse weather (Bijelic et al., 2018b); a 77 GHz radar with 1° resolution; two Velodyne LiDARs namely HDL64 S3D and VLP32C; a far-infrared (FIR) thermal camera; a weather station with the ability to sense temperature, wind speed and direction, humidity, barometric

pressure, and dew point; and a proprietary road-friction sensor. All the above are time-synchronized and ego-motion corrected with the help of the inertial measurement unit (IMU). Their fusion is entropy-steered, which means regions in the captures with low entropy can be attenuated, while entropy-rich regions can be amplified in the feature extraction. All the data collected by the exteroceptive sensors are concatenated for the entropy estimation process and the training was done by using clear weather only which demonstrated a strong adaptation. The fused detection performance was proven to be evidently improved than LiDAR or image-only under fog conditions. The blemish in this modality is that the amount of sensors exceeds the normal expectation of an ADS system. More sensors require more power supply and connection channels which is a burden to the vehicle itself and proprietary weather sensors are not exactly cost-friendly. Even though such an algorithm is still real-time processed, given the bulk amount of data from multiple sensors, the response and reaction time becomes something that should be worried about.

#### 4. Perception enhancement algorithms and experimental validations

Sensors can be treated as the means of ADS perception and one of the main purposes of perception is to extract critical information that is essential to the safe navigation of an AV. This information could mean moving objects either on or close to the road including various vehicles, pedestrians, and non-traffic participants such as playing children or animals, and also static objects including traffic lights, road signs, parked cars, trees, and city infrastructures because those are what we would pay attention to when we are driving as humans. In order to avoid collisions, we first need to know the existence of objects and their locations, followed by their movement directions and speeds, i.e. object detection and tracking. General object detection in the computer vision area is to determine the presence of objects of certain classes in an image, and then determine the size of them through a rectangular bounding box, which is the label in nowadays autonomous driving datasets. YOLO (You Only Look Once) (Redmon et al., 2016) is now one of the most popular single-stage approaches in 2D with spatially separated bounding boxes and provides object class probabilities. Meanwhile, multi-stage detectors such as Region-based CNN (R-CNN) (Ren et al., 2015) models first extract the regions of the pertinent objects and then further determine the objects' location and do the classification. On the other hand, the detection of an object captured by sensors of ADS such as LiDAR and radar is manifested by a signal return. With adequate signal densities, some voxel-based or point-based 3D methods such as PointPillars (Lang et al., 2019), Second (Yan et al., 2018) and Voxel-FPN (Kuang et al., 2020), allow to correctly identify object classes in the point cloud.

As established in the previous context, the signal intensity attenuation and noise disturbance caused by weather phenomena impair the ADS sensors' abilities to carry out their original duties and make the risk index of autonomous driving climb rapidly. Efforts have been made on restoring or improving perception performances. For example for pedestrian detection, recognition of the particular micro-Doppler spectra (Steinbauer et al., 2021) and multi-layer deep learning approaches (Li et al., 2019) are used in bad weather. Thermal datasets specifically targeting pedestrians (Tumas et al., 2020) or large-scale simulation dataset (Liu et al., 2020) are also being established. In this section, perception enhancement methods aiming to mediate the effects of adverse weather, and to improve detection abilities will be introduced, in the order of rain, fog, snow, light-related conditions, and contamination, as well as experimental validations.

#### 4.1. Rain

De-raining technique has been deeply studied by the computer vision field. The detection and removal of raindrops can be divided into falling raindrops and adherent raindrops that accumulated on the protective covers of cameras (Hamzeh and Rawashdeh, 2021). For rain streaks removal, several training and learning methods have been put to use including Quasi-Sparsity-based training (Wang et al., 2021a) and continual learning (Zhou et al., 2021). Quan et al. (2021) proposed a cascaded network architecture to remove rain streaks and raindrops in a one-go while presenting their own real-world rain dataset. Their raindrop removal and rain streak removal work in a complementary way and the results are fused via an attention-based fusion module. They effectively achieved de-raining on various types of rain with the help of neural architecture search and their designated de-raining search space.

Ni et al. (2021) introduced a network that can realize both removal and rendering. They constructed a Rain Intensity Controlling Network (RIC-Net) that contains three sub-networks: background extraction, high-frequency rain streak elimination, and main controlling. Histogram of oriented gradient (HOG) and auto-correlation loss are used to facilitate the orientation consistency and repress repetitive rain streaks. They trained the network all the way from drizzle to downpour rain and validation using real data shows superiority.

Like common de-noising methods, a close loop of both generation and removal can present better performance. Wang et al. (2021b) handled the single image rain removal (SIRR) task by first building a full Bayesian generative model for rainy images. The physical structure is constructed by parameters including direction, scale, and thickness. The good part is that the generator can automatically generate diverse and non-repetitive training pairs so that efficiency is ensured. Similar rain generation is proposed by Ye et al. (2021) using disentangled image translation to close the loop. Furthermore, Yue et al. (2021) surpassed image frames and achieved semi-supervised video de-raining with a dynamic rain generator. The dynamical generator consists of both an emission and transition model to simultaneously construct the rain streaks' spatial and dynamic parameters like the three mentioned above. They use deep neural networks (DNNs) for semi-supervised learning to help the generalization for real cases.

While de-raining has been extensively studied using various training and learning methods, most of the algorithms have met challenges on adherent raindrops and performed poorly when the rain rates or the dynamism of the scene get higher. Detection of adherent raindrops seems to be easy to achieve given the presumed optical conditions are met, but real-time removal of adherent raindrops inevitably brings the trade-off of processing latencies regardless of the performance (Hamzeh and Rawashdeh, 2021).

#### 4.2. Fog

##### 4.2.1. Fog in point clouds

Fog plays a heavy role in the line of perception enhancement in adverse weather conditions, mainly due to two reasons. First, the rapid and advanced development of fog chamber test environments, and second, the fog format commonality of all kinds of weather including wet weather and haze and dust, in other words, the diminution of visibility in a relatively uniform way. Early in 2014, Pfennigbauer et al. (2014) brought up the idea of online waveform processing of range-finding in fog and dense smoke conditions. Different from the traditional mechanism of time-of-flight (TOF) LiDAR, their RIEGL VZ-1000 laser identifies the targets by the signatures of reflection properties (reflectivity and directivity), size, shape, and orientation with respect to the laser beam, which means, this echo-digitizing LiDAR system is capable of recording the waveform of the targets which makes it possible to identify the nature of the detected target, i.e. fog and dense smoke by recognizing their waveforms. Furthermore, since the rate

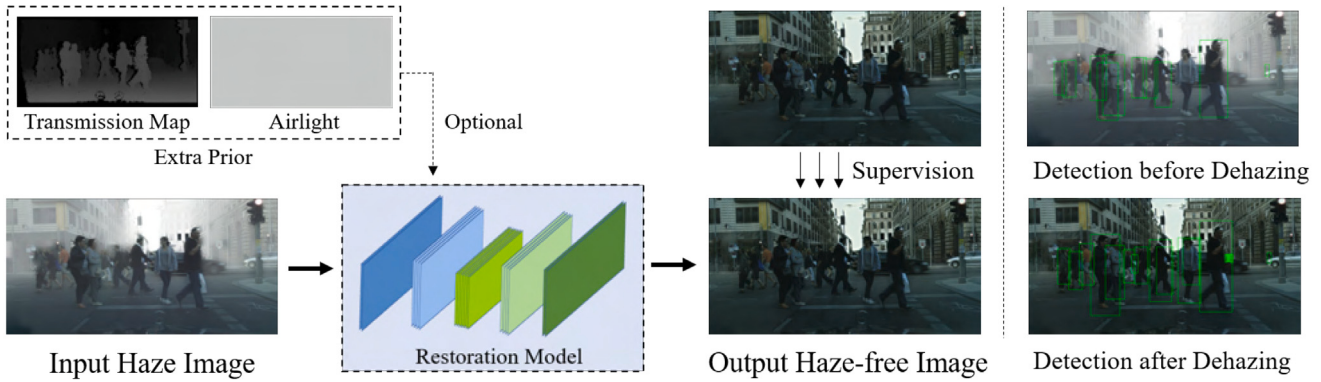


Fig. 10. Illustration of de-hazing methods based on atmospheric scattering model (Yang et al., 2022).

of amplitude decay caused by the fog follows a certain mathematical pattern with regard to the density of the fog, they realized visibility range classification and thusly were able to filter out false targets that do not belong in this range. Even though their experiments were confined within a critically close range (30 m), they paved a way for recovering targets hidden inside fog and smoke, regardless of the attenuation and scattering effects as long as the signal power stays above the designated floor level, because too low a visibility could block the detection almost entirely. Most importantly, the concept of waveform identification brought the multi-echo technique to the commercial LiDAR markets.

SICK AG company developed an HDDM+ (High Definition Distance Measurement Plus) technology (Theilig, 2021), which receives multiple echoes at a very high repetition rate. The uniqueness of the waveform of fog, rain, dust, snow, leaves, and fences are all recognizable to their MRS1000 3D LiDAR (SICK Sensor Intelligence, 2021) and the accuracy of object detection and measurement is largely guaranteed. They are also capable of setting a region of interest (ROI), whose boundaries are established based on max and min signal level and max and min detection distance. Such technology provides a very promising solution to the problem of agglomerate fog during heavy rain and other extremely low visibility conditions.

Wallace et al. (2020) explored the possibility of implementing Full Waveform LiDAR (FWL) in fog conditions. This system records a distribution of returned light energy, and thus can capture more information compared to discrete return LiDAR systems. They evaluated 3D depth images performance using FWL in a fog chamber at a 41 m distance. This type of LiDAR can be classified as a single-photon LiDAR and 1550 nm wavelength, which Tobin et al. (2021) also used to reconstruct the depth profile of moving objects through fog-like high-level obscurant at a distance up to 150 m. The high sensitivity and high-resolution depth profiling that single-photon LiDAR offers make it appealing in remote, complex, and highly scattering scenes. But this raises a question of 1550 nm wavelength and OPA manufacturing difficulties which we will discuss in Section 7.2.1.

Point cloud de-noising is a common approach and one of the typical works in fog is the CNN-based WeatherNet constructed by Heinzler et al. (2020). Their model trained from both fog chamber data and augmented road data is able to distinguish the clusters in point clouds caused by fog or rain and hence remove them with high accuracy. Lin and Wu (2021) implemented the nearest neighbor segmentation algorithm and Kalman filter on the point cloud with an improvement rate of less than 20% within the 2 m range. Shamsudin et al. (2016) proposed algorithms for fog elimination from 3D point clouds after detection. Clusters are separated using intensity and geometrical distribution and targeted and removed. The restriction is that their environment is an indoor laboratory and the algorithms are designed for building search and rescue robots whose working condition has too low a visibility to be adapted into outdoor driving scenarios where beam divergence and reflectance are significantly larger in the far field than in the near field.

#### 4.2.2. Fog in images

Due to the sensitivity of image collecting sensors to external environments, especially under hazy weather, outdoor images will experience serious degradation, such as blurring, low contrast, and color distortion (Narasimhan and Nayar, 2002). It is not helpful for feature extraction and has a negative effect on subsequent analysis. Therefore, image de-hazing has drawn extensive attention.

The purpose of image de-hazing is to remove the bad effects from adverse weather, enhance the contrast and saturation of the image and restore the useful features. In a word, estimating the clean image from the hazy input. Currently, existing methods can be divided into two categories. One is non-model enhancement methods based on image processing (Histogram Equalization Kim et al., 1998, Negative Correlation Gao et al., 2014, Homomorphic Filter Shen et al., 2014, Retinex Zhou and Zhou, 2013, etc.), another is image restoration methods based on atmospheric scattering model (Contrast Restoration Hautière et al., 2007, Human Interaction Narasimhan and Nayar, 2003, Online Geo-model, Polarization Filtering Schechner et al., 2001). Although the former can improve the contrast and highlight the texture details, it does not take into account the internal mechanism of the haze image. Therefore, the scene depth information is not effectively exploited and it can cause serious color distortion. The latter infers the corresponding haze-free image from the input according to the physical model of atmospheric scattering. Based on it, a haze model can be described as:

$$I(x) = J(x)t(x) - A(1 - t(x)) \quad (1)$$

where  $I(x)$  is the observed hazy image,  $J(x)$  is the scene radiance to be recovered.  $A$  and  $t(x)$  are the global atmospheric light and the transmission map, respectively. Consider the input  $I$  is an RGB color image, at each position, only the three intensity values are already known while  $J$ ,  $t$ , and  $A$  remain unknown. In general, the model itself is an ill-posed (He et al., 2010) problem which means its solution involves many unknown parameters (such as scene depth, atmospheric light, etc.). Therefore, many de-hazing methods will first attempt to compute one or two of these unknown parameters under some physics constraint and then put them together into a restoration model to get the haze-free image.

Until a few years ago, the single image de-hazing algorithm based on physical priors was still the focus. It usually predefines some constraints, prior or assumptions of the model parameters first, and then restores the clean image under the framework of atmospheric scattering model, such as contrast prior (Tan, 2008), airlight hypothesis (Tarel and Hautiere, 2009). However, deducing these physical priors requires professional knowledge and it is not always available when applied to different scenes. With the advance of deep learning theory, more and more researchers introduced this data-driven method into the field.

Chen et al. (2021) find that de-hazing models trained on synthetic images usually generalize poorly to real-world hazy images due to

the domain gap between synthetic and real data. They proposed a principled synthetic-to-real de-hazing (PSD) framework which includes two steps. First, a chosen de-hazing model backbone is pre-trained with synthetic data. Then, real hazy images are used to fine-tune the backbone in an unsupervised manner. The loss function of the unsupervised training is based on dark channel prior, bright channel prior and contrast limited adaptive histogram equalization.

Considering the problem that the existing deep learning-based de-hazing methods do not exploit hazy samples for supervision, Wu et al. (2021) proposed a novel ACER-Net, which can effectively generate high-quality haze-free images by contrastive regularization (CR) and highly compact autoencoder-like based de-hazing network. It defines a hazy image, whose corresponding restored image is generated by a de-hazing network and its clear image as negative, anchor and positive respectively. CR ensures that the restored image is pulled closer to the clear image and pushed away from the hazy image in the representation space. Zhang et al. (2021a) employ temporal redundancy from neighborhood hazy frames to perform video de-hazing. Authors collect a real-world video de-hazing dataset containing pairs of real hazy and corresponding haze-free videos. Besides, they propose a confidence-guided and improved deformable network (CG-IDN), in which a confidence-guided pre-de-hazing module and the cost volume can benefit the deformable alignment module by improving the accuracy of the estimated offsets.

Existing deep de-hazing models have such high computational complexity that makes them unsuitable for ultra-high-definition (UHD) images. Therefore, Zheng et al. (2021a) propose a multi-guide bilateral learning framework for 4K resolution image de-hazing. The framework consists of three deep CNNs, one for extracting haze-relevant features at a reduced resolution, one for learning multiple full-resolution guidance maps corresponding to the learned bilateral model, and the final one fuses the high-quality feature maps into a de-hazed image.

Recently in image de-hazing, an unpaired image-to-image translation that aims to map images from one domain to another come into focus. It gets boosted by generative adversarial networks (GAN) that have the ability to generate photorealistic images. CycleGAN (Zhu et al., 2017), DiscGAN (Kim et al., 2017), and DualGAN (Yi et al., 2017) are three pioneering methods, which introduce the cycle-consistency constraint to build the connection. Note that, this method does not require a one-to-one correspondence between source and target, which is more suitable for de-hazing. Because it is almost impossible to collect different weather conditions while keeping the background unchanged at the pixel level, considering that the atmospheric light changes all the time.

Engin et al. (2018) proposed Cycle-Dehaze which is an improved version of CycleGAN that combines cycle consistency and perceptual losses in order to improve the quality of textural information. Shao et al. (2020) proposed a domain adaptation paradigm that introduces an image translation module that translates haze images between the real and synthesis domain. Such methods are just getting started, and the results of de-hazing are often unsatisfactory (artifacts exist). But its feature does not require paired images to have the potential to build more robust models.

Although the field has approached maturity, the mainstream methods still use synthesis data to train models. Because collecting pairs of hazy and haze-free ground-truth images need to capture both images with identical scene radiance, which is almost impossible in real road scenes. Inevitably, the existing de-hazing quality metrics are restricted to non-reference image quality metrics (NRIQA) (Mittal et al., 2012). Recent works start to collect haze datasets utilizing a professional haze/fog generator that imitates the real conditions of haze scenes (Antutti et al., 2018), or multiple weather stacking architecture (Musat et al., 2021) which generates images with diverse weather conditions by adding, swapping out and combining components. Hopefully, this new trend could lead to more effective metrics and boost the existing algorithms to deploy on the ADS.

#### 4.2.3. GAN-based de-hazing model experimental evaluation

We did an evaluation on our own GAN-based model as shown in Fig. 10. Specifically, on the architecture of CycleGAN (Zhu et al., 2017), we added weather layer loss and spatial feature transform technique to disentangle hazy images from the front hazy layer, which keeps the background content in the de-hazing process to a maximum extent. The model is trained on Cityscapes (Cordts et al., 2016) and Foggy Cityscapes datasets (Sakaridis et al., 2018). After training the GAN-based de-hazing model, we first apply it to the hazy input. Then we use the state-of-the-art pedestrian detector in the CityScapes dataset to verify the significance of de-hazing. The results show that the amount of valid detection is increased after haze removal, especially the ones that are partially obscured in the back. For more details about this GAN-based de-hazing model, please refer to Yang et al. (2022).

### 4.3. Snow

#### 4.3.1. Snow covering

Perception of pertinent elements is difficult in snow due to the snow covering, which autonomous robots experienced in pathfinding. Yinka et al. (2014) proposed a drivable path detection system in 2014, aiming at extracting and removing the rain or snow in the visual input. They distinguish the drivable and non-drivable paths by their different RGB element values since the white color of snow is conspicuous compared to road surfaces, and then apply a filtering algorithm based on modeling the intensity value pixel of the image captured on a rainy or snowy day to achieve removal. Their output is in mono color condition and the evaluation based on 100 frames of road pictures shows close to 100% in pathfinding. Although the scenario is rather simple where only some snow is accumulated by the roadsides, this lays a good foundation for ADS when dealing with the same problem in snow conditions.

#### 4.3.2. Snowfall

The degradation of signal or image clarity caused by snowfall is one of the major issues of snow perception. The coping method once again returns to the de-noising technique, and many snow filters emerge for LiDAR point cloud. Charron et al. (2018) extensively explained the deficiency of 2D median filter and conventional radius outlier removal (ROR) before proposing their own dynamic radius outlier removal (DROR) filter. As snowfall is a dynamic process, only the data from the lasers pointing to the ground is suitable for a 2D median filter while it is not necessary from the beginning. The data are quite sparse in the vertical field of view above ground and the 2D filter could not handle the noise point removal and edge smoothing properties well. Hence 3D point cloud ROR filter is called for. 3D ROR filter iterates through each point in the point cloud and examines the contiguous points within a certain vicinity (search radius), and if the number of points found is less than the specified minimum ( $k_{min}$ ), then this point would be considered as noise and removed, which fits the pattern of snowfall where snowflakes are small individual solid objects. The problem is directly implementing this filter in the three-dimensional sense would cause the undesirable removal of points in the environment far away and compromise the LiDAR's perception ability in terms of precognition, as shown in Fig. 11(d). To prevent this problem, Charron's group applied the filter dynamically by setting the search radius of each point ( $SR_p$ ) according to their original geometric properties, as shown in Eq. (2), and successfully preserved the essential points in the point clouds far away from the center (6 m–18 m) while removing the salt and pepper noise near the center (within 6 m) in the point clouds with a precision improvement of nearly 4 times of normal ROR filters, as shown in Fig. 11(e).

$$SR_p = \beta_d(r_p\alpha) \quad (2)$$

$r_p$  is the range from the sensor to the point  $p$ ,  $\alpha$  is the horizontal angular resolution of the LiDAR, and the product of  $(r_p\alpha)$  represents point spacing, which is expected to be computed assuming that the laser

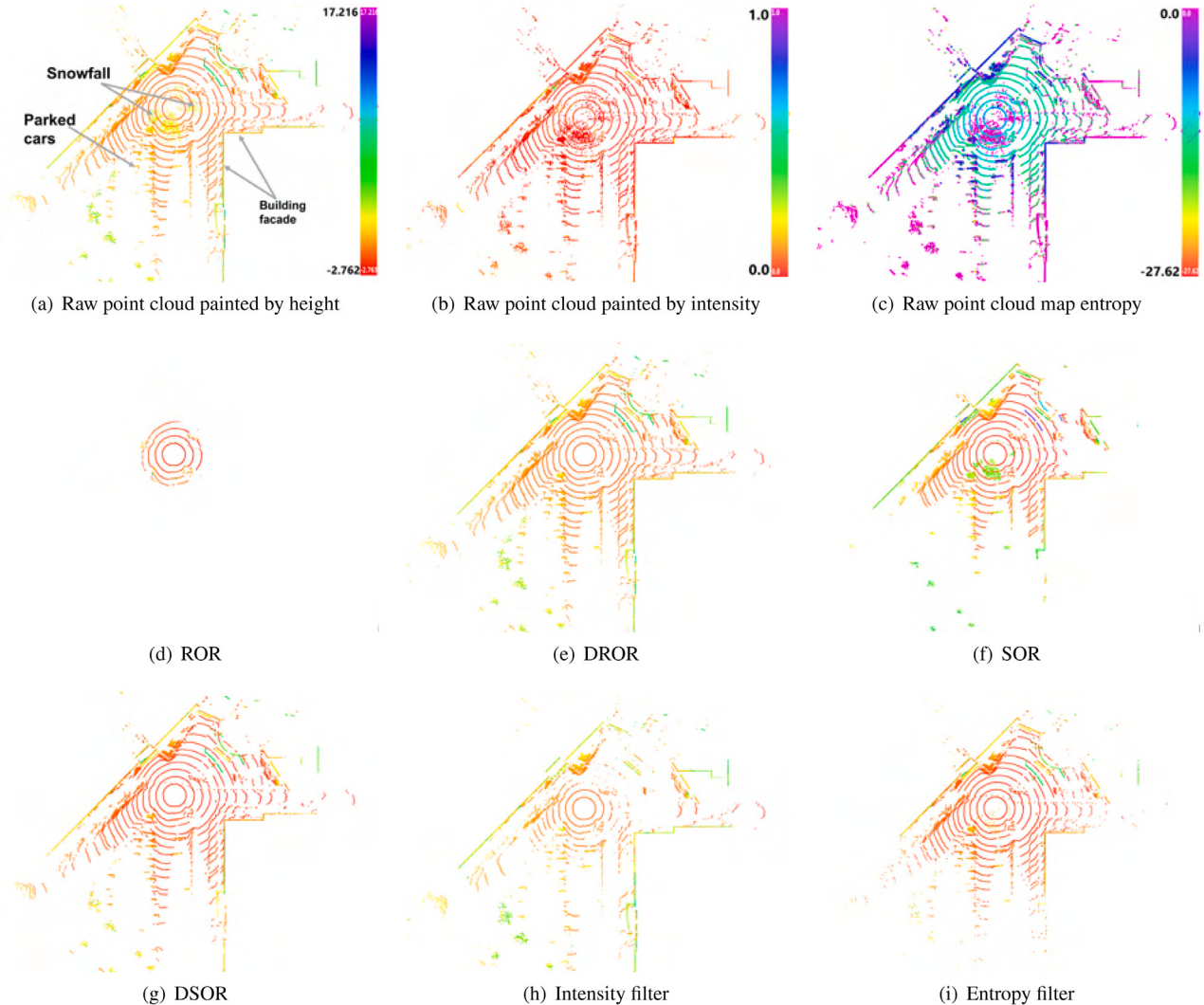


**Fig. 11.** Velodyne HDL-32 LiDAR point clouds in snowfall conditions with different de-noising methods, produced using Canadian adverse driving conditions (CADC) dataset (Pitropov et al., 2021). (a) Raw point cloud painted by height; (b) Raw point cloud painted by intensity; (c) Map entropy; (d) to (i) are painted by height (Z axis), and share the same color scale as (a). (For interpretation of the references to color in this figure legend, the reader is referred to the web version of this article.)

beam is reflecting off a perpendicular surface. So the multiplication factor  $\beta_d$  is meant to account for the increase in point spacing for surfaces that are not perpendicular to the LiDAR beams (Charron et al., 2018).

On the other hand, Park et al. (2020) proposed a low-intensity outlier removal (LIOR) filter based on the intensity difference between snow particles and real objects. It can also preserve important environmental features as the DROR filter does, but somehow maintain more points in the cloud than DROR because LIOR's threshold is more targeted based on the subject's optical properties. It could be an advantage in accuracy given the right circumstances. Advanced snow filters are still being developed (Wang et al., 2022).

The de-snowing technique for cameras works in a similar way as de-hazing. Zhang et al. (2021b) proposed a deep dense multi-scale network (DDMSNet) for snow removal. Snow is first processed by a coarse removal network with three modules, pre-processing module, a core module, and a post-processing module, each containing a different combination of dense block and convolutional layers. The output is a coarse result where the negative effect of falling snow is preliminarily eliminated and is fed to another network to acquire semantic and geometric labels. The DDMSNet learns from the semantic and geometry priors via self-attention and generates clean images without snow. The interesting part is that they use Photoshop to create large-scale snowy

images out of Cityscapes and KITTI datasets to do the evaluation. Despite the fact that this is indeed totally capable of performing state-of-art snow removal, it is still necessary to introduce advanced methods of simulating photo-realistic snow images.

Von Bernuth et al. (2019) simulated and evaluated snowflakes in three steps: first, reconstruct the 3D real-world scene with depth information in OpenGL; then snowflakes are distributed into the scene following physical and meteorological principles, including the motion blur that comes from wind, gravitation or the speed of vehicle displacement; finally, OpenGL renders the snowflakes in the realistic images. The depth information is critical for reconstructing the scene, so the images are either gathered from stereo cameras or other sensors in the real world like the two datasets mentioned above, or from simulators like Vires VTD or CARLA whose depth information is perfectly quantifiable. The snowflakes have two forms: flat crystal as if in 2D, and thick aggregated flakes constructed by three pairwise perpendicular quads in 3D, which ensure the synthetic snow looks like reality as closely as possible. A comparison of such methods of snow generating shows a stunning resemblance with real-world snowy images. No doubt that de-noising with synthetic snowy and foggy images can help the machine learning process and benefit camera perception enhancement in adverse weather conditions to a great extent.

#### 4.3.3. Point cloud de-snowing validations

In this section, we present experimental validations on some common point cloud de-snowing filters including the ROR and DROR from above and an entropy filter we proposed by ourselves. In addition to Figs. 11(d) and 11(e) we produced for illustration, we also present the raw point cloud in height and intensity scale, and an intensity filter; the map entropy of the raw point cloud and an entropy filter; as well as testing and validating SOR and DSOR filters in Fig. 11, as comparisons for better references. All the validations are based on a scene captured from the Canadian adverse driving conditions (CADC) dataset (Pitropov et al., 2021) where buildings, trees, and parked cars are widely present, as shown in Fig. 11(a).

Fig. 11(f) shows the Statistical Outlier Removal Filter (SOR), which removes any point whose mean distance to its  $k$  nearest neighbors exceeds the threshold when iterating each point. The threshold  $T$  for filtering is computed as:

$$T = \mu + \sigma\beta_s \quad (3)$$

where  $\mu$  is the global mean of the distances from all points to their  $k$  nearest neighbors;  $\sigma$  is the global standard deviation of the distances; and  $\beta_s$  is a specified multiplier parameter. Fig. 11(f) is acquired with the selection of  $k = 50$  and  $\beta_s = 0.3$ . The selection of  $k$  is the consideration of the approximate points number of an average actual object's points cluster based on the signal density of the Velodyne HDL-32E LiDAR used. Too big a  $k$  value makes a certain point's mean distance to its  $k$  neighbors inappropriately large, which could result in falsely accusing this point as snow, and vice versa. The rise of  $\beta_s$  results in the rise in threshold  $T$ , which makes the filter's tolerance higher, ending up in a weaker ability to remove snow points. On the other hand, too small a  $\beta_s$  makes the filter remove more non-snow points.  $\beta_s = 0.3$  is a middling choice. It can be seen that ROR's flaw has been largely improved but at the cost of de-noising performance.

With Dynamic Statistical Outlier Removal (DSOR), as shown in Fig. 11(g), the advantages of DROR and SOR are combined, i.e. the filter threshold of SOR is dynamically changed with range (Kurup and Bos, 2021). The dynamic threshold  $T_d$  is set by:

$$T_d = r(Tr_p) \quad (4)$$

where  $T$  is from Eq. (3) and  $r_p$  is the distance of every point from the sensor, same as in Eq. (2).  $r = 0.05$  serves as a multiplicative factor for point spacing. Larger  $r$  leads to a milder filter. It turns out the performance is no less than DROR in both de-noising and preserving environmental features, and even faster in terms of computing.

Fig. 11(h) is a direct intensity filter where all the points with intensity values outside of the interval of [0.03, 0.15] are filtered out (intensity varies from [0,1]). This interval is set based on several trial-and-error attempts. It can be seen that the result is somehow acceptable but the problem is how to determine the exact interval in different scenes that can both filter out snowfall and keep objects. Therefore, the practical use of the intensity filter is limited.

Fig. 11(c) shows the entropy representation of the original raw point cloud scene. The entropy  $h$  of a certain point  $q_k$  in the point cloud is computed by:

$$h(q_k) = \frac{1}{2} \ln |2\pi e \Sigma(q_k)| \quad (5)$$

in which  $\Sigma(q_k)$  is the sample covariance of mapped points in a local radius  $r$  ( $r = 0.25$  m in our case) around  $q_k$ . When  $r$  is high, the entropy of a certain point is likely to increase due to the weak correlation with neighbor points. Fig. 11(i) is the result after the solitary points (points with less than 15 neighbors) with high entropy being filtered out (Razlaw et al., 2015). As we can see, when the snowfall is very dense, the entropy filter is still having trouble filtering them all.

#### 4.4. Light related influences

##### 4.4.1. Strong light and glare

Notwithstanding the severe influences of strong light and glare on AV, there is very limited literature specifically targeting the solution to light-related problems. Back in 2014, Maddern et al. (2014) studied the effect on an AV caused by light condition changes during the 24 h of a day, and managed to improve the performance and robustness of vision-based autonomous driving by implementing illumination invariant transform, which removed almost all variation due to sunlight intensity, direction, spectrum and shadow present in the raw RGB images. Commonly the idea is to count on the redundancies and robustness of certain fusion modalities that are equipped with sensors agnostic to strong light.

Yahiaoui et al. (2020) developed their own sunshine glare dataset in autonomous driving called WoodScape, including situations like direct sunlight in the sky or sun glares on dry roads, road marks being wiped off by sun glares on wet roads, sun glares on reflective surfaces, etc. The glare is detected by an image processing algorithm with several processing blocks including color conversion, adaptive thresholding, geometric filters, and blob detection, and trained with CNN network.

##### 4.4.2. Reflections and shadows

Glare and strong light might not be removed easily, but reflections in similar conditions are relatively removable with the help of the absorption effect (Zheng et al., 2021b), reflection-free flash-only cues (Lei and Chen, 2021), and photo exposure correction (Afifi et al., 2021) techniques in the computer vision area. The principle follows reflection alignment and transmission recovery and it could relieve the ambiguity of the images well, especially in panoramic images which are commonly used in ADS (Hong et al., 2021). It is limited to recognizable reflections and fails in extremely strong lights where image content knowledge is not available. A special reflection is the mirage effect on hot roads. It has a weakness: the high-temperature area on the road is fixed and that fits the feature of a horizon which could be confusing (Young, 2015). Kumar et al. (2019) implemented horizon detection and depth estimation methods and managed to mark out a mirage in a video. The lack of mirage effects in datasets makes it hard to validate the real accuracy.

The same principle applies to shadow conditions as well, where the original image element is intact with a little low brightness in certain regions (Fu et al., 2021). Such image processing uses similar computer vision techniques as in previous paragraphs and can also take the route of first generating shadows and then removing them (Liu et al., 2021b). The Retinex algorithm can also be used for image enhancement in low-light conditions (Pham et al., 2020b).

##### 4.4.3. Thermal imaging validations

In order to show the superiority of thermal imaging over normal RGB cameras, especially in adverse light conditions such as the strong light condition, we did some validations of a couple of thermal imaging enhancement algorithms based on the same scene in Fig. 4.

We can see from Fig. 12 that under direct strong light the highlighted objects were detected at 40 m from the Xenon light source when illuminance is maximum (200 klx) but in all cases, there are not enough measurement points to achieve recognition, but the thermal camera still remains part of the abilities to distinguish the rectangle board beneath the light source which normal camera could not. In addition, we applied multiscale retinex transformation (Petro et al., 2014), and the parvo cellular representation of a bio-inspired retina method (Benoit et al., 2010) to the thermal image to enhance perception. The multi-scale retinex transformation has the ability of image color restoration and contrast enhancement, while the parvo cellular retina model provides accurate structuring of video data by noise and illumination variant removal and static and dynamic contour enhancement.

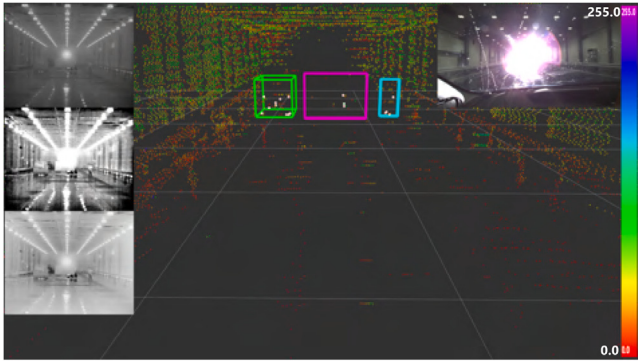


**Fig. 12.** Strong light affects negatively the LiDAR data (point cloud colored by intensity) and the RGB camera image (top right inset). In the experiment, the vehicle is located 40 m from the Xenon light source with a peak illuminance of 200 klx. Objects are barely detected: four 3D points for the mannequin (cyan box), three points for the reflective targets (magenta box), and ten points for the black vehicle (green box), classification is not possible. However, the thermal camera is resilient to illumination and the objects are clearly discernible (top left inset). Multiscale retinex transformation (left middle inset). Parvo cellular representation of a bio-inspired retina method (left bottom inset). (For interpretation of the references to color in this figure legend, the reader is referred to the web version of this article.)

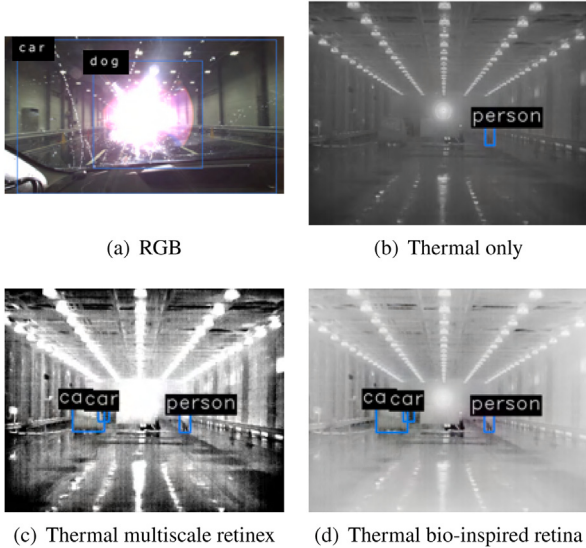


**Fig. 13.** Object classification results using YOLO3 on RGB and thermal camera images with strong light. (a) RGB camera; (b) thermal; (c) multiscale retinex enhancement; (d) bio-inspired retina enhancement.

Furthermore, we tested and compared the YOLO3 (Redmon and Farhadi, 2018) object classification results in Fig. 13 among the RGB camera and each one of the thermal imaging from above. Three objects are defined: person (the mannequin), car 1 (the vehicle in front), and car 2 (the vehicle at the back). 10 s of camera frames were analyzed while the car approached the strong light source. It can be seen from Fig. 13(a), that a normal visible camera is almost blinded and the light source halo is recognized as “dog”. The recall rates are all zero for the three classes. In Fig. 13(b), partial ability is regained where the person can be recognized but not the cars from behind. The recall rates are only 44.3%, 0%, and 60% respectively for the three classes. Multiscale retinex enhancement and bio-inspired retinex enhancement successfully captured all three elements with good accuracy. Multiscale retinex (Petro et al., 2014) enhancement (Fig. 13(c)) has recall rates of 58.6%, 30% and 62.9% respectively; and bio-inspired retina (Benoit et al., 2010) enhancement (Fig. 13(d)) has 67.1%, 45% and 78.6% respectively.

#### 4.5. Contamination

As we summarized in Table 1, contamination influences the perception of ADS sensors in a fierce way, as shown in the contamination effect on the backup camera in Fig. 14. As a result, the robustness and adaptability of the system are facing a rigorous test. Uřičář et al. (2021) created a dataset called SoilingNet having both opaque and transparent soiling (Uřičář et al., 2019), and developed a GAN-based data augmentation for camera lens soiling detection in autonomous driving. Different from rain or snow, the general soiling is normally considered opaque or semi-transparent, so a complementary sensing method might not be able to perform with enough accuracy. Once again, artificial generations of soiling image are relied on because of the near-impossibility of acquiring both soiled images and clean images with paired backgrounds under real driving conditions. The CycleGAN network would generate an image with a random soiling pattern, which provides a blurred mask obtained from the semantic segmentation network applied with a Gaussian smoothing filter on the generated soiled image, and finally, the synthetic version of the soiled image is composed with the original image and the soiled pattern estimated via the mask. The degree of similarity is very close to the real soiled effect shown in Fig. 14(c). The only problem is that CycleGAN does not have the restraint on soiling a designed region of the image but transforms the whole image, so they apply restrictions on the mask area only and modify the network to a new DirtyGAN. Furthermore, they used this DirtyGAN to generate a Dirty dataset based on their previous dataset WoodScape (Yahiaoui et al., 2020) and the degradation evaluation based on the Cityscapes dataset is proven well. Although the removal or interpretation of the soiled image was not discussed in this work, it sure provides a possibility of the same training approach as de-hazing and de-noising.

Trierweiler et al. (2020) made an automatic control over the wiper and nozzle based on the detection of the total internal reflection on the windshield. Due to the difference in reflectivity and intensity distribution between liquid, like raindrops, and solid, like dust, they are able to differentiate the physical status of the pollution on the cover glass of the ADS sensors by splitting the out-coupled intensity from the red light diffuser into two sections. Compared to current rain sensors who can only trigger wipers, this model knows whether it is necessary to trigger the nozzle to clean up the pollution. One concern is that the windshield of a car might not maintain a uniform curvature everywhere, so the practicability of the installation of such a detection device and its operation consistency remains challenged.

### 5. Classification and localization algorithms in adverse weather

Beyond object recognition purposes, the integrity of an ego vehicle’s sensing ability to surrounding conditions is equally critical, including the ego vehicle’s position and its surrounding conditions. In this section, we will introduce sensing enhancement methods in classification tasks and localization tasks under adverse weather conditions.

#### 5.1. Classifications

##### 5.1.1. Weather classification

Perception enhancement fundamentally enables ADS to navigate through various inclement weather conditions, but it mainly focuses on how to ignore the interference or compensate for the negative effects. At some point, it is also important to do weather classification as a way to sense the surrounding conditions. At first, weather classification was limited to binary weather classification like distinguishing clear or not (Lu et al., 2014) on single images. Further machine learning techniques like kernel learning achieved multi-class weather classifications including sunny, rain, fog, and static snow. At this stage, the classification task is realized by setting classifiers with the unique features of each kind of weather. Sunny features come from the clear



**Fig. 14.** Contamination effect on a Cadillac XT5 back-up camera. The mud contamination is formed naturally from off-road driving after rain. Vehicle testing and images courtesy of Mr. Dawei Wang, Pan Asia Technical Automotive Center Co., Ltd.<sup>4</sup> (For interpretation of the references to color in this figure legend, the reader is referred to the web version of this article.)

sky region of a picture and form a highly multi-dimensional feature vector; when sky elements are not included in the picture, a strong shadow region with confident boundaries becomes the indicator of sunny conditions. Rain streak is hard to capture in images so HOG features are extracted from the image to be the rain feature vector. Falling snow is considered noise, while pixels with certain gray levels are defined as snowflakes. Haze is determined by dark channels, where some pixels have very low intensities in at least one color channel which is the dark channel (Zhang and Ma, 2015). With the development in AI technologies, machine learning neural networks such as deep CNN are used by Elhoseiny et al. (2015) in this task to enhance feature extraction and learning performance.

In meteorology, rain is observed and measured by weather radar and stationary rain gauges. Considering carrying a weather station on a car like (Bijelic et al., 2020) is not practical for commercial generalization, people started in an early stage to realize vehicle-based binary (wet/dry) precipitation observations (Haberlandt and Sester, 2010; Hill, 2015). Karlsson et al. did an estimation on the real-time rainfall rate out of automotive LiDAR point cloud under both static and dynamic conditions in a weather chamber using probabilistic methods (Karlsson et al., 2021). Goodin et al. (2019) tried to establish the relationship between the two parameters: rain rate, as manifested by the rain scattering coefficient, and the max range of the LiDAR sensor for a 90% reflective target in clear conditions, and successfully generated a quantitative equation between rain rate and sensor performance. Bartos et al. (2019) raised the idea of producing high-accuracy rainfall maps using windshield wipers measurement on connected vehicles in 2019. It is a very leading concept considering the network of connected vehicles has not been constructed on a large scale. Simply the status (on/off) of windshield wipers serves as the perfect indicator of binary rainfall state compared to traditional sensing methods like rain gauges. This work is supposed to help city flash flood warnings and facilitate stormwater infrastructure's real-time operation, but the involvement of cars provides a line of thought on vehicle-based rain sensing.

Al-Haija et al. (2020) came up with a powerful ResNet-18 CNN network including a transfer learning technique to do multi-class weather classification based on the pre-training of multi-class weather recognition on the ImageNet dataset. However, the class set in this network is still restricted to sunrise, shine, rain, and cloudy, whose impacts on ADS are limited. Dhananjaya et al. (2021) tested the ResNet-18 network on their own weather and light level (bright, moderate, and low) dataset and achieved a rather low accuracy, suggesting improvement room on weather classification in images. In order to better suit autonomous driving purposes, fine-sorted and precise classification is needed, with the possibility of going beyond camera images only.

Heinzler et al. (2019) achieved a pretty fine weather classification with a multi-echo LiDAR sensor only. The point cloud is firstly

transformed into a grid matrix and the presence of rain or fog can be easily noticed by the occurrence of secondary echoes on objects. Then, different from recording the echoes of each kind of condition, the mean distance of each echo and their mathematical properties like variance are used for detailed classification as the covariance matrices are influenced by different levels of rain or fog and the change in the point cloud or to say the matrix is visible. Nearest Neighbor classifier (kNN) and a Support Vector Machine (SVM) are applied as classifiers and rain classification is largely improved. It can be imagined that the test result might not be as good when using a LiDAR sensor with a smaller vertical FOV due to the insufficient number of points and also in dynamic scenarios compared to static scenes. That means this method still has its reliance on controlled environments and the robustness might not meet level 4 or higher autonomy requirements.

Dannheim et al. (2014) proposed to use the fusion data from both LiDAR and camera to do weather classification several years before. Their main classifier was based on the intensity difference generated by the backscattering effect of rain and fog and no neural network was mentioned in their image processing. From the author's point of view, combining both advanced image detection and LiDAR data processing mentioned above to realize fine weather classification could be worth exploring.

### 5.1.2. Visibility classification

The term visibility was initially referred to as the subjective estimation of human observers. In order to measure the meteorological quantity, or to say the transparency of the atmosphere, the meteorological optical range (MOR) (Dunlop, 2008) is defined objectively. In the context of autonomous driving, when visibility is quantified as specific numbers, it normally means MOR. For example, each distinct version of fog scenarios in the Foggy Cityscapes (Sakaridis et al., 2018) dataset is characterized by a constant MOR. As weather conditions often bring visibility degradation of different levels, it is helpful to gain awareness of visibility dropping to avoid detection errors and collisions in advance. It is possible to estimate the visibility range in foggy conditions by profiling the LiDAR signal backscattering effect caused by the tiny droplets, but as mentioned in the previous context, it requires extremely fine-tuned LiDAR power to adapt to the fickle variables. Currently, visibility classification largely relies on camera-based methods with neural networks (Chaabani et al., 2017) and is divided by range classes with intervals of dozens of meters while seldom giving exact pixel-wise visibility values (You et al., 2021). Considering the low cost and the irreplaceable status of cameras in ADS, it is also well-researched.

Chaabani et al. (2017) initially used a neural network with only three layers: feature vector image descriptor as input, a set of fully interconnected computational nodes as a hidden layer, and a vector corresponding to the visibility range classes as output. They used the FROSI (Foggy ROad Sign Images) synthetic dataset (Belaroussi and Gruyer, 2014; Pavlić et al., 2012) for evaluation and were able to classify the visibility from below 60 m to larger than 250 m with

<sup>4</sup> <http://www.patac.com.cn/EN/about.html>.

a spacing of 50 m. They later improved such a network with the combination of deep learning CNN for feature extraction and an SVM classifier (Chaabani et al., 2018). The new network used the AlexNet architecture (Krizhevsky et al., 2012), and the overall recall, precision, and accuracy all reached the state-of-art level and can be used on not only car on-board cameras but roadside cameras which shows further potential in future IoT (Internet of Things) systems.

Duddu et al. (2020) proposed a novel fog visibility range estimation algorithm for autonomous driving applications based on a hybrid neural network. Their input consists of Shannon entropy (Shannon, 1948) and image-based features. Each image captured by the 50-degree-FOV camera is divided into 32 by 32 pixel blocks and the Shannon entropy of each block is calculated and then mapped to corresponding image features extracted from a series of convolutional layers along with maxpool layers, which output three visibility classes: 0–50 m, 50–150 m, and above 150 m. They created their own fog dataset with BOSCH range finder equipment as ground truth to establish the network architecture and the synthetic dataset FORSI is used for public benchmarking. The overall accuracy reached 85% and higher. There are also other similar models like the feed-forward back-propagation neural network (BPNN) (Vaibhav et al., 2020) using data collected from weather monitoring stations as input that can predict the visibility ranges with much smaller spacing at a road-link level. It is unclear whether mobile weather stations equipped on cars are capable of completing visibility classification in real time, but sophisticated sensor fusion could be necessary for conditions beyond fog like snow and rain.

As a matter of fact, there is a correlation between weather and visibility in climatology, and research has been done about the correspondence between how far a driver can see and precipitation rates (Gultepe, 2008), but often at a rather long range (kilometers level) which is not very close to the current AV's visual concern. Miclea et al. (2020) came up with a creative way by setting up a 3-meter-long model chamber with a “toy” road and model cars in it which can be easily filled with almost-homogeneous fog. They successfully identified the correlations between the decrease in optical power and the decrease in visual acuity in a scaling fog condition. Furthermore, Yang et al. (2021) managed to provide a promising prediction of a 903 nm NIR LiDAR's minimum visibility in a fog chamber by determining whether the detecting range of an object with a known distance is true or noisy. In our opinion, sharp visibility declines mostly come from the water screen and unstable mists during wet weather and sometimes do not depend on precipitation rates only. So, the binary condition of visibility safety might have more value than the exact measurement in practical uses.

### 5.1.3. Road surface condition classification

Instant road surface condition changes are direct results of weather conditions, especially wet weather. The information on road conditions can sometimes be an alternative to weather classification. According to the research of Kordani et al. (2018) that at the speed of 80 km/h, the road friction coefficient of rainy, snowy, and icy road surface conditions are 0.4, 0.28 and 0.18 respectively, while average dry road friction coefficient is about 0.7. The dry or wet conditions can be determined in various ways besides road friction or environmental sensors (Shibata et al., 2020). Šabanović et al. (2020) build a vision-based DNN to estimate the road friction coefficient because dry, slippery, slurry, and icy surfaces with decreasing friction can basically be identified as clear, rain, snow, and freezing weather correspondingly. Their algorithm detects not only the wet conditions but is able to classify the combination of wet conditions and pavement types as well. Panhuber et al. (2016) mounted a mono camera behind the windshield and observed the spray of water or dust caused by the leading car and the bird-view of the road features in the surroundings. They determine the road surface's wet or dry condition by analyzing multiple regions of interest with different classifiers in order to merge into a robust result of 86% accuracy.

Road surface detection can also be performed in an uncommon way: audio. The sounds of vehicle speed, tire-surface interactions, and noise under different road conditions or different levels of wetness could be unique, so it is reasonable for Abdić et al. (2016) to train a deep learning network with over 780,000 bins of audio, including low speed when sounds are weak, even at 0 speed because it can detect the sound made by other driving-by vehicles. There are concerns about the vehicle type or tire type's effects on the universality of such a method and the uncertain difficulty degree of the installation of sound collecting devices on vehicles.

## 5.2. Localization and mapping

The awareness of an ego vehicle's own location is as important as knowing other elements' locations in the surrounding environment. In terms of autonomous driving, localization is the sensing of an AV about its ego-position relative to a frame of reference in a given environment (Kuutti et al., 2018). The most common methods currently involved in localization are the Global Positioning System and Inertial Measurement Unit (GPS-IMU), SLAM, and state-of-the-art a-priori map-based localization, which largely relies on the successful detection of certain elements in the surrounding environments and their robustness in weather conditions is of concern. SAR image based road extraction from remote sensing is almost agnostic to weather conditions (Chen et al., 2022) and robust road information segmentation from aerial imagery delivers high-quality HD maps (Fischer et al., 2018). These have laid good foundations to the localization task for autonomous driving in bad weather and helped the development of adverse weather models.

### 5.2.1. Simultaneous localization and mapping

The same-time online map making and localization method are widely deployed in robotics and the change of feature descriptors across seasons compromises SLAM's accuracy. Besides season changing, weather-induced effects including tree foliage falling and growing and snow-covered ground are also part of the reasons. To address the robustness problem of SLAM, Milford and Wyeth (2012) proposed to recognize coherent navigation sequences instead of matching one single image and brought the SeqSLAM as one of the early improvements of SLAM in light, weather, and seasonal changes conditions. SeqSLAM has a weakness of assuming well alignment in different runs which could result in poor performance with uncropped images or different frame rates. Naseer et al. (2015) took it to a further step by first using deep convolutional neural network (DCNN) to extract global image feature descriptors from both given sequences, then leveraging sequential information over a similarity matrix, and finally computing matching hypotheses between sequences to realize the detection of loop closure in datasets from different seasons.

Wenzel et al. (2021) collected data in several European cities under a variety of weather and illumination conditions and presented a Cross-Season Dataset for Multi-Weather SLAM called 4Seasons. They showed centimeter-level accuracy in reference poses and also highly accurate cross-sequence correspondences, on the condition of good GNSS receptions.

Similar to sensor fusion, extra modalities are also enlisted to help localization. Brunner et al. (2013) combined visual and infrared imaging in a traditional SLAM algorithm to do the job. They evaluate the data quality from each sensor first and dispose of the bad ones which might induce errors before combining the data. The principle of introducing thermal cameras here is almost the same as discussed before, only for localization purposes here particularly. Their uniqueness is that they not only tested the modality in low visibility conditions, like dusk or sudden artificial strong light but also tested in the presence of smoke, fire, and extreme heat, which saturate the infrared cameras. There is no guarantee that the flawed data have no weight in the algorithm at all but the combination definitely reduces the error rate compared to



**Fig. 15.** Down-pointing arrow marking the edges of the road covered by snow in Hokkaido, Japan. Image courtesy of Dr. Atsushi Nishimura of Snow and Ice Research Team of CERI (Civil Engineering Research Institute of Cold Region Snow and Ice Reaserch Team, 2021).<sup>5</sup>

a single sensor modality. Their method makes the best of each sensor's strength in adverse conditions.

As robust as visual SLAM may have become, the map's insufficiency in necessary information agnostic to appearance changes is still one of the major problems of SLAM. The localization drift over time and the lack of viability of the map in every driving condition also hinder SLAM from navigating for long distances, which makes it less competitive compared to pre-built map-based localization in autonomous driving (Bresson et al., 2017).

#### 5.2.2. A-priori map

When the elements used for normal localization such as the lane lines, curbs, road barriers, and other landmarks are partially or completely unavailable at the moment, vehicles' localization both in the traveling direction and lateral direction perpendicular to the traveling motion would be hard.

The reference pre-built map that is used for comparing and matching the online readings for localization purposes is called the a-priori map, which is currently the main force in ADS localization. A key method in the assurance of the accuracy of a-priori map-based point cloud matching is landmark searching. A typical example of how humans deal with low certainty localization is the snow pole "Yabane" (down-pointing arrow on a pole) in Hokkaido, Japan, as shown in Fig. 15. The arrows point to the edge of the road and are either flashing or light reflective at night, so this gives the driver a rough idea about their relative position on the road and keeps them from wandering and away from the curb. This concept is important because the occlusion caused by accumulated snow has much more impact on localization than snow precipitation (Baril et al., 2021).

Correspondingly, the idea of fixed landmark searching in AV localization emerges as time requires, similar to the way of robots and AGVs (Automatic Guided Vehicles) reading RFID tags by the route checkpoints in controlled environments and ODDs (Operational Design Domains) to navigate (Hahnel et al., 2004; Roehrig et al., 2014). Enterprises like Ford work closely with companies major in detailed 3D a-priori maps, and their automated sedan would seek for markers such as stop signs or other signposts by the roadsides with either camera or LiDAR when roads are covered by snow or water, and would sense its ego-position by calculating its relative distance against those markers in the a-priori map (Ford Motor Company, 2021). This gives AVs the

ability to locate themselves as accurately as in centimeters with no extra hardware cost even in adverse conditions. However, the potential cost and difficulty lie in the constant updating and maintenance of the a-priori map and that is also what the map companies are working on, towards a more intelligent and efficient system.

Sensible4 uses a LiDAR-based volumetric probabilistic distribution (Sauliala, 2021) approach for mapping and localization in all-weathers, which reduces the amount of information and details in the map, and instead captures the distribution of patches of the surface (surfels). They create such maps from year-long LiDAR data, therefore the common elements of the road are modeled regardless of the season.

Aldibaja et al. (2021) described the general reasons for lateral localization drifting by converting map images into edge profiles to represent the road marks in a series of LiDAR signal reflectivity peaks. Accumulated snow on the roadside creates sharp intensity peaks with irregular distribution for LiDARs while wet elements from snow-rain weather leave a track of line with low reflectivity on the road. The wearings of old roads and vegetation whose branches reach into the road space also create anomalies sometimes. These confuse the LiDAR about the actual whereabouts of the lane lines and the boundaries of the road area which leads to wrong lateral movements. Aldibaja's group proposed to use the Principal Component Analysis (PCA) method to extract dominant edge profile distribution patterns and eliminate the "fake" lane lines via edge profile matching (Aldibaja et al., 2016, 2017). Also by patching the missing LiDAR elements based on leading eigenvectors (eigenroads), a reliable LiDAR profile was reconstructed. The error in the lateral movement was reduced to 15 cm with a localization accuracy of 96.4% in critical environments (Aldibaja et al., 2021).

Cornick et al. (2016) created a new map-based localization called Localized Ground-Penetrating RADAR (LGPR). As the name implied, their system mounted at the under-frame of a car sends electromagnetic pulses toward the ground and measures the unique reflection profiles from under the surface. With highly efficient process units matching the identifiers with registration data, they manage to acquire the precise location of an ego vehicle up to the speed of highway standards (at least 100 km/h). Different from common automotive radar, this system uses 100 MHz to 400 MHz radar with the ability in operating under all kinds of rough environments. Not only does it achieve at least equal or better accuracy than traditional localization methods, but it also shows a great advantage in navigating water puddles or snowdrifts. It does have limitations though. When the saturation of soil reaches a certain level of around 30%, the attenuation it caused for radar at their operating range could reach 10 dB/m (Hoekstra and Delaney, 1974). Also, margins have been reserved because snow melting salt attenuates the RF signal severely.

Multi-sensory place recognition is proven to be more robust (Żywaniowski et al., 2020). The radar extension of the Oxford Robotcar dataset (Barnes et al., 2020) used only Navtech radar to accomplish map building and localization in rain and snow, thanks to radar's specialty in harsh weather. Wolcott and Eustice (2017) developed a robust LiDAR localization using multi-resolution Gaussian mixture maps. They discretized the point cloud into grids of 2D and expand Gaussian mixture distribution on the height direction. This helps compress point clouds into 2.5D maps with parametric representations. They demonstrated the ability to navigate in all kinds of road texture conditions including constructions, and during harsh weather like snow. While their tests showed a small increase of root square mean (RSM) error in normal downtown conditions compared to traditional reflectivity-based localization, they did decrease the RSM error rate by around 80% on both lateral and longitudinal sides in snowy conditions (Wolcott and Eustice, 2015).

<sup>5</sup> <https://www.ceri.go.jp/index.html>.

**Table 3**

Coverage of weather conditions in common autonomous driving datasets.

Dataset	Synthesis	Rain	Fog/Haze/ Smog	Snow	Strong light/ Contamination	Night	Sensors
LIBRE (Carballo et al., 2020)	–	✓	✓	–	✓Strong light	–	10 LiDARs, Camera, IMU, GNSS, CAN, 360° 4K cam, Event cam, Infrared cam
Foggy Cityscape (Sakaridis et al., 2018)	✓	–	✓	–	–	–	–
CADCD (Pitropov et al., 2021)	–	–	–	✓	–	–	1 LiDAR, 8 Cameras, GNSS, IMU
Berkley DeepDrive (Yu et al., 2020)	–	✓	✓	✓	–	✓	Cameras
Mapillary (Neuhold et al., 2017)	–	✓	✓	✓	–	✓	Mobile phones, Tablets, Action cameras, Professional capturing rigs
EuroCity (Braun et al., 2019)	–	✓	✓	✓	–	✓	2 Cameras
Oxford RobotCar (Maddern et al., 2017)	–	✓	–	✓	–	✓	3 LiDARs, 3 Cameras, Stereo cam, GPS (Radar extension: 360° radar)
nuScenes (Caesar et al., 2020)	–	✓	–	–	–	✓	1 LiDAR, 6 Cameras, 5 Radars, GNSS, IMU
D2-City (Che et al., 2019)	–	✓	✓	✓	✓Contamination	–	Dashcams
DDD17 (Binias et al., 2017)	–	✓	–	–	–	✓	Dynamic and active-pixel vision camera
Argoverse (Chang et al., 2019)	–	✓	–	–	–	✓	2 LiDARs, 7 Cameras ring, 2 Stereo cameras, GNSS
Waymo Open (Sun et al., 2020)	–	✓	–	–	–	✓	5 LiDARs, 5 Cameras
A*3D (Pham et al., 2020a)	–	✓	–	–	–	✓	1 LiDAR, 2 Cameras
Snowy Driving (Lei et al., 2020)	–	–	–	✓	–	–	Dashcams
ApolloScape (Huang et al., 2019)	–	✓	–	–	✓Strong light	✓	2 LiDARs, Depth Images, GPS/IMU
SYNTHIA (Ros et al., 2016)	✓	–	–	✓	–	–	–
P.F.B (Richter et al., 2017)	✓	✓	–	✓	–	✓	–
ALSD (Liu et al., 2020)	✓	✓	–	✓	–	✓	–
ACDC (Sakaridis et al., 2021)	–	✓	✓	✓	–	✓	1 Camera
NCLT (Carlevaris-Bianco et al., 2016)	–	–	–	✓	–	–	2 LiDARs, 1 Camera, GPS, IMU
4Seasons (Wenzel et al., 2021)	–	✓	–	–	–	✓	1 Stereo Camera, GNSS, IMU
Raincouver (Tung et al., 2017)	–	✓	–	–	–	✓	Dashcam
WildDash (Zendel et al., 2018)	–	✓	✓	✓	–	✓	Cameras
KAIST multispectral (Choi et al., 2018)	–	–	–	–	✓Strong light	✓	1 LiDAR, 2 Cameras, 1 Thermal (infrared) cam, IMU, GNSS
DENSE (Bijelic et al., 2020)	–	✓	✓	✓	–	✓	1 LiDAR, Stereo Camera, Gated Camera, FIR Camera, Weather Station
A2D2 (Geyer et al., 2020)	–	✓	–	–	–	–	5 LiDARs, 6 Cameras, GPS, IMU
SoilingNet (Ujičář et al., 2019)	–	–	–	–	✓Contamination	–	Cameras
Radiate (Sheeny et al., 2021)	–	✓	✓	✓	–	✓	1 LiDAR, 1 stereo camera, 360° radar, GPS
EU (Yan et al., 2020)	–	–	–	✓	–	✓	4 LiDARs, 2 stereo cameras, 2 fish-eye cameras, radar, RTK GPS, IMU
HSI-Drive (Basterretxea et al., 2021)	–	✓	✓	–	–	✓	1 Photonfocus 25-band hyperspectral camera
WADS (Bos et al., 2020, 2021)	–	✓	–	✓	–	✓	3 LiDARs, 1 camera, NIR camera, LWIR camera, GNSS, IMU, 1550 nm LiDAR
Boreas (Burnett et al., 2022)	–	✓	–	✓	–	✓	1 LiDAR, 1 camera, 1 360° radar, GNSS-INS
DAWN (Kenk and Hassaballah, 2020)	–	✓	✓	✓	✓Sandstorms	–	Camera (images collected from web search)
GROUNDDED (Ort et al., 2021)	–	✓	–	✓	–	–	1 LiDAR, 1 camera, RTK-GPS, LGPR

## 6. Datasets, simulators and facilities

### 6.1. Datasets

Adverse weather research cannot be done without datasets. Many features used in object detection tasks need to be extracted from datasets and almost every algorithm needs to be tested and validated on datasets. In order to better solve the adverse weather problems in autonomous driving, it is essential to have enough data covering each kind of weather. Unfortunately, the majority of the datasets commonly

used for training do not contain too many conditions different from clear weather. Some famous datasets that were collected in tropical areas like nuScenes (Caesar et al., 2020) contain some rain conditions in Singapore, A\*3D (Pham et al., 2020a) has rain conditions at night, and ApolloScape (Huang et al., 2019) includes some strong light and shadow conditions. A summary of the weather conditions coverage and the sensors used for collection in each dataset is shown in Table 3.

Researchers collected weather data that are common in their area of living or used simulation (Liu et al., 2020) to build their own weather datasets. The University of Michigan collected four-season LiDAR data

**Table 4**

Weather conditions and sensors support in simulators.

Simulators	Weather conditions							Sensor support					
	Adjustable	Rain	Fog	Snow	Light/ Time of day	Contamination (Dust, leaf)	LiDAR	Camera	Thermal camera	Radar	GNSS/GPS	Ultrasonic	V2X
CARLA (Dosovitskiy et al., 2017)	✓	✓	✓	–	✓	–	✓	✓	–	✓	✓	✓	–
LG SVL (Rong et al., 2020)	✓	✓	✓	–	✓	–	✓	✓	–	✓	✓	✓	–
dSPACE (dSpace, 2021)	✓	✓	✓	✓	✓	–	✓	✓	–	✓	✓	✓	✓
CarSim (Mechanical Simulation Corporation, 2021)	–	✓	–	✓	✓	–	–	✓	–	✓	✓	✓	–
TASS PreScan (TASS International, 2021)	–	✓	✓	✓	✓	–	✓	✓	–	✓	✓	✓	✓
AirSim (Microsoft, 2021)	✓	✓	✓	✓	✓	✓	✓	✓	✓	–	✓	–	–
PTV Vissim (PTV Group, 2021)	–	✓	✓	✓	–	–	Need to integrate with other platforms						–

**Table 5**

Experimental weather facilities across the world.

Experimental facilities	Adjustable	Rain	Fog	Snow	Light/ Time of day	Contamination (Dust, leaf)	Location	Length	Lanes
JARI special environment proof ground (Japan Automotive Research Institute, 2021)	✓	✓	✓	–	✓	–	Ibaraki, Japan	200 m	3
VTTI Smart roads (Virginia Tech, 2021)	✓	✓	✓	✓	✓	–	Virginia, US	800 m	2
DENSO (Saito, 2021)	✓	✓	–	–	✓	–	Aichi, Japan	200 m	10 m wide
Center for road weather proving ground (KICT, 2021)	✓	✓	✓	✓	✓	✓	Yeoncheon, Korea	600 m	4
CEREMA climatic chamber (Laboratoire régional des ponts et chaussées, 2021)	✓	✓	✓	–	–	–	Clermont-Ferrand, France	31 m	2
NIED cryospheric environment simulator (National Research Institute of Earth Science and Disaster Resilience, 2021)	✓	✓	✓	–	–	–	Yamagata, Japan	N/A	N/A
CATARC proving ground (Wang et al., 2020)	✓	✓	✓	✓	✓	–	Yancheng, China	60 km track	2 or more
CERI Tomakomai cold region test road (Civil Engineering Research Institute of Cold Region, 2021)	✓	–	–	✓	–	–	Hokkaido, Japan	21 hectare ring track	2
Sod5G finnish meteorological institute (Sukuvaara et al., 2022)	Equipped with 5G network and weather stations	–	–	✓	✓	–	Sodankylä, Finland	11 km track	2

using a Segway robot on the campus at an early stage (Carlevaris-Bianco et al., 2016). Pitropov et al. (2021) presented the first AV dataset that focuses on snow conditions specifically, called the Canadian adverse driving conditions (CADC) dataset. The variety of winter was collected by 8 cameras and LiDAR and GNSS+INS in Waterloo, Canada, with their LiDAR de-noising-modified (Charron et al., 2018). The large amount of snow enables researchers to test object detection, localization, and mapping in all kinds of snow conditions, which is hard to realize in artificial environments. Oxford RobotCar (Maddern et al., 2017) is among the early datasets that put weights on adverse conditions including heavy rain, snow, direct sunlight, night, and even road and building works. Sakaridis et al. (2018) applied foggy synthesis on the Cityscapes dataset (Cordts et al., 2016) and generated Foggy Cityscapes with over 20 000 clear-weather images, which is wildly used in the de-hazing task. The same team later introduced ACDC (Sakaridis et al., 2021), the Adverse Conditions Dataset with correspondences for training and testing semantic segmentation methods on adverse visual conditions. It covers the visual domain and contains high-quality fine pixel-level semantic annotated fog, nighttime, rain, and snow images. Zheng (2021) uploaded the IUPUI Driving Video/Image Benchmark to the Consumer Digital Video Library, containing sample views from in-car cameras under different illumination and road conditions

when public safety vehicles are on patrol and responding to disasters. Conditions cover snow, rain, direct light, dim-lit conditions, sunny facing the sun, shadow, night, and their caused phenomena such as wet roads, glass reflection, glass icing, raining and dirty windshields, moving wipers, etc. It is the unremitting effort of research on collecting data on cold days and dangerous driving conditions that gives us the opportunity to push research in adverse conditions further to the next level.

## 6.2. Simulators and experimental facilities

The rapid developments of autonomous driving especially in adverse weather conditions benefit a lot from the availability of simulation platforms and experimental facilities like fog chambers or test roads. Virtual platforms such as the well-known CARLA (Dosovitskiy et al., 2017) simulator, as shown in Fig. 16, enable researchers to construct custom-designed complex road environments and non-ego participants with infinite scenarios where it would be extremely hard and costly in real field experiments. Moreover, for weather conditions, the appearance of each kind of weather especially season-related or extreme climates related is not on call at all times. For example, it is impossible for tropical areas to have the opportunity to do snow



Fig. 16. A scenario of a town with wet road surface in fog weather in CARLA simulator.

tests; and natural rain showers might not be durable enough to collect experimental data. Most importantly, adverse conditions are usually dangerous for driving and subjects always face safety threats in normal field tests, while absolute zero physical harm is something that simulators can guarantee. In recent years, various simulation platforms including open source and closed source software have developed adjustable weather conditions and ‘time of day’ plug-ins. Thus, people can test their ADS modalities against rain, snow, fog with different precipitation rates, and strong light in simulators at any time before taking it to the outside (Best et al., 2018). Table 4 lists the weather conditions and sensors supported in some common autonomous driving simulators.

On the other hand, laboratory environments can also replace real field tests with control. Considering the limitation on test fields and safety hazards to the surrounding people or facilities, an enclosed artificial track or chamber with rain/fog/snow making machines offers almost the same environmental conditions with the advantage of controllable precipitation rates and low risks. Table 5 lists out some renowned test facilities with some details about the chambers or tracks.

## 7. Trends, limitations, and developing research directions

This section will discuss the trend of current adverse weather research, the limitations we are facing along the road, potential research directions, and focuses in the future.

### 7.1. Trends toward advanced sensor fusion and sophisticated networks

To some extent, the tendency of industry technology is affected by market needs and preferences. For example, after using mere radar as the main core sensor for years (Braga, 2021), Tesla announced that they started transitioning to a camera-based pure vision Autopilot system (Tesla, 2021b). However, the deficiency of the sole force of each ADS sensor alone in weather does not exactly agree with such a route. Each sensor has its own strength against particular problems, such as the lower signal attenuation radar possesses over LiDAR in rain conditions previously mentioned in Section 2.2. It is in AVs’ best interest to make the best of each sensor’s superiority. As summarized in Section 3, sensor fusion, the combining force of several sensors is still one of the most reliable ways to build a robust system that is agnostic to weather.

Instead of enlisting every help available by appending all kinds of specialized sensors such as the weather station, the sensible way is to pick out the best-performed combination of necessities and maintain a feasible economic cost and computational cost in the meantime. As many fusion combinations have been tried, the choices have not been exhausted yet. Studies on LiDAR-based fusion modalities and thermal-camera-included modalities are starting to emerge recently. Future benchmarking and evaluations at a comprehensive level on advanced sensor fusions should provide the community with one or more well-recognized choices that can make it safer when cruising in weather.

### 7.1.1. Extra LiDAR types

Besides the common LiDARs widely in use, there are also new types of LiDARs on the table right now that have started to lead the major research trend among many technology companies around the world, i.e. solid-state LiDAR and MEMS LiDAR. Unlike traditional rotating LiDARs, solid-state LiDAR needs beam steering to tune the laser direction and one of the popular ways is through the Optical Phased Array (OPA) platform. Thermal optics tuning is currently the dominant method as the thermo-optic coefficients of the two major materials, Si and SiN, have a difference of over an order of magnitude (Sun et al., 2019). The tunability of thermal tuning is somehow limited, whereas wavelength tuning could achieve a tunability of a couple of dozen degrees per 100 nm change around 1550 nm laser wavelength (Wu et al., 2020b). There are also other cutting-edge beam steering techniques, such as metasurfaces (Lio and Ferraro, 2021), starting to emerge these years.

FMCW LiDAR is a technology using continuous waves to do coherent detection which also caught a great deal of attention recently. Unlike traditional LiDAR using amplitude modulation (AM) approach, FMCW LiDAR emits a continuous laser beam to measure the change in frequency of the waveform as it reflects off of an object, which gives it the ability to see as far as more than 300 meters and measuring the instantaneous velocity based on Doppler shift (Li and Ibanez-Guzman, 2020). The longer detection range and the accurate velocity sensing help identify a pertinent quick-moving subject at a distance and give the AV enough time to react. Even though the difference could be as small as a fraction of a second, it would still make a huge difference for a heavy vehicle, like a bus or cargo truck, given its enormous inertia. Most of all, lights that do not match the FMCW LiDAR’s local oscillator are not detected, which provides robustness to interference from solar light and the cross-talk between other AVs or even the ego vehicle’s previous signal itself.

There is an uncommon LiDAR called super-continuum laser (Nishizawa and Yamanaka, 2021), a broadband beam pumped in very short pulse duration. Such technology is commonly used in gas sensing, optical communication, etc., and Outsight AI is the company known for developing it in the ADS field (Outsight, 2021). This kind of LiDAR works in the SWIR (Short-wave Infrared) band and can do multispectral detection in real time. Each wavelength in the SWIR band has a unique reflectance spectral signature based on the object’s material, e.g. snow, ice, skin, cotton, plastic, asphalt, and so on. That way, it is possible to recognize a real person from a mannequin or a poster or to classify the ongoing weather. One hidden problem is that super-continuum lasers normally work at 728–810 nm (Lehtonen et al., 2003) and whether the power level they are using at this wavelength range has any risk to human eyes is not well established. We will further discuss the eye safety and wavelength issue next in Section 7.2.1.

### 7.1.2. Extra camera types

Similar to the Navtech radar (Navtech Radar, 2021a) we mentioned before that has lifted the upper bound of sensor use, cameras that are suitable candidates for advanced sensor fusions will not be limited to plain visible cameras either. Instead, professional cameras have started to be deployed for data collection and replaced conventional imaging devices. Some popular choices of extra and potential camera types that we conclude are shown below:

A stereo camera has two or more lenses with a separate image sensor for each lens, which provides the ability to capture 3D images, just like human binocular vision.

Thermal cameras use infrared radiation to create images. Far-infrared (FIR) cameras operate at 8–12 μm and can see heat sources, while near-infrared (NIR) camera normally operates around 700–1400 nm and can penetrate what visible light could not, like haze, light fog, and smoke (SONY, 2021).

Event camera, such as the dynamic vision sensor (DVS), does not capture images using a shutter as conventional cameras do, but individual and asynchronous pixels that report any brightness changes (Gallego et al., 2019). Event camera offers a very high dynamic range

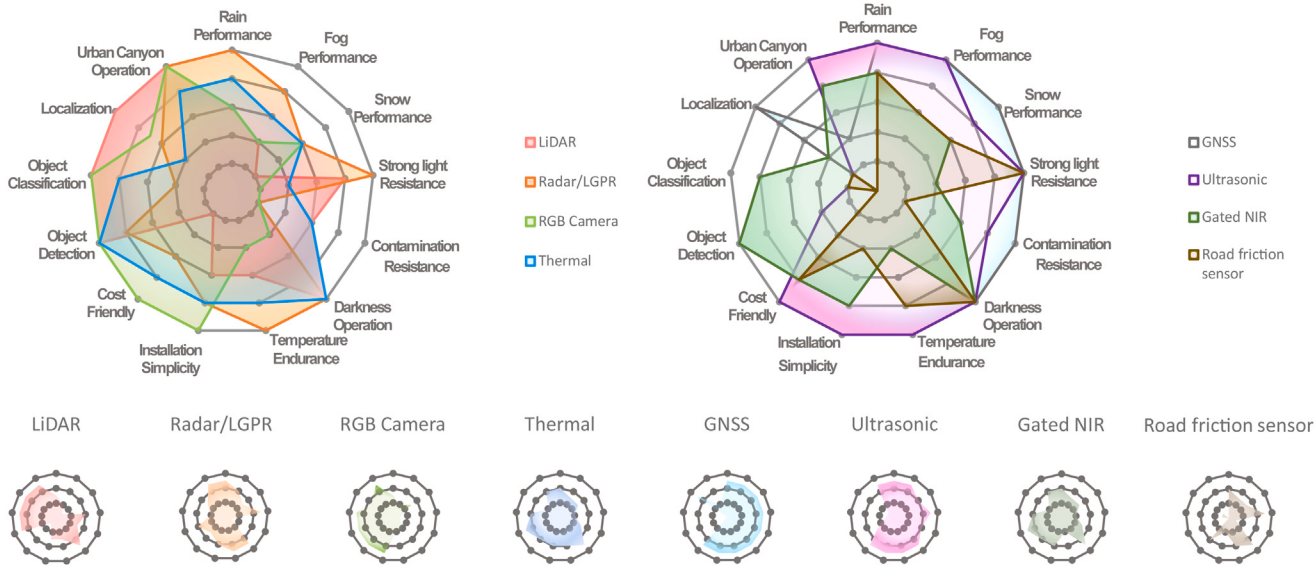


Fig. 17. Sensor performance and characteristics radar map.

and no motion blur, but traditional vision algorithms do not apply to asynchronous events output, so the application on cars normally would require additional algorithms.

For the OpenCV OAK-D AI cameras, the fusion even happens before our definition of sensor fusion, for this type of camera is consisted of a high-resolution RGB camera, a stereo pair, and an Intel Myriad X Visual Processing Unit (VPU), which can produce a depth map with sophisticated neural networks for visual perception (Mallick, 2022).

The High Dynamic Range (HDR) camera is a type of camera that captures three images of the same scene with three different shutter speeds corresponding to different brightness: bright, medium, and dark. An HDR image that reveals both what is in the dark and glare is then produced by the combination of said three (Mann and Picard, 1995). Clearly, such a feature gives HDR camera a strong advantage in the conditions of strong light or shadows, but it has a serious limitation on moving objects because any movement between successive images will cause a staggered-blur strobe effect after combining them together. What is more, due to the need for several images to achieve desired luminance range, extra time is expected, which is a luxury for video conditions. In order to increase the dynamic range of a video, either the frame rate or the resolution is going to be cut in half for the acquirement of two differently exposed images. If we want to preserve full frame rate and resolution, then a CMOS image sensor with dual gain architecture is required. With HDR cameras, visibility drop due to sudden changes in light conditions like the entry and exit of a tunnel is largely mitigated. Benefiting from better color preservation, AV navigating performance when driving into direct sunlight can also be improved (Paul and Chung, 2018).

Hyperspectral imaging technology on the other hand could be the key to the next generation of vision in ADS. Covering an extremely broad spectrum all the way from UV to IR, hyperspectral cameras can record over 100 different wavelengths and filter out visible light interference. The AV situation awareness can be enhanced because this kind of camera can precisely identify the subjects' material signatures by visualizing their spectra. In other words, the material of the detected target can be clearly identified and classified based on its chemical compositions (Brian et al., 2022). The ability to capture more information makes hyperspectral cameras suitable in case of light-related conditions, including darkness, shadow, direct strong light, and even fog. The only obstacle between hyperspectral imaging technology and

its wide deployment in autonomous driving could be the cost of as high as \$20,000–\$100,000 USD, while the number of devices to cover a 360° FOV is not on the low side in the meantime. Good thing is that the reduction of costs is on the horizon and the industry also shows great interest in this promising technology (Brian et al., 2022). Basterretxea et al. (2021) actually already have presented the HSI-Drive dataset collected by only one 25-band hyperspectral camera containing light condition changes, rainy/wet and foggy conditions across four seasons, as shown in Table 3.

### 7.1.3. Sophisticated machine learning methods

Successful sensor fusions rely on the strength of each of their element, but it would be hard to release their full potential on perception and sensing without sophisticated algorithms and machine learning techniques helping with the processing of fusion data (Ahmed et al., 2019). Weather conditions networks training is being conducted on various neural networks including CNN (Heinzler et al., 2020), R-CNN (Ren et al., 2015), DNN (Yue et al., 2021), BPNN (Vaibhav et al., 2020), etc. with numerous advanced algorithms. No matter how hard the dataset is to acquire, the use of artificial equivalent effects of certain weather is starting to dominate this field of research and has proven to be efficient, as introduced in Section 4.

Also, with the rapid development of AI technologies in recent years, it is possible to apply new methods of machine learning in adverse weather solutions. For instance, the active learning of DNN by NVIDIA DRIVE (Shapiro, 2021). Active learning starts with a trained DNN on labeled data, then sorts through the unlabeled data and selects the frames that it does not recognize, which would be then sent to human annotators for labeling and added to the training pool, and completes the learning loop. In a nighttime scenario where raindrops blur the camera lens and make it difficult to detect pedestrians with umbrellas and bicycles, active learning is proven to have over 3 times better accuracy and be able to avoid false positive detection. Other burgeoning machine learning methods such as transfer learning and federated learning could also be very effective on robust AI infrastructure, which is still left to be explored.

## 7.2. Limitations

As stated in Section 2, the degradation of perception is the main limitation of ADS sensors in adverse weather conditions. Hardware limitations including temperature and humidity endurance are something barely considered but should not be ignored. We summarize a radar chart to show the strengths and weaknesses of each sensor in adverse conditions partially based on Table 1, as shown in Fig. 17.

### 7.2.1. 1550 nm LiDAR

Currently, the majority of the market use 905 nm wavelength LiDAR deployment. However, LiDAR upgrade has been put on the agenda by the research community. Kutila et al. (2018) raised using 1550 nm LiDAR to overcome fog conditions because higher optical power is allowed to emit at this wavelength. Before we determine the feasibility of this, it is necessary to bring up the two critical design considerations in LiDAR selection: eye safety and ambient suppression. Most civilian or commercial LiDARs are used in an environment where human eyes are exposed, so the infrared laser of LiDAR must not exceed the maximum permissible exposure (MPE) or cause any damage to retinas, according to the international laser product safety standard (IEC 60825-1:2014) class 1 (International Electrotechnical Commission, 2017). Therefore, the selection of laser wavelength is pretty much narrowed down to two ranges: 800 nm–1000 nm and 1300 nm–1600 nm. That is why current LiDARs made for AVs have the selection of 850 nm,<sup>6</sup> 905 nm,<sup>7</sup> and 1550 nm<sup>8</sup> wavelengths (see Carballo et al. (2020) for a list of other LiDARs and their respective wavelengths), and they also all fall into the window of low solar irradiance, which helps on suppressing the ambient light for the signal receiver with a lower SNR (Sun et al., 2019). We also plot a water extinction coefficient chart as shown in Fig. 18 in order to show that the 1550 nm wavelength is more likely to be absorbed by water. The extinction coefficient  $\alpha_{water}$  is also known as the Lambert absorption coefficient, which is acquired from:

$$\alpha(\lambda) = 4\pi k(\lambda)/\lambda \quad (6)$$

in which  $\lambda$  is wavelength and  $k(\lambda)$  is the extinction coefficient of water at 25 °C. The detail of the acquisition of  $k(\lambda)$  can be found in Hale and Querry (1973). Therefore, a 1550 nm laser can be largely absorbed in the crystalline lens or the vitreous body of an eye so more energy is allowed than 905 nm, which seems to be a good thing considering the power attenuation predicament in weather (Warren, 2019).

However, based on the research of Wojtanowski et al. (2014) on the comparison of 905 nm and 1550 nm performance deterioration due to adverse environmental conditions, 905 nm reaches two times further than 1550 nm in a rain rate of 25 mm/h. There are opinions arguing that light propagation at 1550 nm might suffer less attenuation than at shorter wavelengths, but Kim et al. (2001) suggested that this rule only applies to haze condition (visibility > 2 km), while in fog (visibility < 500 m) the attenuation is independent of wavelength and 905 nm still measures 60% longer than 1550 nm. What is more, 1550 nm waves have approximately 97% worse reflectance in snow compared to 905 nm (Velodyne, 2021a). Less interference from snow does not make up for the insufficiency in object detection.

FMCW LiDAR manufacturers like Aurora (2021) and Aeva (2021) are using 1550 nm wavelength in solid-state and newly proposed concurrent firing LiDAR that excels at remote distance sensing also utilizes the 1550 nm band (Kim et al., 2021). Despite their obvious advantages in higher signal power and anti-interference, the 1550 nm wavelength's ineffectiveness in dealing with water was hardly considered. Some promotion articles may argue that FMCW LiDAR handles the water droplets on the emitter well and can easily filter out the raindrops or

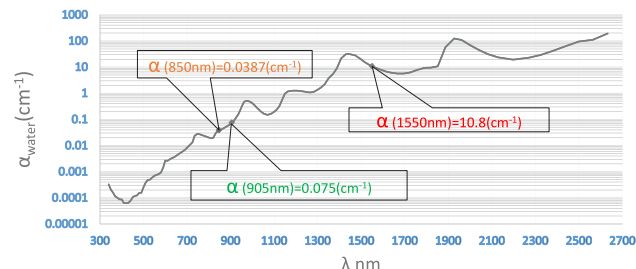


Fig. 18. Water extinction coefficient spectrum. Laser energy absorption by water of 1550 nm is over 100 times larger than that of 905 nm (Palmer and Williams, 1974; Sogandares and Fry, 1997).

snowflakes based on its velocity detecting ability (Crouch, 2021), but the large signal attenuation that comes with the wavelength itself is omitted here and barely any systematic field tests of FMCW LiDAR or concurrent firing LiDAR in adverse weather conditions can be found at this stage.

Still, 1550 nm has great potential in further solid-state LiDAR development and better compatibility with CMOS (Complementary Metal Oxide Semiconductor) technology. New technologies in new kinds of LiDARs, for example, Baraja's spectrum-scan technology (Pulikkasril and Lam, 2019; Tsai et al., 2021), are still being looked forward to.

### 7.2.2. Dataset and tool support

Based on the weather support status we collected in Table 3, rain conditions can be considered adequate in current autonomous driving datasets, while fog and snow are not so much. Fog or haze is not time-sustained weather that is easy to encounter during data collection, so normally fog datasets are acquired from test facilities or simulators such as those shown in Tables 4 and 5. As for snow, due to the difference between falling snow and accumulated snow, the qualities of the snow conditions contained in current datasets vary largely. And since the obvious difficulty of constructing an artificial snow environment compared to rain, experimental facilities' snow condition supports are very much limited. Furthermore, the strong light and contamination supports are seriously lacking in datasets, even rarer in simulators and facilities, which makes the research in this area relatively short. Therefore, as rich as the dataset resources are getting, the limitations on weather support are still realistic problems for perception and sensing research in adverse weather.

## 7.3. Developing research directions

The V2X (Vehicle to Everything) system is an unignorable part of the development of Intelligent Transportation Systems (ITS) and ADS. Regardless of the proficiency of well-experienced drivers, accidents still happen due to asymmetric road information among drivers, and short reaction time. V2X system broadens the range of information gathering from one car's perception to the perception of almost every element on the road. The 'Everything', or X here, can refer to other vehicles, roadside infrastructures, pedestrians, and even UAVs (Unmanned Aerial Vehicles). To have pedestrians included in the V2X or further IoT systems, advanced wearable devices or universal smartphone technical support is needed, which is out of the scope of this survey.

### 7.3.1. V2V

The core of V2V (Vehicle to Vehicle) is information sharing among connected vehicles (CV), which eliminates the problem of information asymmetry from the bottom root. Under normal conditions, visual blockage like a truck in front of the ego vehicle or vehicles beyond direct line of sight due to terrain or intersections is a high risk of accidents. With V2V technology, the ego vehicle gains the ability to acquire the perception data and position information from another car

<sup>6</sup> OS1-64, Ouster LiDAR (Pacala, 2021).

<sup>7</sup> Puck, Velodyne LiDAR (Velodyne, 2021c).

<sup>8</sup> PandarGT, Hesai LiDAR (Yifan David Li, 2021).



**Fig. 19.** V2I infrastructures at Morikoro park in Nagoya, Japan. A self-driving vehicle interacting with the roadside units (RSU). Inset: A LiDAR deployment on a pole. Images courtesy of Mr. Abraham Monrroy-Cano of Perception Engine Inc.<sup>9</sup>

whose view is out of its own reach at the moment (Alam et al., 2019), thus the driver or the ego vehicle can avoid accidents by making proper decisions and adjusting behaviors based on the additional information. In terms of harsh weather, vehicles that first experience or perceive the presence of weather conditions or the change in the road surface conditions can make weather assessments before other vehicles reach this location and then relay the perception data or assessment results to other vehicles to alert them about the dangers. If the adverse conditions cause traffic congestion or accidents, later vehicles can plan a new route according to the information gathered by fore CVs in real time to improve efficiency and safety in intersections and work zones (Horani, 2019). With the V2V technology, truck platooning on highways or docks areas is about to become the first mature application of ADS. According to the evaluation of Ahmed et al. (2020) on the driver's perception of CV in Wyoming, almost 90% of the human test drivers found that the front collision warning and rerouting function are very useful as a benefit of the improved road condition information.

### 7.3.2. V2I

V2I (Vehicle to Infrastructure) as shown in Fig. 19 on the other hand is not as fluid as V2V, but still offers a great deal of potential in intelligent transportation. Roadside units (RSU) compose most of the infrastructure in V2I and have recently become a branch of weather perception research (Vargas Rivero et al., 2020). Sensors installed on an RSU mounted on a pole have a wide angle of view and do not suffer from the water screen on rainy days or the snow whirl in snowy weather. A slightly downward pointing angle also dodges some direct sunlight.

Roadside LiDAR has its own weather perception abilities (Hill and Hamilton, 2017) and can be used to identify local weather conditions (Tian, 2021). Besides, the V2I network also provides the possibility of multi-image-based de-weathering with background filtering and object clustering (Wu et al., 2020a) not involving sophisticated neural networks. With the image of a certain scene in clear weather being captured and stored in infrastructures in advance, a 3-D model without the disturbance from weather can be easily reconstructed and fed to nearby vehicles to help them safely navigate under low visibility and incomplete road information.

### 7.3.3. V2X and IoT

Laux et al. (2016) developed one of the first complete open-source vehicular networking experimental platforms in 2016 that supports most of the features of the European wireless standards at the time (i.e. ETSI ITS-G5), OpenC2X. With its open-source advantage and high compatibility with car sensors such as OBD-II for speed information, new features and updates are easily developed which is a huge contribution of OpenC2X to the V2X community. And now, some V2X technologies have already been put into use to help with adverse weather problems. Jung et al. (2020) developed an ADS with V2X communication aid which is comprised of beyond-line-of-sight perception and extended planning. If we consider V2X as an extra sensor, then such a system is just like a new fusion modality. Ego vehicles' own sensors and other vehicles' sensors and roadside sensors facilitate the data input of perception including those beyond the line of sight. Route, velocity, and real-time traffic information obtained by V2I communication are integrated to extend route planning with an optimal solution. Such modality approaches fully autonomous driving to a great extent but is still limited by the scale of the CV network and connected infrastructure's coverage.

Just like perception enhancement methods, V2X's architecture is also being improved to better deal with weather conditions. Barrachina et al. (2013) propose a V2X-d architecture, which combines V2V and V2I together to overcome each of their own deficiency such as V2V's limited horizontal view and the vulnerability of traditional surveillance cameras on roadside infrastructures. This architecture allows vehicle density estimation in urban areas under all weather conditions which is the ideal way of utilizing the V2X system in autonomous driving. Vaidya et al. (2021) use roadside infrastructures as the nearby processing and storage server of the Edge Cloud and deploy a Fuzzy-Inference system as a road weather hazard assessment method. They take the road surface conditions and surface temperatures gathered from both roadside environmental sensors and CVs as the linguistic variables and the Fuzzy-Inference system outputs consequent slipperiness based on IF-THEN and AND-type and OR-type rules. Overall 10 fuzzy rules have been established. Take one as an example: IF the surface condition is 'ice warning' AND surface temperature is 'low' OR 'very low', THEN slipperiness is 'very slippery'. Such results are processed locally in a segmented network and distributed to nearby CVs. The pressure of computing concentration, the processing time, and the latency of CV communication are all largely reduced.

Onesimu et al. (2021) proposed an IoT-based intelligent accident avoidance system for adverse weather and road conditions. They used a dataset collected by Hjelkrem and Ryeng (2017) which contains not only weather conditions but also the vehicle's speed and weight information which is being used to calculate the proper speed limit of the vehicle under the current condition to avoid collisions. They implemented a Naïve Bayes classifier in the training process to predict the chance of accidents in the network and use Blynk (2021) mobile app to do the hardware control and simulation. This app will display a message containing an accident warning or weather information like 'Accident ahead, Sandstorm' on the back window of a car, and this message will be received by the following car who would act accordingly to prevent accidents from happening and potentially be passed along.

<sup>9</sup> <https://perceptionengine.jp/>.

In recent years, V2X and IoT technologies are starting to enter adverse weather research and provide the Intelligent Transportation System field with a new platform for perception and sensing enhancement. With profuse weather and road data, the reliability and versatility of vehicular networks could be the next focus of future research. Finnish Meteorological Institute (FMI) operates on the Sod5G test track in Arctic weather using ITS-G5 (European standard for vehicular communications based on the IEEE-1609. x and IEEE-802.11p standards) and 5G cellular test networks with real-time road weather data services supported by road weather stations and CV measurements (Perälä et al., 2022).

But of course, all the features just mentioned would require real-time video (rapid image) sharing, or at least high-volume data transmission among infrastructures, vehicles, and electronic devices. That is why the large volume LiDAR point cloud data need to be compressed for V2X transmission (Tu et al., 2019), and also the reason why the telecom community is working on the V2X communication methods towards richer bandwidth and lower latency such as the fifth-generation wireless technology, i.e. 5G (Horani, 2019) to transmit among vehicles and servers. Wi-Fi 6 (2.4 GHz and 5 GHz), based on the IEEE 802.11ax standard (Wi-Fi ALLIANCE, 2021), is currently considered a well-experienced IoT solution, which we could see in our daily lives such as routers and smart appliances. Qorvo for example has started the exploration of enabling a Wi-Fi 6 V2X link in the Telematics Control Unit (TCU) and antenna, and the expansion to Wi-Fi 6E (6 GHz spectrum), a critical band to establish reliable links between vehicles and their surroundings (Qorvo, 2021).

Several cities in the world, like Ann Arbor, Michigan (City of Ann Arbor, Michigan, 2021); Barcelona, Spain (Stott, 2021); and Guangzhou, China (Huanan et al., 2015) have initiated their smart city projects, where thousands of roadside units and sensors would be installed on city infrastructures and form a huge local connected system. Prototypes of V2X and IoT are soon to be expected.

#### 7.3.4. Aerial view

Long before being introduced into autonomous driving, LiDAR technology was widely used in geographical mapping and meteorological monitoring. Terrain, hydrology, forestry, and vegetation cover can be derived from measurements of a LiDAR mounted on planes, or satellites (Ippolito, 1989). The advantage of looking from above is that the view coverage is enormous and there are fewer obstacles than from the ground. With the rapid development of UAVs like drones, it is becoming realistic to do transportation perception from the top view, which sees what could not be seen from the ground. For example at an intersection, an AV can only behave according to its leading vehicle but not something that is beyond direct sight, however, UAV can see the leading vehicle of the leading vehicle and thereafter, foresee risks far away from the subject AV and avoid accidents in advance.

Aerial imagery helps acquire accurate map data and has become a reliable remote sensing resource for autonomous driving (Chen et al., 2022). Vehicle detection and classification can now be done from high-resolution satellite imagery (Ghandour et al., 2018) and driving context recognition can be improved under weather interference with the help of UAVs (Khezaz et al., 2022). Xu et al. (2021) developed a method to detect road curbs off-line using aerial images via imitation learning. They take images from the New York City planimetric dataset (New York City Department of Information Technology and Telecommunications (NYC DOITT), 2021) as input and generate a graph with vertices and edges representing road curbs. Aerial LiDAR makes the AV ego-perception into a macro perspective.

While a UAV could provide supporting information, the UAV itself also faces the challenges of changes in illumination and precipitation, thus might provide significantly less reliable information than in the normal case (Wu et al., 2019). Hence, perception and sensing enhancement research both in the air and on the ground under adverse weather conditions could benefit mutually. Concerns are that aerial views are

not enough to cover all the modern urban environments where tunnels and elevated roads are common. Nonetheless, aerial perception research is being done in the areas of change detection (Hebel et al., 2013), aerial image segmentation, and object detection (Wu et al., 2019).

## 8. Conclusion

In this work, we surveyed the influence of adverse weather conditions on 5 major ADS sensors. Sensor fusion solutions were listed. The core solution to adverse weather problems is perception enhancement and various machine learning and image processing methods such as de-noising were thoroughly analyzed. Additional sensing enhancement methods including classification and localization were also among the discussions. A research tendency towards robust sensor fusions, sophisticated networks and computer vision models is concluded. Candidates for future ADS sensors such as FMCW LiDAR, HDR camera and hyperspectral camera were introduced. The limitations brought by the lack of relevant datasets and the difficulty of 1550 nm LiDAR were thoroughly explained. Finally, we believe that V2X and IoT have a brighter prospect in future weather research. This survey covered almost all types of common weather that pose negative effects on sensors' perception and sensing abilities including rain, snow, fog, haze, strong light, and contamination, and listed out datasets, simulators, and experimental facilities that have weather support.

With the development of advanced test instruments and new technologies in LiDAR architectures, signs of progress have been largely made in the performance of perception and sensing in common wet weather. Rain and fog conditions seem to be getting better with the advanced development in computer vision in recent years, but still have some space for improvement on LiDAR. Snow, on the other hand, is still at the stage of dataset expansion and perception enhancement against snow has some more to dig in. Hence, point cloud processing under extreme snowy conditions, preferably with interaction scenarios either under controlled environments or on open roads is part of our future work. Two major sources of influence, strong light and contamination are still not rich in research and solutions. Hopefully, efforts made towards the robustness and reliability of sensors can carry adverse weather conditions research to the next level.

## Declaration of competing interest

The authors declare that they have no known competing financial interests or personal relationships that could have appeared to influence the work reported in this paper.

## Acknowledgments

## Funding

The author (Y.Z) would like to take this opportunity to thank the "Nagoya University Interdisciplinary Frontier Fellowship" supported by Nagoya University and JST, Japan, the establishment of university fellowships towards the creation of science technology innovation, Grant Number JPMJFS2120, and JSPS KAKENHI, Japan Grant Number JP21H04892 and JP21K12073.

The authors thank Prof. Ming Ding from Nagoya University for his help. We would also like to extend our gratitude to Sensible4, the University of Michigan, Tier IV Inc., Ouster Inc., Perception Engine Inc., and Mr. Kang Yang for their support. In addition, our deepest thanks to VTT Technical Research Center of Finland, the University of Waterloo, Pan Asia Technical Automotive Center Co., Ltd, and the Civil Engineering Research Institute for Cold Region of Japan.

## References

- Abdić, I., Fridman, L., Brown, D.E., Angell, W., Reimer, B., Marchi, E., Schuller, B., 2016. Detecting road surface wetness from audio: A deep learning approach. In: International Conference on Pattern Recognition. ICPR, IEEE, pp. 3458–3463.
- Advanced Navigation, 2021. Spatial FOG dual reference manual version 1.3. URL <https://www.advancednavigation.com/wp-content/uploads/2021/08/Spatial-FOG-Dual-Reference-Manual.pdf>, [Last accessed 12 Dec 2021].
- Aeva, 2021. Perception for all devices. URL <https://www.aeva.ai/>, [Last accessed 14 June 2021].
- Afifi, M., Derpanis, K.G., Ommer, B., Brown, M.S., 2021. Learning multi-scale photo exposure correction. In: Conference on Computer Vision and Pattern Recognition. CVPR, IEEE/CVF, pp. 9157–9167.
- Ahmed, S., Huda, M.N., Rajbhandari, S., Saha, C., Elshaw, M., Kanarachos, S., 2019. Pedestrian and cyclist detection and intent estimation for autonomous vehicles: A survey. *Appl. Sci.* 9 (11), 2335.
- Ahmed, M.M., Yang, G., Gaweesh, S., 2020. Assessment of drivers' perceptions of connected vehicle-human machine interface for driving under adverse weather conditions: preliminary findings from wyoming. *Front. Psychol.* 11, e1889.
- Akita, T., Mita, S., 2019. Object tracking and classification using millimeter-wave radar based on LSTM. In: Intelligent Transportation Systems Conference. ITSC, IEEE, pp. 1110–1115.
- Al-Haija, Q.A., Smadi, M.A., Zein-Sabatto, S., 2020. Multi-class weather classification using ResNet-18 CNN for autonomous IoT and CPS applications. In: International Conference on Computational Science and Computational Intelligence. CSCI, IEEE, pp. 1586–1591.
- Alam, F., Mehmood, R., Katib, I., Altowaijri, S.M., Albeshri, A., 2019. TAAWUN: A decision fusion and feature specific road detection approach for connected autonomous vehicles. *Mob. Netw. Appl.* 1–17.
- Aldibaja, M., Suganuma, N., Yoneda, K., 2016. Improving localization accuracy for autonomous driving in snow-rain environments. In: International Symposium on System Integration. SII, IEEE/SICE, pp. 212–217.
- Aldibaja, M., Suganuma, N., Yoneda, K., 2017. Robust intensity-based localization method for autonomous driving on snow-wet road surface. *IEEE Trans. Ind. Inform.* 13 (5), 2369–2378.
- Aldibaja, M., Yanase, R., Kuramoto, A., Kim, T.H., Yoneda, K., Suganuma, N., 2021. Improving lateral autonomous driving in snow-wet environments based on road-mark reconstruction using principal component analysis. *IEEE Intell. Transp. Syst. Mag.* 13 (4), 116–130.
- Ancuti, C., Ancuti, C.O., Timofte, R., 2018. Ntire 2018 challenge on image dehazing: Methods and results. In: Conference on Computer Vision and Pattern Recognition (CVPR) Workshops. IEEE/CVF, pp. 891–901.
- Andrej, J., Yagar, S., 1993. A temporal analysis of rain-related crash risk. *Accid. Anal. Prev.* 25 (4), 465–472.
- Aurora, 2021. FMCW lidar: The self-driving game-changer. URL <https://aurora.tech/blog/fmcw-lidar-the-self-driving-game-changer>, [Last accessed 14 June 2021].
- Axis Communications, 2021. Product support for AXIS Q1922 thermal network camera. URL <https://www.axis.com/products/axis-q1922/support>, [Last accessed 17 June 2021].
- Balasubramaniam, R., Ruf, C., 2020. Characterization of rain impact on L-Band GNSS-R ocean surface measurements. *Remote Sens. Environ.* 239, 111607.
- Baril, D., Deschênes, S.-P., Gamache, O., Vaidis, M., LaRocque, D., Laconte, J., Kubelka, V., Giguère, P., Pomerleau, F., 2021. Kilometer-scale autonomous navigation in subarctic forests: challenges and lessons learned. arXiv preprint [arXiv:2111.13981](https://arxiv.org/abs/2111.13981).
- Barnes, D., Gadd, M., Murcatt, P., Newman, P., Posner, I., 2020. The oxford radar robotcar dataset: A radar extension to the oxford robotcar dataset. In: International Conference on Robotics and Automation. ICRA, IEEE, pp. 6433–6438.
- Barrachina, J., Sanguesa, J.A., Fogue, M., Garrido, P., Martinez, F.J., Cano, J.-C., Calafate, C.T., Manzoni, P., 2013. V2X-d: A vehicular density estimation system that combines V2V and V2I communications. In: Wireless Days Conference. WD, IEEE/IFIP, pp. 1–6.
- Bartos, M., Park, H., Zhou, T., Kerkez, B., Vasudevan, R., 2019. Windshield wipers on connected vehicles produce high-accuracy rainfall maps. *Sci. Rep.* 9 (1), 1–9.
- Basterretxea, K., Martínez, V., Echanobe, J., Gutiérrez-Zaballa, J., Del Campo, I., 2021. HSI-drive: A dataset for the research of hyperspectral image processing applied to autonomous driving systems. In: 2021 IEEE Intelligent Vehicles Symposium. IV, IEEE, pp. 866–873.
- Beloroussi, R., Gruyer, D., 2014. Impact of reduced visibility from fog on traffic sign detection. In: Intelligent Vehicles Symposium Proceedings. IEEE, pp. 1302–1306.
- Benoit, A., Caplier, A., Durette, B., Hérault, J., 2010. Using human visual system modeling for bio-inspired low level image processing. *Comput. Vis. Image Underst.* 114 (7), 758–773.
- Best, A., Narang, S., Pasqualin, L., Barber, D., Manocha, D., 2018. Autonovi-sim: Autonomous vehicle simulation platform with weather, sensing, and traffic control. In: Conference on Computer Vision and Pattern Recognition (CVPR) Workshops. IEEE/CVF, pp. 1048–1056.
- Bijelic, M., Gruber, T., Mannan, F., Kraus, F., Ritter, W., Dietmayer, K., Heide, F., 2020. Seeing through fog without seeing fog: Deep multimodal sensor fusion in unseen adverse weather. In: Conference on Computer Vision and Pattern Recognition. CVPR, IEEE/CVF, pp. 11682–11692.
- Bijelic, M., Gruber, T., Ritter, W., 2018a. A benchmark for lidar sensors in fog: Is detection breaking down? In: Intelligent Vehicles Symposium (IV). IEEE, pp. 760–767.
- Bijelic, M., Gruber, T., Ritter, W., 2018b. Benchmarking image sensors under adverse weather conditions for autonomous driving. In: Intelligent Vehicles Symposium. IV, IEEE, pp. 1773–1779.
- Binas, J., Neil, D., Liu, S.-C., Delbruck, T., 2017. DDD17: End-to-end DAVIS driving dataset. arXiv preprint [arXiv:1711.01458](https://arxiv.org/abs/1711.01458).
- Blynk, 2021. IoT platform for businesses and developers. URL <https://blynk.io/>, [Last accessed 27 Aug. 2021].
- Bos, J.P., Chopp, D., Kurup, A., Spike, N., 2020. Autonomy at the end of the earth: an inclement weather autonomous driving data set. In: Autonomous Systems: Sensors, Processing, and Security for Vehicles and Infrastructure 2020, Vol. 11415. SPIE, pp. 36–48.
- Bos, J.P., Kurup, A., Chopp, D., Jeffries, Z., 2021. The Michigan Tech autonomous winter driving data set: year two. In: Autonomous Systems: Sensors, Processing, and Security for Vehicles and Infrastructure 2021, Vol. 11748. SPIE, pp. 57–65.
- Braga, B., 2021. What is tesla autopilot?. URL <https://www.jdpower.com/cars-shopping-guides/what-is-tesla-autopilot>, [Last accessed 14 June 2021].
- Braun, M., Krebs, S., Flohr, F., Gavrila, D.M., 2019. Eurocity persons: A novel benchmark for person detection in traffic scenes. *IEEE Trans. Pattern Anal. Mach. Intell.* 41 (8), 1844–1861.
- Bresson, G., Alsayed, Z., Yu, L., Glaser, S., 2017. Simultaneous localization and mapping: A survey of current trends in autonomous driving. *IEEE Trans. Intell. Veh.* 2 (3), 194–220.
- Brian, B., Bryan, M., Chetan, M., Jeff, K., Paul, L., Venkata, V., Vijay, N., 2022. HyperSpectral technology for autonomous vehicles. URL <https://scet.berkeley.edu/wp-content/uploads/UCB-ELPP-Report-Hyperspectral-Technology-for-Autonomous-Vehicles-FINAL.pdf>, [Last accessed 12 Jan 2022].
- Briefs, U., 2015. Mcity grand opening. *Res. Rev.* 46 (3).
- Bright Way Vision, 2021. See through adverse weather, darkness, and glare. URL <https://www.brightwayvision.com/technology>, [Last accessed 17 June 2021].
- Brunner, C., Peynot, T., Vidal-Calleja, T., Underwood, J., 2013. Selective combination of visual and thermal imaging for resilient localization in adverse conditions: Day and night, smoke and fire. *J. Field Robotics* 30 (4), 641–666.
- Burnett, K., Yoon, D.J., Wu, Y., Li, A.Z., Zhang, H., Lu, S., Qian, J., Tseng, W.-K., Lambert, A., Leung, K.Y., et al., 2022. Boreas: A multi-season autonomous driving dataset. arXiv preprint [arXiv:2203.10168](https://arxiv.org/abs/2203.10168).
- Bystrov, A., Hoare, E., Tran, T.-Y., Clarke, N., Gashinova, M., Cherniakov, M., 2016. Road surface classification using automotive ultrasonic sensor. *Procedia Eng.* 168, 19–22.
- Caesar, H., Bankiti, V., Lang, A.H., Vora, S., Liang, V.E., Xu, Q., Krishnan, A., Pan, Y., Baldan, G., Beijbom, O., 2020. Nuscenes: A multimodal dataset for autonomous driving. In: Conference on Computer Vision and Pattern Recognition. CVPR, IEEE/CVF, pp. 11621–11631.
- Carballo, A., Lambert, J., Monrroy, A., Wong, D., Narksri, P., Kitsukawa, Y., Takeuchi, E., Kato, S., Takeda, K., 2020. LIBRE: The multiple 3D LiDAR dataset. In: Intelligent Vehicles Symposium. IV, IEEE, pp. 1094–1101.
- Carlevaris-Bianco, N., Ushani, A.K., Eustice, R.M., 2016. University of Michigan North Campus long-term vision and lidar dataset. *Int. J. Robot. Res.* 35 (9), 1023–1035.
- Carullo, A., Parvis, M., 2001. An ultrasonic sensor for distance measurement in automotive applications. *IEEE Sens. J.* 1 (2), 143.
- Chaabani, H., Kamoun, F., Bargaoui, H., Outay, F., et al., 2017. A neural network approach to visibility range estimation under foggy weather conditions. *Procedia Comput. Sci.* 113, 466–471.
- Chaabani, H., Werghi, N., Kamoun, F., Taha, B., Outay, F., et al., 2018. Estimating meteorological visibility range under foggy weather conditions: A deep learning approach. *Procedia Comput. Sci.* 141, 478–483.
- Chang, M.-F., Lambert, J., Sangkloy, P., Singh, J., Bak, S., Hartnett, A., Wang, D., Carr, P., Lucey, S., Ramanan, D., et al., 2019. Argoverse: 3d tracking and forecasting with rich maps. In: Conference on Computer Vision and Pattern Recognition. CVPR, IEEE/CVF, pp. 8748–8757.
- Charron, N., Phillips, S., Waslander, S.L., 2018. De-noising of Lidar point clouds corrupted by snowfall. In: Conference on Computer and Robot Vision. CRV, IEEE, pp. 254–261.
- Che, Z., Li, G., Li, T., Jiang, B., Shi, X., Zhang, X., Lu, Y., Wu, G., Liu, Y., Ye, J., 2019. D<sup>2</sup>-city: A large-scale dashcam video dataset of diverse traffic scenarios. arXiv preprint [arXiv:1904.01975](https://arxiv.org/abs/1904.01975).
- Chen, Z., Deng, L., Luo, Y., Li, D., Junior, J.M., Gonçalves, W.N., Nurunnabi, A.A.M., Li, J., Wang, C., Li, D., 2022. Road extraction in remote sensing data: A survey. *Int. J. Appl. Earth Obs. Geoinf.* 112, 102833.
- Chen, Z., Wang, Y., Yang, Y., Liu, D., 2021. PSD: Principled synthetic-to-real dehazing guided by physical priors. In: Conference on Computer Vision and Pattern Recognition. CVPR, IEEE/CVF, pp. 7180–7189.
- Choi, Y., Kim, N., Hwang, S., Park, K., Yoon, J.S., An, K., Kweon, I.S., 2018. KAIST multi-spectral day/night data set for autonomous and assisted driving. *IEEE Trans. Intell. Transp. Syst.* 19 (3), 934–948.
- City of Ann Arbor, Michigan, 2021. Ann arbor is developing a smart city strategic plan. URL <https://www.a2gov.org/news/pages/article.aspx?i=630>, [Last accessed 24 May 2021].

- Civil Engineering Research Institute of Cold Region, 2021. Off-site research facilities. URL <https://www.ceri.go.jp/contents/about/about05.html>, [Last accessed 30 Nov 2021].
- Civil Engineering Research Institute of Cold Region Snow and Ice Research Team, 2021. Guidance facilities regarding blizzard visibility impairment (in Japanese). URL <https://www2.ceri.go.jp/jpn/pdf2/b-gp-200710-fubuki.pdf>, [Last accessed 30 Nov 2021].
- Colomb, M., Hirsch, K., André, P., Boreux, J., Lacôte, P., Dufour, J., 2008. An innovative artificial fog production device improved in the European project 'FOG'. *Atmos. Res.* 87 (3–4), 242–251.
- Cordts, M., Omran, M., Ramos, S., Rehfeld, T., Enzweiler, M., Benenson, R., Franke, U., Roth, S., Schiele, B., 2016. The cityscapes dataset for semantic urban scene understanding. In: Conference on Computer Vision and Pattern Recognition. CVPR, IEEE/CVF, pp. 3213–3223.
- Cornick, M., Koehling, J., Stanley, B., Zhang, B., 2016. Localizing ground penetrating radar: A step toward robust autonomous ground vehicle localization. *J. Field Robotics* 33 (1), 82–102.
- Crouch, S., 2021. Frequency-modulated continuous-wave lidar has all-weather capabilities. URL <https://www.laserfocusworld.com/lasers-sources/article/14035383/frequencymodulated-continuouswave-lidar-has-allweather-capabilities>, [Last accessed 14 June 2021].
- Dannheim, C., Icking, C., Mäder, M., Sallis, P., 2014. Weather detection in vehicles by means of camera and LIDAR systems. In: International Conference on Computational Intelligence, Communication Systems and Networks. IEEE, pp. 186–191.
- Dhananjaya, M.M., Kumar, V.R., Yogamani, S., 2021. Weather and light level classification for autonomous driving: Dataset, baseline and active learning. arXiv preprint arXiv:2104.14042.
- Dosovitskiy, A., Ros, G., Codevilla, F., Lopez, A., Koltun, V., 2017. CARLA: An open urban driving simulator. In: Conference on Robot Learning. PMLR, pp. 1–16.
- dSpace, 2021. Over-the-air simulation of echoes for automotive radar sensors. URL <https://www.dspace.com/en/ltd/home/news/engineers-insights/over-the-air-simulation.cfm>, [Last accessed 25 Sep. 2021].
- Duddu, V.R., Pulugurtha, S.S., Mane, A.S., Godfrey, C., 2020. Back-propagation neural network model to predict visibility at a road link-level. *Transp. Res. Interdiscip. Perspect.* 8, 100250.
- Dunlop, S., 2008. A Dictionary of Weather. OUP Oxford.
- Elhoseiny, M., Huang, S., Elgammal, A., 2015. Weather classification with deep convolutional neural networks. In: International Conference on Image Processing. ICIP, IEEE, pp. 3349–3353.
- Engin, D., Genç, A., Kemal Ekenel, H., 2018. Cycle-dehaze: Enhanced cyclegan for single image dehazing. In: Proceedings of the IEEE Conference on Computer Vision and Pattern Recognition Workshops. pp. 825–833.
- Fersch, T., Buhmann, A., Koelpin, A., Weigel, R., 2016. The influence of rain on small aperture LiDAR sensors. In: German Microwave Conference (GeMiC). IEEE, pp. 84–87.
- Filgueira, A., González-Jorge, H., Lagüela, S., Díaz-Vilarino, L., Arias, P., 2017. Quantifying the influence of rain in LiDAR performance. *Measurement* 95, 143–148.
- Fischer, P., Azimi, S.M., Roschlau, R., Krauß, T., 2018. Towards HD maps from aerial imagery: Robust lane marking segmentation using country-scale imagery. *ISPRS Int. J. Geo-Inf.* 7 (12), 458.
- FLIR, 2021. Fused AEB with thermal can save lives. URL <https://www.flir.com/globalassets/industrial/oem/adas/flir-thermal-aeb-white-paper---final-v1.pdf>, [Last accessed 22 Oct. 2021].
- Ford Motor Company, 2021. From autonomy to snowconomy: How ford fusion hybrid autonomous research vehicle can navigate in winter. URL <https://media.ford.com/content/fordmedia/fna/us/en/news/2016/03/10/how-fusion-hybrid-autonomous-vehicle-can-navigate-in-winter.html>, [Last accessed 31 May 2021].
- Frenzel, L., 2021. Ultrasonic sensors: A smart choice for shorter-range applications. URL <https://www.electronicdesign.com/industrial-automation/article/21806202/ultrasonic-sensors-a-smart-choice-for-shorter-range-applications>, [Last accessed 17 Aug. 2021].
- Fritzsche, P., Kueppers, S., Briese, G., Wagner, B., 2016. Radar and LiDAR sensorfusion in low visibility environments. In: International Conference on Informatics in Control, Automation and Robotics. ICINCO, pp. 30–36.
- Fritzsche, P., Kueppers, S., Briese, G., Wagner, B., 2018. Fusing LiDAR and radar data to perform SLAM in harsh environments. In: Informatics in Control, Automation and Robotics. Springer, pp. 175–189.
- Fu, L., Zhou, C., Guo, Q., Juefei-Xu, F., Yu, H., Feng, W., Liu, Y., Wang, S., 2021. Auto-exposure fusion for single-image shadow removal. In: Conference on Computer Vision and Pattern Recognition. CVPR, IEEE/CVF, pp. 10571–10580.
- Gadd, M., De Martini, D., Marchegiani, L., Newman, P., Kunze, L., 2020. Sense-Assess-eXplain (SAX): Building trust in autonomous vehicles in challenging real-world driving scenarios. In: 2020 IEEE Intelligent Vehicles Symposium. IV, IEEE, pp. 150–155.
- Gallego, G., Delbrück, T., Orchard, G., Bartolozzi, C., Taba, B., Censi, A., Leutenegger, S., Davison, A., Conradt, J., Daniilidis, K., et al., 2019. Event-based vision: A survey. arXiv preprint arXiv:1904.08405.
- Gao, T., Gao, F., Zhang, G., Liang, L., Song, Y., Du, J., Dai, W., 2018. Effects of temperature environment on ranging accuracy of lidar. In: Tenth International Conference on Digital Image Processing (ICDIP 2018), Vol. 10806. SPIE, pp. 1915–1921.
- Gao, Y., Hu, H.-M., Wang, S., Li, B., 2014. A fast image dehazing algorithm based on negative correction. *Signal Process.* 103, 380–398.
- Gao, X., Roy, S., Xing, G., 2021. MIMO-SAR: A hierarchical high-resolution imaging algorithm for mmwave FMCW radar in autonomous driving. *IEEE Trans. Veh. Technol.* 70 (8), 7322–7334.
- Garmin Ltd., 2021. VIRB 360 owner's manual. URL [https://www8.garmin.com/manuals/webhelp/virb360/EN-US/VIRB\\_360\\_OM\\_EN-US.pdf](https://www8.garmin.com/manuals/webhelp/virb360/EN-US/VIRB_360_OM_EN-US.pdf), [Last accessed 17 June 2021].
- Gernot, C., 2007. GPS signal disturbances by water in various states. In: International Technical Meeting of the Satellite Division of the Institute of Navigation (ION GNSS). ION, pp. 2187–2195.
- Geyer, J., Kassahun, Y., Mahmudi, M., Ricou, X., Durgesh, R., Chung, A.S., Hauswald, L., Pham, V.H., Mühllegg, M., Dorn, S., et al., 2020. A2D2: Audi autonomous driving dataset. arXiv preprint arXiv:2004.06320.
- Ghandour, A.J., Krayem, H.A., Jezzini, A.A., 2018. Autonomous vehicle detection and classification in high resolution satellite imagery. In: 2018 International Arab Conference on Information Technology. ACIT, IEEE, pp. 1–5.
- Goodin, C., Carruth, D., Doude, M., Hudson, C., 2019. Predicting the influence of rain on LiDAR in ADAS. *Electronics* 8 (1), 89.
- Groves, P.D., 2014. The complexity problem in future multisensor navigation and positioning systems: A modular solution. *J. Navig.* 67 (2), 311–326.
- Gultepe, I., 2008. Measurements of light rain, drizzle and heavy fog. In: Precipitation: Advances in Measurement, Estimation and Prediction. Springer, pp. 59–82.
- Guo, J., Kurup, U., Shah, M., 2020. Is it safe to drive? An overview of factors, metrics, and datasets for drivability assessment in autonomous driving. *IEEE Trans. Intell. Transp. Syst.* 21 (8), 3135–3151.
- Haberlandt, U., Sester, M., 2010. Areal rainfall estimation using moving cars as rain gauges—a modelling study. *Hydrol. Earth Syst. Sci.* 14 (7), 1139–1151.
- Hahnel, D., Burgard, W., Fox, D., Fishkin, K., Philipose, M., 2004. Mapping and localization with RFID technology. In: International Conference on Robotics and Automation. ICRA, 1, IEEE, pp. 1015–1020.
- Hale, G.M., Querry, M.R., 1973. Optical constants of water in the 200-nm to 200- $\mu\text{m}$  wavelength region. *Appl. Opt.* 12 (3), 555–563.
- Hamzeh, Y., Rawashdeh, S.A., 2021. A review of detection and removal of raindrops in automotive vision systems. *J. Imaging* 7 (3), 52.
- Hasirlioglu, S., Doric, I., Lauerer, C., Brandmeier, T., 2016. Modeling and simulation of rain for the test of automotive sensor systems. In: Intelligent Vehicles Symposium. IV, IEEE, pp. 286–291.
- Hautière, N., Tarel, J.-P., Aubert, D., 2007. Towards fog-free in-vehicle vision systems through contrast restoration. In: Conference on Computer Vision and Pattern Recognition. CVPR, IEEE/CVF, pp. 1–8.
- He, K., Sun, J., Tang, X., 2010. Single image haze removal using dark channel prior. *IEEE Trans. Pattern Anal. Mach. Intell.* 33 (12), 2341–2353.
- Hebel, M., Arens, M., Stilla, U., 2013. Change detection in urban areas by object-based analysis and on-the-fly comparison of multi-view ALS data. *ISPRS J. Photogramm. Remote Sens.* 86, 52–64.
- Heinzler, R., Piewak, F., Schindler, P., Stork, W., 2020. Cnn-based lidar point cloud de-noising in adverse weather. *IEEE Robot. Autom. Lett.* 5 (2), 2514–2521.
- Heinzler, R., Schindler, P., Seekircher, J., Ritter, W., Stork, W., 2019. Weather influence and classification with automotive lidar sensors. In: Intelligent Vehicles Symposium. IV, IEEE, pp. 1527–1534.
- Hill, D.J., 2015. Assimilation of weather radar and binary ubiquitous sensor measurements for quantitative precipitation estimation. *J. Hydroinform.* 17 (4), 598–613.
- Hill, C.J., Hamilton, B.A., 2017. Concept of Operations for Road Weather Connected Vehicle and Automated Vehicle Applications. Technical Report, United States. Federal Highway Administration.
- Hjelkrem, O.A., Ryeng, E.O., 2017. Driver behaviour data linked with vehicle, weather, road surface, and daylight data. *Data Brief* 10, 511–514.
- Hoekstra, P., Delaney, A., 1974. Dielectric properties of soils at UHF and microwave frequencies. *J. Geophys. Res.* 79 (11), 1699–1708.
- Hong, Z., Petillot, Y., Wang, S., 2020. Radarslam: Radar based large-scale slam in all weathers. In: International Conference on Intelligent Robots and Systems. IROS, IEEE/RSJ, pp. 5164–5170.
- Hong, Y., Zheng, Q., Zhao, L., Jiang, X., Kot, A.C., Shi, B., 2021. Panoramic image reflection removal. In: Conference on Computer Vision and Pattern Recognition. CVPR, IEEE/CVF, pp. 7762–7771.
- Horani, M., 2019. Improved Vision-based Lane Line Detection in Adverse Weather Conditions Utilizing Vehicle-to-Infrastructure (V2I) Communication (Ph.D. thesis). Oakland University.
- Huanan, Z., Shijun, L., Hong, J., 2015. Guangzhou smart city construction and big data research. In: International Conference on Behavioral, Economic and Socio-Cultural Computing. BESC, IEEE, pp. 143–149.
- Huang, X., Wang, P., Cheng, X., Zhou, D., Geng, Q., Yang, R., 2019. The apolloscape open dataset for autonomous driving and its application. *IEEE Trans. Pattern Anal. Mach. Intell.* 42 (10), 2702–2719.

- Ijaz, M., Ghassemlooy, Z., Le Minh, H., Rajbhandari, S., Perez, J., 2012. Analysis of fog and smoke attenuation in a free space optical communication link under controlled laboratory conditions. In: International Workshop on Optical Wireless Communications. IWOW, IEEE, pp. 1–3.
- International Electrotechnical Commission, 2017. IEC 60825-1:2014/ISH1:2017 Edition 3.0 2014/05 Safety of Laser Products – Part 1: Equipment Classification and Requirements. Standard IEC 60825-1:2014/ISH1:2017, IEC, Geneva, CH, URL <https://webstore.iec.ch/publication/3587>.
- International Telecommunication Union, 2021. Recommendation ITU-R P.838-3 Specific attenuation model for rain for use in prediction methods. URL [https://www.itu.int/dms\\_pubrec/itu-r/rec/p/R-REC-P.838-3-200503-I!!PDF-E.pdf](https://www.itu.int/dms_pubrec/itu-r/rec/p/R-REC-P.838-3-200503-I!!PDF-E.pdf), [Last accessed 14 June 2021].
- Ippolito, L.J., 1989. Propagation Effects Handbook for Satellite Systems Design: A Summary of Propagation Impairments on 10 to 100 GHz Satellite Links with Techniques for System Design, Vol. 1082. National Aeronautics and Space Administration, Scientific and Technical Information Division.
- Japan Automotive Research Institute, 2021. Special environment proving ground. URL <http://www.jari.or.jp/tabid/563/Default.aspx>, [Last accessed 25 Sep. 2021].
- Jebson, S., 2007. Fact Sheet Number 3: Water in the Atmosphere. National Meteorological Library and Archive.
- John, V., Mita, S., Lakshmanan, A., Boyali, A., Thompson, S., 2021. Deep visible and thermal camera-based optimal semantic segmentation using semantic forecasting. *J. Auton. Veh. Syst.* 1 (2), 021006.
- Jokela, M., Kutila, M., Pykönén, P., 2019. Testing and validation of automotive point-cloud sensors in adverse weather conditions. *Appl. Sci.* 9 (11), 2341.
- Judd, K.M., Thornton, M.P., Richards, A.A., 2019. Automotive sensing: Assessing the impact of fog on LWIR, MWIR, SWIR, visible, and lidar performance. In: Infrared Technology and Applications XLV, Vol. 11002. SPIE, pp. 322–334.
- Jung, C., Lee, D., Lee, S., Shim, D.H., 2020. V2X-communication-aided autonomous driving: system design and experimental validation. *Sensors* 20 (10), 2903.
- Kamemura, T., Takagi, H., Pal, C., Ohsumi, A., 2008. Development of a long-range ultrasonic sensor for automotive application. *SAE Int. J. Passeng. Cars-Electron. Electr. Syst.* 1 (2008-01-0910), 301–306.
- Karlsson, R., Wong, D.R., Kawabata, K., Thompson, S., Sakai, N., 2021. Probabilistic rainfall estimation from automotive lidar. arXiv preprint [arXiv:2104.11467](https://arxiv.org/abs/2104.11467).
- Kenk, M.A., Hassaballah, M., 2020. DAWN: vehicle detection in adverse weather nature dataset. arXiv preprint [arXiv:2008.05402](https://arxiv.org/abs/2008.05402).
- Kehez, A., Hina, M.D., Ramdane-Cherif, A., 2022. Perception enhancement and improving driving context recognition of an autonomous vehicle using UAVs. *J. Sensor Actuator Netw.* 11 (4), 56.
- KICT, 2021. An opening ceremony of the center for road weather proving ground, yeoncheon. URL [https://www.kict.re.kr/board.es?mid=a20601000000&bid=newsnotice&act=view&list\\_no=13372](https://www.kict.re.kr/board.es?mid=a20601000000&bid=newsnotice&act=view&list_no=13372), [Last accessed 25 Sep. 2021].
- Kim, G., Ashraf, I., Eom, J., Park, Y., 2021. Concurrent firing light detection and ranging system for autonomous vehicles. *Remote Sens.* 13 (9), 1767.
- Kim, T., Cha, M., Kim, H., Lee, J.K., Kim, J., 2017. Learning to discover cross-domain relations with generative adversarial networks. In: International Conference on Machine Learning. PMLR, pp. 1857–1865.
- Kim, I.I., McArthur, B., Korevaar, E.J., 2001. Comparison of laser beam propagation at 785 nm and 1550 nm in fog and haze for optical wireless communications. In: Optical Wireless Communications III, Vol. 4214. International Society for Optics and Photonics, pp. 26–37.
- Kim, T.K., Paik, J.K., Kang, B.S., 1998. Contrast enhancement system using spatially adaptive histogram equalization with temporal filtering. *IEEE Trans. Consum. Electron.* 44 (1), 82–87.
- Kordani, A.A., Rahmani, O., Nasiri, A.S.A., Boroomandrad, S.M., 2018. Effect of adverse weather conditions on vehicle braking distance of highways. *Civ. Eng. J.* 4 (1), 46–57.
- Krizhevsky, A., Sutskever, I., Hinton, G.E., 2012. Imagenet classification with deep convolutional neural networks. *Adv. Neural Inf. Process. Syst.* 25, 1097–1105.
- Kuang, H., Wang, B., An, J., Zhang, M., Zhang, Z., 2020. Voxel-FPN: Multi-scale voxel feature aggregation for 3D object detection from LiDAR point clouds. *Sensors* 20 (3), 704.
- Kumar, H., Gupta, S., Venkatesh, K.S., 2019. A novel method for inferior mirage detection in video. In: Digital Image & Signal Processing. DISP.
- Kurup, A., Bos, J., 2021. DSOR: A scalable statistical filter for removing falling snow from LiDAR point clouds in severe winter weather. arXiv preprint [arXiv:2109.07078](https://arxiv.org/abs/2109.07078).
- Kutila, M., Pykönén, P., Holzhüter, H., Colomb, M., Duthon, P., 2018. Automotive LiDAR performance verification in fog and rain. In: International Conference on Intelligent Transportation Systems. ITSC, IEEE, pp. 1695–1701.
- Kutila, M., Pykönén, P., Ritter, W., Sawade, O., Schäufele, B., 2016. Automotive LiDAR sensor development scenarios for harsh weather conditions. In: International Conference on Intelligent Transportation Systems. ITSC, IEEE, pp. 265–270.
- Kuutti, S., Fallah, S., Katsaros, K., Dianati, M., McCullough, F., Mouzakitis, A., 2018. A survey of the state-of-the-art localization techniques and their potentials for autonomous vehicle applications. *IEEE Internet Things J.* 5 (2), 829–846.
- Laboratoire régional des ponts et chaussées, 2021. Site de clermont-ferrand. URL <https://www.cerema.fr/fr/cerema/directions/cerema-centre-est/site-clermont-ferrand>, [Last accessed 25 Sep. 2021].
- Lambert, J., Carballo, A., Cano, A.M., Narksri, P., Wong, D., Takeuchi, E., Takeda, K., 2020. Performance analysis of 10 models of 3D LiDARs for automated driving. *IEEE Access* 8, 131699–131722.
- Lang, A.H., Vora, S., Caesar, H., Zhou, L., Yang, J., Beijbom, O., 2019. Pointpillars: Fast encoders for object detection from point clouds. In: Conference on Computer Vision and Pattern Recognition. CVPR, pp. 12697–12705.
- Laris, M., 2018. Transportation Waymo launches nation's first commercial self-driving taxi service in Arizona. Wash. Post 6, 2018.
- Laux, S., Pannu, G.S., Schneider, S., Tiemann, J., Klingler, F., Sommer, C., Dressler, F., 2016. OpenC2X—An open source experimental and prototyping platform supporting ETSI ITS-G5. In: 2016 IEEE Vehicular Networking Conference. VNC, IEEE, pp. 1–2.
- Lehtonen, M., Genty, G., Ludvigsen, H., Kaivola, M., 2003. Supercontinuum generation in a highly birefringent microstructured fiber. *Appl. Phys. Lett.* 82 (14), 2197–2199.
- Lei, C., Chen, Q., 2021. Robust reflection removal with reflection-free flash-only cues. In: Conference on Computer Vision and Pattern Recognition. CVPR, IEEE/CVF, pp. 14811–14820.
- Lei, Y., Emaru, T., Ravankar, A.A., Kobayashi, Y., Wang, S., 2020. Semantic image segmentation on snow driving scenarios. In: International Conference on Mechatronics and Automation. ICMA, IEEE, pp. 1094–1100.
- Li, Y., Ibanez-Guzman, J., 2020. Lidar for autonomous driving: The principles, challenges, and trends for automotive lidar and perception systems. *IEEE Signal Process. Mag.* 37 (4), 50–61.
- Li, G., Yang, Y., Qu, X., 2019. Deep learning approaches on pedestrian detection in hazy weather. *IEEE Trans. Ind. Electron.* 67 (10), 8889–8899.
- Lin, S.-L., Wu, B.-H., 2021. Application of Kalman filter to improve 3D LiDAR signals of autonomous vehicles in adverse weather. *Appl. Sci.* 11 (7), 3018.
- Lio, G.E., Ferraro, A., 2021. LiDAR and beam steering tailored by neuromorphic metasurfaces dipped in a tunable surrounding medium. *Photonics* 8 (3).
- Liu, Z., Cai, Y., Wang, H., Chen, L., Gao, H., Jia, Y., Li, Y., 2021a. Robust target recognition and tracking of self-driving cars with radar and camera information fusion under severe weather conditions. *IEEE Trans. Intell. Transp. Syst.*
- Liu, D., Cui, Y., Cao, Z., Chen, Y., 2020. A large-scale simulation dataset: Boost the detection accuracy for special weather conditions. In: International Joint Conference on Neural Networks. IJCNN, IEEE, pp. 1–8.
- Liu, Z., Yin, H., Wu, X., Wu, Z., Mi, Y., Wang, S., 2021b. From shadow generation to shadow removal. In: Conference on Computer Vision and Pattern Recognition. CVPR, IEEE/CVF, pp. 4927–4936.
- Lu, C., Lin, D., Jia, J., Tang, C.-K., 2014. Two-class weather classification. In: Conference on Computer Vision and Pattern Recognition. CVPR, IEEE/CVF, pp. 3718–3725.
- Lufft, 2021. StaRWIS-UMB-Stationary Road Weather Information Sensor. URL <https://www.lufft.com/products/road-runway-sensors-292/starwis-umb-stationary-road-weather-information-sensor-2317/>, [Last accessed 17 June 2021].
- Maddern, W., Pascoe, G., Linegar, C., Newman, P., 2017. 1 year, 1000 km: The Oxford robotcar dataset. *Int. J. Robot. Res.* 36 (1), 3–15.
- Maddern, W., Stewart, A., McManus, C., Upcroft, B., Churchill, W., Newman, P., 2014. Illumination invariant imaging: Applications in robust vision-based localisation, mapping and classification for autonomous vehicles. In: International Conference on Robotics and Automation (ICRA), Visual Place Recognition in Changing Environments Workshop, Vol. 2. p. 3.
- Mai, N.A.M., Duthon, P., Khoudour, L., Crouzil, A., Velastin, S.A., 2021. 3D object detection with SLS-fusion network in foggy weather conditions. *Sensors* 21 (20), 6711.
- Mallick, S., 2022. Introduction to OAK-D and DepthAI. URL [https://learnopencv.com/introduction-to-opencv-ai-kit-and-depthai/?utm\\_source=rss&utm\\_medium=rss&utm\\_campaign=introduction-to-opencv-ai-kit-and-depthai](https://learnopencv.com/introduction-to-opencv-ai-kit-and-depthai/?utm_source=rss&utm_medium=rss&utm_campaign=introduction-to-opencv-ai-kit-and-depthai), [Last accessed 22 Jan 2022].
- Mann, S., Picard, R.W., 1995. On being ‘undigital’ with digital cameras: Extending dynamic range by combining differently exposed pictures. In: Imaging Science & Technology Annual Conference (IS&T). pp. 442–448.
- Mardirosian, R., 2021. Lidar vs. camera: driving in the rain. URL <https://ouster.com/zh-cn/blog/lidar-vs-camera-comparison-in-the-rain>, [Last accessed 15 May 2021].
- Mechanical Simulation Corporation, 2021. Unreal engine marketplace showcase. URL [https://www.carsim.com/publications/newsletter/2021\\_03\\_17.php](https://www.carsim.com/publications/newsletter/2021_03_17.php), [Last accessed 25 Sep. 2021].
- Mehra, A., Mandal, M., Narang, P., Chamola, V., 2021. ReViewNet: A fast and resource optimized network for enabling safe autonomous driving in hazy weather conditions. *IEEE Trans. Intell. Transp. Syst.* 22 (7), 4256–4266.
- Miclea, R.-C., Dughir, C., Alexa, F., Sandru, F., Silea, I., 2020. Laser and LiDAR in a system for visibility distance estimation in fog conditions. *Sensors* 20 (21), 6322.
- Microsoft, 2021. AirSim. URL <https://microsoft.github.io/AirSim/>, [Last accessed 25 Sep. 2021].
- Milford, M.J., Wyeth, G.F., 2012. SeqSLAM: Visual route-based navigation for sunny summer days and stormy winter nights. In: International Conference on Robotics and Automation. ICRA, IEEE, pp. 1643–1649.
- Mittal, A., Moorthy, A.K., Bovik, A.C., 2012. No-reference image quality assessment in the spatial domain. *Trans. Image Process.* 21 (12), 4695–4708.
- Mohammed, A.S., Amamou, A., Ayevide, F.K., Kelouwani, S., Agbossou, K., Zioui, N., 2020. The perception system of intelligent ground vehicles in all weather conditions: A systematic literature review. *Sensors* 20 (22), 6532.

- Musat, V., Fursa, I., Newman, P., Cuzzolin, F., Bradley, A., 2021. Multi-weather city: Adverse weather stacking for autonomous driving. In: International Conference on Computer Vision. ICCV, IEEE, pp. 2906–2915.
- Narasimhan, S.G., Nayar, S.K., 2002. Vision and the atmosphere. *Int. J. Comput. Vis.* 48 (3), 233–254.
- Narasimhan, S.G., Nayar, S.K., 2003. Interactive (de) weathering of an image using physical models. In: IEEE Workshop on Color and Photometric Methods in Computer Vision, Vol. 6. France, p. 1.
- Naseer, T., Ruhnke, M., Stachniss, C., Spinello, L., Burgard, W., 2015. Robust visual SLAM across seasons. In: International Conference on Intelligent Robots and Systems. IROS, IEEE/RSJ, pp. 2529–2535.
- National Oceanic and Atmospheric Administration, 2021. Getting traction: Tips for traveling in winter weather. URL [https://www.weather.gov/wrn/getting\\_traction](https://www.weather.gov/wrn/getting_traction), [Last accessed 03 May 2021].
- National Research Institute of Earth Science and Disaster Resilience, 2021. Snow and ice disaster prevention experiment building. URL <https://www.bosai.go.jp/study/snow.html>, [Last accessed 25 Sep. 2021].
- Naughton, K., 2021. Self-driving cars succumb to snow blindness as driving lanes disappear. URL <https://www.autonews.com/article/20160210/OEM06/160219995/self-driving-cars-succumb-to-snow-blindness-as-driving-lanes-disappear>, [Last accessed 15 May 2021].
- Navtech Radar, 2021a. ClearWay software and sensors CTS350-X & CTS175-X technical specifications. URL <https://navtechradar.com/clearway-technical-specifications/>, [Last accessed 22 Oct. 2021].
- Navtech Radar, 2021b. FMCW radar. URL <https://navtechradar.com/explore/fmcw-radar/>, [Last accessed 22 Nov 2021].
- Neuhold, G., Ollmann, T., Rota Bulo, S., Kotschieder, P., 2017. The mapillary vistas dataset for semantic understanding of street scenes. In: International Conference on Computer Vision. ICCV, IEEE, pp. 4990–4999.
- New York City Department of Information Technology and Telecommunications (NYC DOITT), 2021. GIS & mapping. URL <https://www1.nyc.gov/site/doitt/residents/gis-3d-data.page>, [Last accessed 20 Oct. 2021].
- Ni, S., Cao, X., Yue, T., Hu, X., 2021. Controlling the rain: From removal to rendering. In: Conference on Computer Vision and Pattern Recognition. CVPR, IEEE/CVF, pp. 6328–6337.
- Nishizawa, N., Yamanaka, M., 2021. Characteristics of spectral peaking in coherent supercontinuum generation. In: 2021 Conference on Lasers and Electro-Optics. CLEO, IEEE, pp. 1–2.
- Norouzian, F., Marchetti, E., Hoare, E., Gashinova, M., Constantinou, C., Gardner, P., Cherniakov, M., 2019. Experimental study on low-THz automotive radar signal attenuation during snowfall. *IET Radar Sonar Navig.* 13 (9), 1421–1427.
- Olsen, R., Rogers, D.V., Hodge, D., 1978. The  $aR^b$  relation in the calculation of rain attenuation. *IEEE Trans. Antennas and Propagation* 26 (2), 318–329.
- Onesimus, J.A., Kadam, A., Sagayam, K.M., Elngar, A.A., 2021. Internet of things based intelligent accident avoidance system for adverse weather and road conditions. *J. Reliab. Intell. Environ.* 1–15.
- Ort, T., Gilitschenski, I., Rus, D., 2021. GROUNDED: The localizing ground penetrating radar evaluation dataset. In: Robotics: Science and Systems, Vol. 2.
- Osche, G.R., Young, D.S., 1996. Imaging laser radar in the near and far infrared. *Proc. IEEE* 84 (2), 103–125.
- Outsight, 2021. Smarter vehicles and robots. URL <https://www.outsight.ai/smarter-vehicles-and-robots>, [Last accessed 14 June 2021].
- Pacala, A., 2021. How multi-beam flash lidar works. URL <https://ouster.com/blog/how-multi-beam-flash-lidar-works/>, [Last accessed 26 Nov 2021].
- Palfy, A., Pool, E., Baratam, S., Kooij, J.F., Gavrila, D.M., 2022. Multi-class road user detection with 3+ 1D radar in the view-of-delft dataset. *IEEE Robot. Autom. Lett.* 7 (2), 4961–4968.
- Palmer, K.F., Williams, D., 1974. Optical properties of water in the near infrared. *J. Opt. Soc. Amer.* 64 (8), 1107–1110.
- Panhuber, C., Liu, B., Scheickl, O., Wies, R., Isert, C., 2016. Recognition of road surface condition through an on-vehicle camera using multiple classifiers. In: SAE-China Congress 2015: Selected Papers. Springer, pp. 267–279.
- Park, J.-I., Park, J., Kim, K.-S., 2020. Fast and accurate desnowing algorithm for LiDAR point clouds. *IEEE Access* 8, 160202–160212.
- Patole, S.M., Torlak, M., Wang, D., Ali, M., 2017. Automotive radars: A review of signal processing techniques. *IEEE Signal Process. Mag.* 34 (2), 22–35.
- Paul, N., Chung, C., 2018. Application of HDR algorithms to solve direct sunlight problems when autonomous vehicles using machine vision systems are driving into sun. *Comput. Ind.* 98, 192–196.
- Pavlić, M., Belzner, H., Rigoll, G., Ilić, S., 2012. Image based fog detection in vehicles. In: Intelligent Vehicles Symposium. IEEE, pp. 1132–1137.
- Perälä, T., Määnpää, K., Sukuvaara, T., 2022. Autonomous miniature vehicle for testing 5G intelligent traffic weather services. In: 2022 IEEE 95th Vehicular Technology Conference(VTC2022-Spring). IEEE, pp. 1–6.
- Petro, A.B., Sbert, C., Morel, J.-M., 2014. Multiscale retinex. *Image Process. Line* 71–88.
- Pfennigbauer, M., Wolf, C., Weinkopf, J., Ullrich, A., 2014. Online waveform processing for demanding target situations. In: Laser Radar Technology and Applications XIX, and Atmospheric Propagation XI, Vol. 9080. SPIE, pp. 142–151.
- Pham, Q.-H., Sevestre, P., Pahwa, R.S., Zhan, H., Pang, C.H., Chen, Y., Mustafa, A., Chandrasekhar, V., Lin, J., 2020a. A\*3D dataset: Towards autonomous driving in challenging environments. In: International Conference on Robotics and Automation. ICRA, IEEE, pp. 2267–2273.
- Pham, L.H., Tran, D.N.-N., Jeon, J.W., 2020b. Low-light image enhancement for autonomous driving systems using DriveRetinex-Net. In: International Conference on Consumer Electronics-Asia (ICCE-Asia). IEEE, pp. 1–5.
- Pitropov, M., Garcia, D.E., Rebello, J., Smart, M., Wang, C., Czarnecki, K., Waslander, S., 2021. Canadian adverse driving conditions dataset. *Int. J. Robot. Res.* 40 (4–5), 681–690.
- PTV Group, 2021. Virtual testing of autonomous vehicles with PTV VisSim. URL <https://www.ptvgroup.com/en/solutions/products/ptv-vissim/areas-of-application/autonomous-vehicles-and-new-mobility/>, [Last accessed 25 Sep. 2021].
- Pulikkaseril, C., Lam, S., 2019. Laser eyes for driverless cars: the road to automotive LiDAR. In: 2019 Optical Fiber Communications Conference and Exhibition. OFC, IEEE, pp. 1–4.
- Qian, K., Zhu, S., Zhang, X., Li, L.E., 2021. Robust multimodal vehicle detection in foggy weather using complementary lidar and radar signals. In: Conference on Computer Vision and Pattern Recognition. CVPR, IEEE/CVF, pp. 444–453.
- Qorvo, 2021. Qorvo at CES 2020: Innovative solutions for 5g, IoT, Wi-Fi 6 and V2X. URL <https://www.qorvo.com/design-hub/blog/qorvo-at-ces-2020>, [Last accessed 22 June 2021].
- Quan, R., Yu, X., Liang, Y., Yang, Y., 2021. Removing raindrops and rain streaks in one go. In: Conference on Computer Vision and Pattern Recognition. CVPR, IEEE/CVF, pp. 9147–9156.
- Radecki, P., Campbell, M., Matzen, K., 2016. All weather perception: Joint data association, tracking, and classification for autonomous ground vehicles. arXiv preprint [arXiv:1605.02196](https://arxiv.org/abs/1605.02196).
- Rapp, J., Tachella, J., Altmann, Y., McLaughlin, S., Goyal, V.K., 2020. Advances in single-photon lidar for autonomous vehicles: Working principles, challenges, and recent advances. *IEEE Signal Process. Mag.* 37 (4), 62–71.
- Rasmussen, R.M., Vivekanandan, J., Cole, J., Myers, B., Masters, C., 1999. The estimation of snowfall rate using visibility. *J. Appl. Meteorol.* 38 (10), 1542–1563.
- Rasshofer, R.H., Spies, M., Spies, H., 2011. Influences of weather phenomena on automotive laser radar systems. *Adv. Robot. Sci.* 9 (B. 2), 49–60.
- Rawashdeh, N.A., Bos, J.P., Abu-Alrub, N.J., 2021. Drivable path detection using CNN sensor fusion for autonomous driving in the snow. In: Autonomous Systems: Sensors, Processing, and Security for Vehicles and Infrastructure 2021, Vol. 11748. SPIE, pp. 36–45.
- Razlaw, J., Droeischel, D., Holz, D., Behnke, S., 2015. Evaluation of registration methods for sparse 3D laser scans. In: 2015 European Conference on Mobile Robots. ECMR, IEEE, pp. 1–7.
- Redmon, J., Divvala, S., Girshick, R., Farhadi, A., 2016. You only look once: Unified, real-time object detection. In: Conference on Computer Vision and Pattern Recognition. CVPR, IEEE/CVF, pp. 779–788.
- Redmon, J., Farhadi, A., 2018. Yolov3: An incremental improvement. arXiv preprint [arXiv:1804.02767](https://arxiv.org/abs/1804.02767).
- Ren, S., He, K., Girshick, R., Sun, J., 2015. Faster r-cnn: Towards real-time object detection with region proposal networks. *Adv. Neural Inf. Process. Syst.* 28.
- Reway, F., Huber, W., Ribeiro, E.P., 2018. Test methodology for vision-basedadas algorithms with an automotive camera-in-the-loop. In: IEEE International Conference on Vehicular Electronics and Safety. ICVES, IEEE, pp. 1–7.
- Rexing, 2021. V1P-4K. URL <https://www.rexingusa.com/products/rexing-v1p/>, [Last accessed 22 Dec 2021].
- Richter, S.R., Hayder, Z., Koltun, V., 2017. Playing for benchmarks. In: International Conference on Computer Vision. ICCV, IEEE, pp. 2213–2222.
- Ricoh, 2021. SV-M-S1 Product specifications. URL [https://industry.ricoh.com/en/fa\\_camera\\_lens/sv-m-s1/spec.html](https://industry.ricoh.com/en/fa_camera_lens/sv-m-s1/spec.html), [Last accessed 17 June 2021].
- Roehrig, C., Heller, A., Hess, D., Kuenemund, F., 2014. Global localization and position tracking of automatic guided vehicles using passive RFID technology. In: International Symposium on Robotics (ISR/Robotik). VDE, pp. 1–8.
- Rogers, R., Vaughan, M., Hostetler, C., Burton, S., Ferrare, R., Young, S., Hair, J., Oblad, M., Harper, D., Cook, A., et al., 2014. Looking through the haze: evaluating the CALIPSO level 2 aerosol optical depth using airborne high spectral resolution lidar data. *Atmos. Meas. Tech.* 7 (12), 4317–4340.
- Rong, G., Shin, B.H., Tabatabaei, H., Lu, Q., Lemke, S., Mozeiko, M., Boise, E., Uhm, G., Gerow, M., Mehta, S., et al., 2020. Lgsvl simulator: A high fidelity simulator for autonomous driving. In: International Conference on Intelligent Transportation Systems. ITSC, IEEE, pp. 1–6.
- Ros, G., Sellart, L., Materzynska, J., Vazquez, D., Lopez, A.M., 2016. The synthia dataset: A large collection of synthetic images for semantic segmentation of urban scenes. In: Conference on Computer Vision and Pattern Recognition. CVPR, IEEE/CVF, pp. 3234–3243.
- Šabanović, E., Žurauski, V., Prentkovskis, O., Skrnikj, V., 2020. Identification of road-surface type using deep neural networks for friction coefficient estimation. *Sensors* 20 (3), 612.
- SAE On-Road Automated Driving, 2014. Taxonomy and Definitions for Terms Related to Driving Automation Systems for On-Road Motor Vehicles, Surface Vehicle Recommended Practice SAE J3016:2014. SAE International.

- Saito, Y., 2021. Denso's Nakuda Test Center evaluates sensors by reproducing darkness and heavy rain indoors. URL <https://monoist.atmarkit.co.jp/mn/articles/1612/12/news035.html>, [Last accessed 25 Sep. 2021].
- Sakaridis, C., Dai, D., Van Gool, L., 2018. Semantic foggy scene understanding with synthetic data. *Int. J. Comput. Vis.* 126 (9), 973–992.
- Sakaridis, C., Dai, D., Van Gool, L., 2021. ACDC: The adverse conditions dataset with correspondences for semantic driving scene understanding. arXiv preprint [arXiv:2104.13395](https://arxiv.org/abs/2104.13395).
- Sauliala, T., 2021. Sensible4's positioning—How our autonomous vehicles know where they're going?. URL <https://sensible4.fi/2020/06/17/sensible4-positioning-how-our-autonomous-vehicles-know-where-theyre-going/>, [Last accessed 12 Dec. 2021].
- Schechner, Y.Y., Narasimhan, S.G., Nayar, S.K., 2001. Instant dehazing of images using polarization. In: Conference on Computer Vision and Pattern Recognition, Vol. 1. CVPR, IEEE/CVF, pp. 325–332.
- SenS HiPe, 2021. SenS HiPe long exposure SWIR camera. URL <https://pembrokeinstruments.com/swir-cameras/SenS-HiPe/>, [Last accessed 17 June 2021].
- Shamsudin, A.U., Ohno, K., Westfchel, T., Takahiro, S., Okada, Y., Tadokoro, S., 2016. Fog removal using laser beam penetration, laser intensity, and geometrical features for 3D measurements in fog-filled room. *Adv. Robot.* 30 (11–12), 729–743.
- Shannon, C.E., 1948. A mathematical theory of communication. *Bell Syst. Tech. J.* 27 (3), 379–423.
- Shao, Y., Li, L., Ren, W., Gao, C., Sang, N., 2020. Domain adaptation for image dehazing. In: Proceedings of the IEEE/CVF Conference on Computer Vision and Pattern Recognition. pp. 2808–2817.
- Shapiro, D., 2021. What is active learning? Finding the right self-driving training data doesn't have to take a swarm of human labelers. URL <https://blogs.nvidia.com/blog/2020/01/16/what-is-active-learning/?LinkId=100000011660647>, [Last accessed 02 Nov. 2021].
- Sharma, V., Sergeyev, S., 2020. Range detection assessment of photonic radar under adverse weather perceptions. *Opt. Commun.* 472, 125891.
- Sheeny, M., De Pellegrin, E., Mukherjee, S., Ahrabian, A., Wang, S., Wallace, A., 2021. RADITE: A radar dataset for automotive perception in bad weather. In: International Conference on Robotics and Automation. ICRA, IEEE, pp. 1–7.
- Shen, H., Li, H., Qian, Y., Zhang, L., Yuan, Q., 2014. An effective thin cloud removal procedure for visible remote sensing images. *ISPRS J. Photogramm. Remote Sens.* 96, 224–235.
- Shibata, Y., Arai, Y., Saito, Y., Hakura, J., 2020. Development and evaluation of road state information platform based on various environmental sensors in snow countries. In: International Conference on Emerging Internetworking, Data & Web Technologies. Springer, pp. 268–276.
- SICK Sensor Intelligence, 2021. 3D LiDAR sensors MRS1000. URL <https://www.sick.com/us/en/detection-and-ranging-solutions/3d-lidar-sensors/mrs1000/c/g387152>, [Last accessed 24 Aug 2021].
- Sogardares, F.M., Fry, E.S., 1997. Absorption spectrum (340–640 nm) of pure water. I. Photothermal measurements. *Appl. Opt.* 36 33, 8699–8709.
- SONY, 2021. NIR (near-infrared) imaging cameras. URL <https://www.infinitioptics.com/technology/nir-near-infrared>, [Last accessed 21 Oct. 2021].
- SONY Semiconductor Solutions Corporation, 2021. Sony to release a stacked SPAD depth sensor for automotive LiDAR applications, an industry first contributing to the safety and security of future mobility with enhanced detection and recognition capabilities for automotive LiDAR applications. URL <https://www.sony-semicon.co.jp/e/news/2021/2021090601.html>, [Last accessed 21 Oct. 2021].
- Spooren, N., Geelen, B., Tack, K., Lambrechts, A., Jayapala, M., Ginat, R., David, Y., Levi, E., Grauer, Y., 2016. RGB-NIR active gated imaging. In: Electro-Optical and Infrared Systems: Technology and Applications XIII, Vol. 9987. SPIE, pp. 19–29.
- Steinhauser, D., Held, P., Thöresz, B., Brandmeier, T., 2021. Towards safe autonomous driving: Challenges of pedestrian detection in rain with automotive radar. In: European Radar Conference (EuRAD). IEEE, pp. 409–412.
- Stott, H., 2021. Barcelona future: Smart city. URL <https://www.barcelona-metropolitan.com/living/barcelona-future-smart-city/>, [Last accessed 7 Oct 2021].
- Sukuvaara, T., Mäenpää, K., Perälä, T., Hippi, M., Rimaili, A., 2022. Winter testing track environment for the intelligent traffic road weather services development. In: Druskininkai, Lithuania (14–16TH JUNE 2022). p. 131.
- Sun, P., Kretschmar, H., Dotiwalla, X., Chouard, A., Patnaik, V., Tsui, P., Guo, J., Zhou, Y., Chai, Y., Caine, B., et al., 2020. Scalability in perception for autonomous driving: Waymo open dataset. In: Conference on Computer Vision and Pattern Recognition. CVPR, IEEE/CVF, pp. 2446–2454.
- Sun, X., Zhang, L., Zhang, Q., Zhang, W., 2019. Si photonics for practical LiDAR solutions. *Appl. Sci.* 9 (20), 4225.
- Swatantran, A., Tang, H., Barrett, T., DeCola, P., Dubayah, R., 2016. Rapid, high-resolution forest structure and terrain mapping over large areas using single photon lidar. *Sci. Rep.* 6 (1), 1–12.
- Tan, R.T., 2008. Visibility in bad weather from a single image. In: Conference on Computer Vision and Pattern Recognition. CVPR, IEEE/CVF, pp. 1–8.
- Tarel, J.-P., Hautiere, N., 2009. Fast visibility restoration from a single color or gray level image. In: International Conference on Computer Vision. ICCV, IEEE, pp. 2201–2208.
- TASS International, 2021. PreScan overview. URL <https://tass.plm.automation.siemens.com/prescan-overview>, [Last accessed 25 Sep. 2021].
- Tebaldini, S., Manzoni, M., Tagliaferri, D., Rizzi, M., Monti-Guarnieri, A.V., Prati, C.M., Spagnolini, U., Nicoli, M., Russo, I., Mazzucco, C., 2022. Sensing the urban environment by automotive SAR imaging: Potentials and challenges. *Remote Sens.* 14 (15), 3602.
- Tesla, 2021a. Summon your tesla from your phone. URL <https://www.tesla.com/blog/summon-your-tesla-your-phone>, [Last accessed 14 June 2021].
- Tesla, 2021b. Transitioning to Tesla vision. URL <https://www.tesla.com/support/transitioning-tesla-vision>, [Last accessed 14 May 2021].
- Texas Instruments, 2021. AWR1642 single-chip 77- and 79-GHz FMCW radar sensor datasheet. URL <https://www.ti.com/product/AWR1642>, [Last accessed 17 June 2021].
- Theilig, T., 2021. HDDM+—Innovative technology for distance measurement from SICK. URL [https://www.sick.com/media/docs/1/11/511/Whitepaper\\_HDDM\\_INNOVATIVE TECHNOLOGY\\_FOR\\_DISTANCE\\_en\\_IM0076511.PDF](https://www.sick.com/media/docs/1/11/511/Whitepaper_HDDM_INNOVATIVE TECHNOLOGY_FOR_DISTANCE_en_IM0076511.PDF), [Last accessed 24 Sep. 2021].
- Thrun, S., Montemerlo, M., Dahlkamp, H., Stavens, D., Aron, A., Diebel, J., Fong, P., Gale, J., Halpenny, M., Hoffmann, G., Lau, K., Oakley, C., Palautucci, M., Pratt, V., Stang, P., Strohband, S., Dupont, C., Jendrossek, L.-E., Koelen, C., Markey, C., Rummel, C., van Niekerk, J., Jensen, E., Alessandrini, P., Bradski, G., Davies, B., Ettinger, S., Kaehler, A., Nefian, A., Mahoney, P., 2006. Stanley: The robot that won the DARPA Grand Challenge. *J. Field Robotics* 23 (9), 661–692.
- Tian, Y., 2021. Identification of Weather Conditions Related to Roadside LiDAR Data (Ph.D. thesis). University of Nevada, Reno.
- Tobin, R., Halimi, A., McCarthy, A., Soan, P.J., Buller, G.S., 2021. Robust real-time 3D imaging of moving scenes through atmospheric obscurant using single-photon LiDAR. *Sci. Rep.* 11 (1), 1–13.
- Trenberth, K.E., Zhang, Y., 2018. How often does it really rain? *Bull. Am. Meteorol. Soc.* 99 (2), 289–298.
- Trierweiler, M., Caldelas, P., Gröninger, G., Peterseim, T., Neumann, C., 2019. Influence of sensor blockage on automotive LiDAR systems. In: IEEE SENSORS. pp. 1–4. <http://dx.doi.org/10.1109/SENSORS43011.2019.8956792>.
- Trierweiler, M., Peterseim, T., Neumann, C., 2020. Automotive LiDAR pollution detection system based on total internal reflection techniques. In: Light-Emitting Devices, Materials, and Applications XXIV, Vol. 11302. SPIE, pp. 135–144.
- Tsai, D., Worrall, S., Shan, M., Lohr, A., Nebot, E., 2021. Optimising the selection of samples for robust lidar camera calibration. arXiv preprint [arXiv:2103.12287](https://arxiv.org/abs/2103.12287).
- Tu, C., Takeuchi, E., Carballo, A., Miyajima, C., Takeda, K., 2019. Motion analysis and performance improved method for 3D LiDAR sensor data compression. *IEEE Trans. Intell. Transp. Syst.* 22 (1), 243–256.
- Tumas, P., Nowosielski, A., Serakis, A., 2020. Pedestrian detection in severe weather conditions. *IEEE Access* 8, 62775–62784.
- Tung, F., Chen, J., Meng, L., Little, J.J., 2017. The raincouver scene parsing benchmark for self-driving in adverse weather and at night. *Robot. Autom. Lett. (RA-L)* 2 (4), 2188–2193.
- University of Michigan, 2021. Mcity driverless shuttle: What we learned about consumer acceptance of automated vehicles. URL <https://mcity.umich.edu/wp-content/uploads/2020/10/mcity-driverless-shuttle-whitepaper.pdf>, [Last accessed 06 May 2021].
- Uříčák, M., Křížek, P., Sistu, G., Yogamani, S., 2019. Soilingnet: Soiling detection on automotive surround-view cameras. In: Intelligent Transportation Systems Conference. ITSC, IEEE, pp. 67–72.
- Uříčák, M., Sistu, G., Rashed, H., Vobecky, A., Kumar, V.R., Krizek, P., Burger, F., Yogamani, S., 2021. Let's get dirty: GAN based data augmentation for camera lens soiling detection in autonomous driving. In: Winter Conference on Applications of Computer Vision. WACV, IEEE/CVF, pp. 766–775.
- Vachmanus, S., Ravankar, A.A., Emaru, T., Kobayashi, Y., 2021. Multi-modal sensor fusion-based semantic segmentation for snow driving scenarios. *IEEE Sens. J.* 21 (15), 16839–16851.
- Vaibhav, V., Konda, K.R., Kondapalli, C., Praveen, K., Kondoju, B., 2020. Real-time fog visibility range estimation for autonomous driving applications. In: International Conference on Intelligent Transportation Systems. ITSC, IEEE, pp. 1–6.
- Vaidya, B., Kaur, P.P., Mouftah, H.T., 2021. Provisioning road weather management using edge cloud and connected and autonomous vehicles. In: International Wireless Communications and Mobile Computing. IWCMC, IEEE, pp. 1424–1429.
- Vaisala, 2022. Present weather and visibility sensors PWD10, PWD12, PWD20, and PWD22. URL <https://www.vaisala.com/sites/default/files/documents/PWD-Series-Datasheet-B210385EN.pdf>, [Last accessed 04 Feb 2022].
- Vargas Rivero, J.R., Gerbich, T., Teiluf, V., Buschardt, B., Chen, J., 2020. Weather classification using an automotive LIDAR sensor based on detections on asphalt and atmosphere. *Sensors* 20 (15), 4306.
- Varghese, J.Z., Boone, R.G., et al., 2015. Overview of autonomous vehicle sensors and systems. In: International Conference on Operations Excellence and Service Engineering. pp. 178–191.
- Velodyne, 2021a. A guide to lidar wavelengths for autonomous vehicles and driver assistance. URL <https://velodynelidar.com/blog/guide-to-lidar-wavelengths/>, [Last accessed 06 June 2021].
- Velodyne, 2021b. HDL-64E spec sheet. URL <https://velodynesupport.zendesk.com/hc/en-us/articles/115003632634-HDL-64E-Spec-Sheet>, [Last accessed 10 Oct. 2021].

- Velodyne, 2021c. A smart, powerful lidar solution. URL <https://velodynelidar.com/products/puck/>, [Last accessed 21 Oct. 2021].
- Velodyne, 2021d. Velodyne Alpha Prime datasheet. URL [https://velodynelidar.com/wp-content/uploads/2019/12/63-9679\\_Rev-1\\_DATASHEET\\_ALPHA-PRIME\\_Web.pdf](https://velodynelidar.com/wp-content/uploads/2019/12/63-9679_Rev-1_DATASHEET_ALPHA-PRIME_Web.pdf), [Last accessed 21 Oct. 2021].
- Vertens, J., Zürn, J., Burgard, W., 2020. Heatnet: Bridging the day-night domain gap in semantic segmentation with thermal images. In: International Conference on Intelligent Robots and Systems. IROS, IEEE/RSJ, pp. 8461–8468.
- Virginia Tech, 2021. Virginia smart roads highway section. URL <https://www.vtti.vt.edu/facilities/highway-section.html>, [Last accessed 25 Sep. 2021].
- Von Bernuth, A., Volk, G., Bringmann, O., 2019. Simulating photo-realistic snow and fog on existing images for enhanced CNN training and evaluation. In: Intelligent Transportation Systems Conference. ITSC, IEEE, pp. 41–46.
- VSLabs, 2021. Research & testing on ADAS & autonomous vehicle technologies. URL <https://vsl-labs.com/>, [Last accessed 21 Oct. 2021].
- Wallace, A.M., Halimi, A., Buller, G.S., 2020. Full waveform lidar for adverse weather conditions. IEEE Trans. Veh. Technol. 69 (7), 7064–7077.
- Wang, Y., Li, K., Hu, Y., Chen, H., 2020. Modeling and quantitative assessment of environment complexity for autonomous vehicles. In: Chinese Control and Decision Conference. CCDC, IEEE, pp. 2124–2129.
- Wang, Y., Ma, C., Zeng, B., 2021a. Multi-decoding deraining network and quasi-sparsity based training. In: Conference on Computer Vision and Pattern Recognition. CVPR, IEEE/CVF, pp. 13375–13384.
- Wang, W., You, X., Chen, L., Tian, J., Tang, F., Zhang, L., 2022. A scalable and accurate de-snowing algorithm for LiDAR point clouds in winter. Remote Sens. 14 (6), 1468.
- Wang, H., Yue, Z., Xie, Q., Zhao, Q., Zheng, Y., Meng, D., 2021b. From rain generation to rain removal. In: Conference on Computer Vision and Pattern Recognition. CVPR, IEEE/CVF, pp. 14791–14801.
- Warren, M.E., 2019. Automotive LiDAR technology. In: Symposium on VLSI Circuits. pp. C254–C255.
- Wenzel, P., Wang, R., Yang, N., Cheng, Q., Khan, Q., von Stumberg, L., Zeller, N., Cremers, D., 2021. 4Seasons: A cross-season dataset for multi-weather SLAM in autonomous driving. In: DAGM German Conference on Pattern Recognition. GCPR, Deutsche Arbeitsgemeinschaft für Mustererkennung (DAGM), pp. 404–417.
- Wi-Fi ALLIANCE, 2021. Generational Wi-Fi® user guide. URL [https://www.wi-fi.org/download.php?file=/sites/default/files/private/Generational\\_Wi-Fi\\_User\\_Guide\\_20181003.pdf](https://www.wi-fi.org/download.php?file=/sites/default/files/private/Generational_Wi-Fi_User_Guide_20181003.pdf), [Last accessed 22 June 2021].
- Wojtanowski, J., Zygmunt, M., Kaszczuk, M., Mierczyk, Z., Muzal, M., 2014. Comparison of 905 nm and 1550 nm semiconductor laser rangefinders' performance deterioration due to adverse environmental conditions. Opto-Electron. Rev. 22 (3), 183–190.
- Wolcott, R.W., Eustice, R.M., 2015. Fast LiDAR localization using multiresolution Gaussian mixture maps. In: International Conference on Robotics and Automation. ICRA, IEEE, pp. 2814–2821.
- Wolcott, R.W., Eustice, R.M., 2017. Robust LiDAR localization using multiresolution Gaussian mixture maps for autonomous driving. Int. J. Robot. Res. 36 (3), 292–319.
- Wu, H., Qu, Y., Lin, S., Zhou, J., Qiao, R., Zhang, Z., Xie, Y., Ma, L., 2021. Contrastive learning for compact single image dehazing. In: Conference on Computer Vision and Pattern Recognition. CVPR, IEEE/CVF, pp. 10551–10560.
- Wu, Z., Suresh, K., Narayanan, P., Xu, H., Kwon, H., Wang, Z., 2019. Delving into robust object detection from unmanned aerial vehicles: A deep nuisance disentanglement approach. In: Proceedings of the IEEE/CVF International Conference on Computer Vision. pp. 1201–1210.
- Wu, J., Xu, H., Tian, Y., Pi, R., Yue, R., 2020a. Vehicle detection under adverse weather from roadside LiDAR data. Sensors 20 (12), 3433.
- Wu, D., Yi, Y., Zhang, Y., 2020b. High-efficiency end-fire 3D optical phased array based on a multi-layer Si<sub>3</sub>N<sub>4</sub>/SiO<sub>2</sub> platform. Appl. Opt. 59 (8), 2489–2497.
- Xu, Z., Sun, Y., Liu, M., 2021. iCurb: Imitation learning-based detection of road curbs using aerial images for autonomous driving. Robot. Autom. Lett. (RA-L) 6 (2), 1097–1104.
- Yahiaoui, L., Uřičář, M., Das, A., Yogamani, S., 2020. Let the sunshine in: Sun glare detection on automotive surround-view cameras. Electron. Imaging 2020 (16), 80–81.
- Yan, Y., Mao, Y., Li, B., 2018. Second: Sparsely embedded convolutional detection. Sensors 18 (10), 3337.
- Yan, Z., Sun, L., Krajník, T., Ruichek, Y., 2020. EU long-term dataset with multiple sensors for autonomous driving. In: International Conference on Intelligent Robots and Systems. IROS, IEEE/RSJ, pp. 10697–10704.
- Yang, H., Carballo, A., Takeda, K., 2022. Disentangled bad weather removal GAN for pedestrian detection. In: 2022 IEEE 95th Vehicular Technology Conference:(VTC2022-Spring). IEEE, pp. 1–6.
- Yang, B., Guo, R., Liang, M., Casas, S., Urtasun, R., 2020. Radarnet: Exploiting radar for robust perception of dynamic objects. In: European Conference on Computer Vision. Springer, pp. 496–512.
- Yang, T., Li, Y., Ruichek, Y., Yan, Z., 2021. Performance modeling a near-infrared ToF LiDAR under fog: A data-driven approach. IEEE Trans. Intell. Transp. Syst. 1–10.
- Ye, Y., Chang, Y., Zhou, H., Yan, L., 2021. Closing the loop: Joint rain generation and removal via disentangled image translation. In: Conference on Computer Vision and Pattern Recognition. CVPR, IEEE/CVF, pp. 2053–2062.
- Yeong, D.J., Velasco-Hernandez, G., Barry, J., Walsh, J., et al., 2021. Sensor and sensor fusion technology in autonomous vehicles: A review. Sensors 21 (6), 2140.
- Yi, Z., Zhang, H., Tan, P., Gong, M., 2017. Dualgan: Unsupervised dual learning for image-to-image translation. In: Proceedings of the IEEE International Conference on Computer Vision. pp. 2849–2857.
- Yifan David Li, K.S., 2021. Hesai introduces PandarGT-third-gen solid-state lidar. URL <https://www.hesaitech.com/en/media/3>, [Last accessed 26 Nov 2021].
- Yinka, A.O., Ngwira, S.M., Tranos, Z., Sengar, P.S., 2014. Performance of drivable path detection system of autonomous robots in rain and snow scenario. In: International Conference on Signal Processing and Integrated Networks. SPIN, IEEE, pp. 679–684.
- Yogamani, S., Hughes, C., Horgan, J., Sistu, G., Varley, P., O'Dea, D., Uricár, M., Milz, S., Simon, M., Amende, K., et al., 2019. Woodscape: A multi-task, multi-camera fisheye dataset for autonomous driving. In: Proceedings of the IEEE/CVF International Conference on Computer Vision. pp. 9308–9318.
- Yoneda, K., Suganuma, N., Yanase, R., Aldibaja, M., 2019. Automated driving recognition technologies for adverse weather conditions. IATSS Res. 43 (4), 253–262.
- You, J., Jia, S., Pei, X., Yao, D., 2021. DMRVisNet: Deep multi-head regression network for pixel-wise visibility estimation under foggy weather. arXiv preprint arXiv:2112.04278.
- Young, A.T., 2015. Inferior mirages: an improved model. Appl. Opt. 54 (4), B170–B176.
- Yu, F., Chen, H., Wang, X., Xian, W., Chen, Y., Liu, F., Madhavan, V., Darrell, T., 2020. Bdd100k: A diverse driving dataset for heterogeneous multitask learning. In: Conference on Computer Vision and Pattern Recognition. CVPR, IEEE/CVF, pp. 2636–2645.
- Yue, Z., Xie, J., Zhao, Q., Meng, D., 2021. Semi-supervised video deraining with dynamical rain generator. In: Conference on Computer Vision and Pattern Recognition. CVPR, IEEE/CVF, pp. 642–652.
- Yurtsever, E., Lambert, J., Carballo, A., Takeda, K., 2020. A survey of autonomous driving: Common practices and emerging technologies. IEEE Access 8, 58443–58469.
- Zang, S., Ding, M., Smith, D., Tyler, P., Rakotoarivelo, T., Kaafar, M.A., 2019. The impact of adverse weather conditions on autonomous vehicles: how rain, snow, fog, and hail affect the performance of a self-driving car. IEEE Veh. Technol. Mag. 14 (2), 103–111.
- Zendel, O., Honauer, K., Murschitz, M., Steininger, D., Dominguez, G.F., 2018. Wilddash-creating hazard-aware benchmarks. In: European Conference on Computer Vision. ECCV, pp. 402–416.
- Zhang, X., Dong, H., Pan, J., Zhu, C., Tai, Y., Wang, C., Li, J., Huang, F., Wang, F., 2021a. Learning to restore hazy video: A new real-world dataset and a new method. In: Conference on Computer Vision and Pattern Recognition. CVPR, IEEE/CVF, pp. 9239–9248.
- Zhang, K., Li, R., Yu, Y., Luo, W., Li, C., 2021b. Deep dense multi-scale network for snow removal using semantic and depth priors. IEEE Trans. Image Process. 30, 7419–7431.
- Zhang, Z., Ma, H., 2015. Multi-class weather classification on single images. In: International Conference on Image Processing. ICIP, IEEE, pp. 4396–4400.
- Zheng, J.Y., 2021. IUPUI driving videos and images in all weather and illumination conditions. arXiv preprint arXiv:2104.08657.
- Zheng, Z., Ren, W., Cao, X., Hu, X., Wang, T., Song, F., Jia, X., 2021a. Ultra-high-definition image dehazing via multi-guided bilateral learning. In: Conference on Computer Vision and Pattern Recognition. CVPR, IEEE/CVF, pp. 16185–16194.
- Zheng, Q., Shi, B., Chen, J., Jiang, X., Duan, L.-Y., Kot, A.C., 2021b. Single image reflection removal with absorption effect. In: Conference on Computer Vision and Pattern Recognition. CVPR, IEEE/CVF, pp. 13395–13404.
- Zhou, M., Xiao, J., Chang, Y., Fu, X., Liu, A., Pan, J., Zha, Z.-J., 2021. Image de-raining via continual learning. In: Conference on Computer Vision and Pattern Recognition. CVPR, IEEE/CVF, pp. 4907–4916.
- Zhou, J., Zhou, F., 2013. Single image dehazing motivated by retinex theory. In: International Symposium on Instrumentation and Measurement, Sensor Network and Automation. IMSNA, IEEE, pp. 243–247.
- Zhu, J.-Y., Park, T., Isola, P., Efros, A.A., 2017. Unpaired image-to-image translation using cycle-consistent adversarial networks. In: Proceedings of the IEEE International Conference on Computer Vision. pp. 2223–2232.
- Żywanowski, K., Banaszczuk, A., Nowicki, M.R., 2020. Comparison of camera-based and 3D LiDAR-based place recognition across weather conditions. In: International Conference on Control, Automation, Robotics and Vision. ICARCV, IEEE, pp. 886–891.



**Yuxiao Zhang** received the B.S. degree in mechanical engineering from Wuhan University of Technology, China, and the M.S.Eng from the University of Michigan, USA. From 2019 to 2020, he worked as a Research Assistant at the Integrated Nano Fabrication and Electronics Laboratory of the College of Engineering and Computer Science at the University of Michigan. He is currently pursuing a Ph.D. degree with the Graduate School of Informatics, Nagoya University, Japan. His main research interests are LiDAR sensors and robust perception for autonomous driving systems.



**Alexander Carballo** received the Dr. Eng. degree from the Intelligent Robot Laboratory, University of Tsukuba, Japan. From 1996 to 2006, he was a Lecturer with the School of Computer Engineering, Costa Rica Institute of Technology. From 2011 to 2017, he worked in LiDAR research and development at Hokuyo Automatic Company, Ltd. From 2017, he joined Nagoya University as Designated Associate Professor affiliated to the Institutes of Innovation for Future Society. Lastly, from 2022 he was appointed permanent Associate Professor at the Graduate School of Engineering in Gifu University, Japan. He is a professional member of IEEE Intelligent Transportation Systems Society (ITSS), IEEE Robotics and Automation Society (RAS), Robotics Society of Japan (RSJ), Asia Pacific Signal and Information Processing Association (APSIPA), the Society of Automotive Engineers of Japan (JSCE), and the Japan Society of Photogrammetry and Remote Sensing (JSPRS). His main research interests include LiDAR sensors, robotic perception, and autonomous driving.



**Hanting Yang** received his B.S. degree and M.E. degree from Beijing University of Civil Engineering and Architecture. He is currently pursuing a Ph.D. degree with the Graduate School of Informatics, Nagoya University, Japan. His main research interests are image processing, deep learning, and robust vision perception for autonomous vehicles.



**Kazuya Takeda** received the B.E. and M.E. degrees in electrical engineering and the D.Eng. degree from Nagoya University, Nagoya, Japan, in 1983, 1985, and 1994, respectively. From 1986 to 1989, he was with the Advanced Telecommunication Research (ATR) Laboratories, Osaka, Japan. He was a Visiting Scientist with the Massachusetts Institute of Technology (MIT), from November 1987 to April 1988. From 1989 to 1995, he was a Researcher and Research Supervisor with the KDD R&D Laboratories, Kamifukuoka, Japan. From 1995 to 2003, he was an Associate Professor with the Faculty of Engineering, Nagoya University. Since 2003, he has been a Professor with Graduate School of Informatics, Nagoya University and currently is the Head of the Takeda Laboratory, Nagoya University. Currently, he also serves as Vice President of Nagoya University. He is a fellow of IEICE (the Institute of Electronics, Information and Communications Engineers) and a senior member of IEEE. Prof. Takeda has served as one of academic leaders in various signal processing fields. Currently, he is a BoG (Board of Governors) member of IEEE ITS Society, Asia-Pacific Signal and Information Processing Association (APSIPA) and vice president of Acoustical Society Japan. He is a co-founder and director of Tier IV, Inc. His main focus is in the field of signal processing technology research for acoustic, speech and vehicular applications. In particular, understanding human behavior through data centric approaches utilizing signal corpora of real driving behavior.